01 Jun 1995

Design of automotive structural components using high strength sheet steels effect of strain rate on the structural strength of cold-formed steel hybrid beams

Chi-Ling Pan

Wei-Wen Yu
Missouri University of Science and Technology, wwy4@mst.edu

Civil Engineering Study 95-4
Cold-Formed Steel Series

Twentieth Progress Report

DESIGN OF AUTOMOTIVE STRUCTURAL COMPONENTS
USING HIGH STRENGTH SHEET STEELS

EFFECT OF STRAIN RATE ON THE STRUCTURAL STRENGTH OF COLD-FORMED STEEL HYBRID BEAMS

by

Chi-Ling Pan
Post-Doctoral Fellow

Wei-Wen Yu
Project Director

A Research Project Sponsored by the American Iron and Steel Institute

June 1995

Department of Civil Engineering
University of Missouri-Rolla
Rolla, Missouri

TABLE OF CONTENTS

LIST OF TABLES

LIST OF TABLES (cont.)

LIST OF TABLES (cont.)

LIST OF FIGURES

LIST OF FIGURES (cont.)

LIST OF FIGURES (cont.)

I. INTRODUCTION

In cold-formed steel design, local buckling is one of the major design features because of the use of large width-to-thickness ratios for compression elements. For the purpose of determining the load-carrying capacity of automotive components, the effective width approach has been used. In view of the fact that the design criteria for effective design width included in the AISI Automotive Steel Design Manual[1] are based on the test results for static loading condition, an investigation was conducted at University of Missouri-Rolla from January 1988 through December 1991 to study the validity of these effective design width formulas for the design of cold-formed steel automotive components subjected to dynamic loads. The results showed that the effective cross-sectional area calculated on the basis of the dynamic yield stresses can be employed in the determination of ultimate loads. The test results of material properties, stub columns, and beams with evaluations were summarized in the Eighteenth Progress Report[2].

In the previous UMR research, stub column and beam specimens fabricated from two different sheet steels (35XF and 50XF) were tested under different strain rates to study the behavior of stiffened and unstiffened compression elements. Because the previous studies were limited only to the structural members which were assembled with the same material in a given section, this portion of the research was concentrated on a study of the structural strength of hybrid automotive structural components using different sheet steels. In the first phase of the investigation, two selected sheet steels (25AK and 50SK) have

been tested in order to study the effect of strain rate on the tensile and compressive mechanical properties. The nominal yield strengths of these two types of sheet steels were 25 and 50 ksi and the range of strain rates used in the tests varied from 10^{-4} to 1.0 in./in./sec.. The test results obtained from this study were presented in the Seventeenth Progress Report[3]. The structural behavior and strength of cold-formed steel stub columns assembled with these two selected sheet steels were studied experimentally and analytically under dynamic loads. In the second phase of the investigation, ninety-six (96) box-shaped stub columns and forty-eight (48) hat-shaped stub columns were tested under the strain rates varied from 10^{-4} to 10^{-1} in./in./sec. at the University of Missouri-Rolla. In addition, fifty-two (52) drop tower tests of stub columns were conducted at General Motors Corporation. Details of stub column tests with evaluations were presented in the Nineteenth Progress Report[4]. The test results showed that a good prediction for the ultimate strength of hybrid stub columns can be achieved by employing the dynamic material properties in the calculation of the effective cross-sectional area.

The study of beam specimens fabricated from two types of sheet steels (25AK and 50SK) subjected to dynamic loads was initiated in October 1993. A total of 72 hat-shaped beams were tested to investigate the structural behavior and strength of hybrid sections using different sheet steels. The range of strain rates used in the beam tests were from 10^{-4} to 10^{-2} in./in./sec.. The test results of beam specimens are reported herein.

A review of the available literature on the effect of impact loads or dynamic loads on the structural strength of beams is presented in Chapter II of this report.

The experimental investigation of the structural behavior of hat-shaped beam specimens subjected to dynamic loads is discussed in Chapter III. In Chapter IV, the test data for beam specimens are evaluated and presented. Finally, the research findings are summarized in Chapter V.

II. REVIEW OF LITERATURE

A. GENERAL

In recent years, more economic and lighter vehicles have been produced by automotive manufacturers for the sake of fuel economy. High strength sheet steels have been favorably used to accomplish the construction of such automobiles. The design information for using sheet steels is provided in the AISI Automotive Steel Design Manual[1].

In the current AISI Automotive Steel Design Manual[1], the design criteria for effective design width are based on the test results under static loading condition. Therefore, the objective of this experimental investigation was to study whether the available effective design formulas using dynamic material properties can be adequately used for the design of hybrid structural members fabricated from two different materials subjected to dynamic loads.

A review of the structural behavior of compression elements under static loads, the development of effective width formulas for the prediction of maximum strength of compression elements, and the current effective width formulas used in the AISI Automotive Steel Design Manual[1] were discussed and presented in the Nineteenth Progress Report[4]. In Section B of this chapter, some of the developments resulted from the previous research for the response of structural members subjected to dynamic loads are reviewed. Particular attention is focused on those items related to beams. A brief discussion for some of the previous

research related to the structural strength of hybrid beams is presented in Section C.

B. RESPONSE OF FLEXURAL MEMBERS TO DYNAMIC LOADS

In 1955, Parkes[5] examined the permanent deformation of mild steel cantilever beams subjected to dynamic transverse loads and found that a simple rigid, perfectly plastic analysis overestimated the final maximum deflections. In 1958, Parkes[6] investigated encastre beams with impact loading applied transversely at any point on their span. The supports of beams were prevented from rotating but were free to move axially. Test specimens were made from mild steel, brass and duralumin. He found that the mild steel is the most sensitive to strain rate as compared with other two materials. Taking the strain-rate sensitivity into account one can improve the correlation between theoretical and experimental results. Similar discovery was also found by Ezra[7] in 1958. Ezra developed a mathematical model to analyze the response of simply supported beams subjected to a concentrated impact load at midspan. His model allows the use of plastic moment, taking account of yield stress as affected by strain rate. The theoretical values showed increasingly better agreements with the test results as the impact speed of the test increases.

In 1962, Ting and Symonds[8] tested the cantilever beam with an attached tip mass subjected to a rapid transverse velocity change at the base. The predictions of plastic deformation showed good agreement with corresponding experimental results when considering the strain-rate

dependence of yield stress and geometry changes. Bodner and Symonds[9] (1962) examined the plastic deformations of cantilever beams with tip mass under two loading conditions: (1) the base of the cantilever was impacted against a solid support and (2) the tip mass was loaded either by an explosive charge, or being hit by a rifle bullet. Two materials (mild steel and aluminum alloy) were used to fabricate the specimens. Theoretical results were initially obtained from the use of a rigid-plastic theory. It was concluded that the strain rate effects gave good agreements with the test results.

Rawlings[10] (1963) reported on his experimental investigation of strain-rate effects on yield loads for beam tests. He tested a series of simply supported beams fabricated from mild steel using two-point loading system so that a plastic hinge could be formed in the central portion of a beam. All loads were applied by large falling masses. The results for the relationship between lower yield value and the time taken to yield obtained from beam tests showed good agreements with the relationship obtained from material tests.

Using the experimental results of Parkes, Ting[11] (1965) developed a formula for cantilever beams loaded dynamically on the basis of rigid-plastic theory, which took into account large geometric changes. His results compared very favorably with Parkes' experimental results. He concluded that not all discrepancies between the theory and experimental results can be attributed to strain-rate effect, as had been previously assumed.

In 1965, Florence and Firth[12] tested the pinned and clamped beams without axial restraints, subjected to uniformly distributed impulses. It was concluded that a rigid-plastic analysis considering strain-hardening effect in an approximate manner during the second stage of motion instead of considering strain-rate effect, gave somewhat better agreement with the experimental results than a rigid-plastic analysis.

Similar results were found by Jones[13] (1967). He developed the method for estimating the combined influence of strain-hardening and strain-rate sensitivity on the permanent deformation of rigid-plastic structures loaded dynamically. A study is made of the particular case of a beam supported at the ends by immovable frictionless pins and loaded with a uniform impulse. He found that when considering strain-hardening alone for beams with small L/H (half-length to thickness) ratios, or strain-rate sensitivity alone for physically small beams, then permanent deflections are predicted, which compare rather favorably with those given for the same value of λ (impulse parameter) by an analysis retaining their combined influence.

Aspden and Campbell[14] (1966) were the first to conduct dynamic flexural tests in which transient records were taken of moment -rotation characteristics. They used small-scale specimens, 0.75 inches long by 0.375 inches wide by 0.125 inches thick, supported at their ends by beams and loaded as four point loading system by a falling weight. They compared their high speed flexural test results with those obtained under dynamic compression using a hydraulically operated machine, and with slow speed tests in an Instron machine. Like Rawlings, Aspden and

Campbell observed evidence of high initial peak moments of resistance. For the highest rate of strain in their beams, the dynamic 'upper yield moment' was about 80% higher than the corresponding moment in a low speed test. Figure 2.1 shows the variation of upper and lower yield moments with different strain-rate at surface of specimen. They noticed that attaining the maximum peak moment of resistance, the value decreased below that which would be derived from test results by assuming plane sections remain plane. They attributed the difference of about 10% to non-uniform strain distribution throughout the experiment during the loading process. Based on the empirical equation (Equation 2.1) for prediction of dynamic yield stresses under constant strain rate derived by Cowper and Symonds, Aspden and Campbell integrated Equation 2.1 through the thickness of a beam and found that the dynamic bending moment is related to the associated beam curvature rate according to the expression given in Equation 2.2.

$$\frac{\sigma}{\sigma_0} = 1 + \left(\frac{\dot{\varepsilon}}{D}\right)^{1/p} \tag{2.1}$$

where σ = dynamic yield stress

σ_0 = static yield stress

$\dot{\varepsilon}$ = strain rate

D and p = strain-rate sensitivity coefficients

$$\frac{M}{M_0} = 1 + \frac{2p}{2p+1}\left(\frac{\dot{\kappa}H}{2D}\right)^{1/p} \tag{2.2}$$

where M = dynamic bending moment

$M_0 = \sigma_y H^2/4$, static collapse moment

$\dot{\kappa}$ = curvature rate

H = thickness of the beam

In 1971, Culver, Zanoni, and Osgood[15] of Carnegie-Mellon University reported on thin-walled beam sections subjected to dynamic loading, as part of a large program of dynamic loading on cold-formed steel structural sections. Two methods of analysis were used in this study. The linear elastic and the non-linear methods including local buckling effects, were used to compare with the test results. A comparison of results showed that it was sufficient to predict bending moments from nominal linear elastic analysis considering local buckling effects.

Symonds and Jones[16] (1972) reviewed the earlier work on plastic response to impulsive loading of beams which were clamped against end rotations and axial displacements, taking account for small finite transverse displacements and for strain-rate dependence of the yield stress. New solutions were derived from the rigid-plastic analysis which included both effects and were compared with experimental results. They concluded that the rigid-plastic interation theory with simple strain-rate corrections provides satisfactory agreement with deflections measured from tests of small beams for deflections up to about seven times the beam thickness.

Forrestal, Wesenberg, and Sagartz[17,18] have developed a simple method for incorporating the approximate influence of material elasticity on the dynamic plastic response of beams. An exact elastic analysis was first undertaken for a dynamic beam problem which remains valid until the maximum stress reaches yield. If the beam material is

strain-rate sensitive, then this yield stress is calculated from Cowper-Symonds constitutive law (Equation 2.1), using the corresponding strain-rate predicted by elastic analysis. The subsequent plastic behavior is controlled by a constant yield stress. There was an excellent agreement with the peak displacements recorded during experiments on simply supported beams using 1018 steel and type 304 stainless steel as shown in Figure 2.2.

In 1989, Kassar[19] tested three different sheet steels (35XF, 50XF, and 100XF) and 30 beams fabricated from 35XF sheet steel under dynamic loads. Based on the test results, it was found that the mechanical properties of sheet steels (yield stress, proportional limit, and ultimate tensile strength) and the load-carrying capacity of beams increase with increasing strain rates. In addition, Pan[2] tested 30 beams fabricated from 50XF sheet steel. The results showed that the effective cross-sectional area calculated on the basis of the dynamic yield stresses can be employed in the determination of load-carrying capacity of beams.

C. Response of Hybrid Flexural Members under Static Loads

High strength steels show more favorable price-to-strength ratios than structural carbon steels. That is, when high strength steels are compared with carbon steels in price and yield stress, the increase in price for high strength steels is less than the increase in yield stress. As a result, the application of high strength steels to structures can often results in significant material-cost savings[20].

In 1963, Geerhard Haaijer[20] studied the I-shaped hybrid beam and girder analytically. By using a plastic analysis, a hybrid beam consisting of a web of structural carbon steel (yield point 33,000 psi) and flanges of "T-1" steel (yield strength 100,000 psi) was studied. Figure 2.3[20] shows a schematic moment-verse-curvature curve and the distribution of strains and stresses across the section for three stages of loading. During Stage I, all stresses are smaller than the yield stresses of the respective parts; thus, the behavior of the beam is completely elastic. The end of Stage I is reached when the maximum stress in the web equals the yield stress of the web. During Stage II, part of the web is yielding but the flanges are still elastic. Stage III is reached when the flanges also start to yield. The fully plastic moment, M_p, is determined from the condition that the entire section reaches yield. Therefore, M_p is the true measure of the bending strength of the beam.

In the analysis of I-shaped beams and girders, Haaijer[20] found that the web depth-to-thickness, α, has a major influence on the efficiency of such beams. The minimum cross-section area that is required to support a given moment is proportional to the inverse of the cube root of α. It is obvious that significant weight savings can be obtained by constructing beams with large web depth-to-thickness ratios. He concluded that through the optimum design of structural members the application of higher strength steels can lead to lighter weight structures and often to significant material-cost savings as well.

In 1964, Ronald Frost and Charles Schilling[21] studied the behavior of hybrid beams consisting of higher-strength steel flanges connected with lower-strength steel webs, under pure bending and combined shear and bending. Three types of beams were studied , one with a 100,000-psi yield strength flange and a 50,000-psi yield point web, one with a 100,000-psi yield strength flange and a 33,000-psi yield point web, and one homogeneous 100,000-psi yield strength beam were tested for the comparison purpose.

The test results showed that the experimental maximum moments for the hybrid beams with the 50,000-psi and 33,000-psi steel webs were, respectively, 4.8% and 7.7% less than the experimental maximum moment for the homogeneous 100,000-psi steel beam. The shear strengths, V_p, of the three beams differed considerably more than did the bending strength, M_p, because practically all the shear strength of a beam is contributed by the web, whereas most of the bending strength is contributed by the flanges. It was founded by Frost and Schilling[21] that the theoretical ratios of shear to bending strength, V_p/M_p, of the hybrid beams with the 50,000-psi and 33,000-psi steel webs were, respectively, 37.8% and 63.5% less than the ratio for the homogenous 100,000-psi steel beam.

Frost and Schilling[21] suggested that the maximum bending strength of a hybrid beam may be considered to be (1) the moment causing the cross section to become fully plastic, M_p, or (2) the moment causing initial yielding in the flange, M_{yf}, because it has been demonstrated that the yielding which occurs in the webs of hybrid beams has little effect on the behavior of such beams.

In 1968, A paper titled "Design of Hybrid Steel Beams" was prepared by the Subcommittee 1 on Hybrid Beams and Girders of the Joint ASCE-AASHO Committee on Flexural Members[22]. The methods and procedure for computing composite and noncomposite hybrid beams were discussed in this paper. The design suggestions recommended by this Subcommittee are not intended to apply to the following cases:

(1) Noncomposite hybrid beams that are unsymmetrical with respect to either the neutral axis or an axis in the plane of the web. Hybrid steel beams used in composite construction may themselves be unsymmetrical with respect to the neutral axis.

(2) Noncomposite hybrid beams with different steels in the two flanges.

(3) Composite hybrid beams in which the steel top flange has a large area or higher yield strength than the bottom flange.

(4) Composite or noncomposite hybrid beams subjected to significant axial loads, that is, axial loads that exceed 15% of the allowable load for a homogenous beam of the same dimensions fabricated from the flange steel.

Because web yielding has little effect on the bending behavior of hybrid beams, the conclusion of this paper showed that composite and noncomposite hybrid beams can be efficiently designed on the basis of the initial flange-yield moment. Specifically, an allowable flange stress that is slightly below the allowable stress normally used for the flange steel can be applied and the bending stress in the web need not be checked. The shear stress in the web, however, must be limited to the normal allowable stress for the web steel.

In 1969, Lew, Natarajan, and Toprac[23] studied the static behavior of hybrid plate girders comprised of A514 steel flange and A36 steel webs. The minimum yield point of A514 steel is 100 ksi and is 36 ksi for A36 steel. The test program included eleven bending tests, two shear tests and one combined bending and shear test. Three of the bending specimens had one-sided longitudinal stiffeners placed at the upper fifth point of the web.

From the test results, they found that the strain distributions in the compression partion of the web were considerably less than the predicted by beam theory. The reduction of strains in the web causes a redistribution of compressive stresses from the web to the compression flange. However, the strain distributions indicated no significant increase in strains in the compression flange although a definite reduction in the web strain was present. This difference in the flange-strain distributions can be explained from the fact that a portion of the total moment resisted by the flanges in hybrid girder cross sections is considerably larger than the portion resisted by the flanges of homogeneous girders. They also found that hybrid girders having slender webs subjected to a constant moment may fail in vertical buckling of the compression flange prior to general yielding in the flange. The ultimate strength was not significantly increased by the use of longitudinal stiffeners. Nor did such stiffeners prevent the vertical buckling of the compression flange.

III. EXPERIMENTAL INVESTIGATION

A. GENERAL

The recent research project sponsored by the American Iron and Steel Institute (AISI) at University of Missouri-Rolla has been concentrated on a study of the effect of strain rate on mechanical properties of sheet steels and the structural behavior and strength of cold-formed steel hybrid members fabricated from two different materials subjected to dynamic loads. The materials used in this phase of the study were 25AK and 50SK sheet steels with nominal yield strengths of 25 and 50 ksi, respectively. A total of 72 hat-shaped beams were fabricated from these two materials. These specimens were cold-formed to shape by Rose Metal Products Inc. in Springfield, Missouri.

The configurations of beam specimens are shown in Figure 3.1. The designation of test specimens is presented in Table 3.1. As shown in Figure 3.2, four groups of test specimens were used in this investigation:

(1) Group W - hat-shaped beams which were assembled by using a hat section fabricated from 25AK sheet steel and a plate of 50SK sheet steel. The stiffened flange of the hat section was in compression.

(2) Group Z - hat-shaped beams which were assembled by using a hat section fabricated from 25AK sheet steel and a plate of 50SK sheet steel. The stiffened flange of the hat section was in tension.

(3) Group S - hat-shaped beams which were assembled by using a hat section fabricated from 50SK sheet steel and a plate of 25AK sheet steel. The stiffened flange of the hat section was in compression.

(4) Group K - hat-shaped beams which were assembled by using a hat section fabricated from 50SK sheet steel and a plate of 25AK sheet steel. The stiffened flange of the hat section was in tension.

Tables 3.2 through 3.5 list the specimen number, test speed, strain rate, and width-to-thickness ratio (w/t) of each individual test specimen. The selected strain rates used in the tests were 10^{-4}, 10^{-3}, and 10^{-2}. in./in./sec.. A total of 72 beam specimens were tested and are discussed in this report.

B. MATERIAL PROPERTIES

The sheet steels used to fabricate beam specimens were 25AK and 50SK. The mechanical properties of these two types of sheet steels were presented in the Seventeenth Progress Report[3]. Tables 3.6 and 3.7 summarize the average values of mechanical properties including yield strength (F_y) in tension and compression, proportional limit (F_{pr}), tensile strength (F_u), and elongation in 2-inch gage length for 25AK and 50SK sheet steels which were tested under different strain rates. The nominal thicknesses of the 25AK and 50SK sheet steels were 0.078 inch and 0.074 inch, respectively.

Figures 3.3 and 3.4 show comparisons of typical stress-strain relationships for the 25AK sheet steel subjected to longitudinal tension

and compression under four strain rates of 10^{-4}, 10^{-2}, 10^{-1}, and 1.0 in./in./sec.. The typical stress-strain relationships for 50SK sheet steel under tension and compression are shown in Figures 3.5 and 3.6. Based on the material test results, empirical equations were derived and presented in the Eighteenth Progress Report[2] and Reference 28 and 29. The compression yield strength and proportional limit obtained from the material tests were used to evaluate the strength of beam specimens.

C. BEAM TESTS

1. Specimens. Beam tests were used to study the local buckling and postbuckling strengths of compression elements. In order to investigate the behavior and strength of stiffened compression elements, the webs of hat-shaped beam specimens were designed to be fully effective without web buckling and crippling according to the AISI Specification for the Design of Cold-Formed Steel Structural Members[24].

As shown in Figure 3.7, a hat section and a plate were assembled by attaching the plate to the unstiffened flanges of the hat section to form a hat-shaped beam. All test specimens were fabricated by Rose Metal Company using spot welded connections. Spot welds of one-inch spacing were used on each unstiffened flange of hat sections for all beams regardless the lengths of specimens. Tables 3.8 through 3.11 give the lengths and dimensions of beam specimens fabricated from 25AK and 50SK sheet steels. For the specimens with the stiffened flange of hat section on the compression side, the w/t ratios of stiffened flanges ranged from 9.26 to 63.33 and from 24.78 to 69.69 for Group W and Group

S, respectively. For the specimens with the plate on the compression side, the w/t ratios of plates ranged from 25.61 to 82.49 and from 37.09 to 79.46 for Group Z and Group K, respectively. The dimension w for plates represents the distance between two spot welds, or w = BP-BL.

During the test, four-inch wide loading plates were used at the loading points (one-fourth of span length) for all specimens of Group Z and Group K, and the specimens with small w/t ratios of Group W and Group S as shown in Figure 3.8. Aluminum bars were attached to two sides of loading plates to prevent the loading plate from movement. For the specimens with medium and large w/t ratios of Group W and Group S, T-sections were connected to the beam webs at loading points to prevent web crippling failure as shown in Figure 3.9.

2. Strain Measurements. Six foil strain gages were used to measure strains at the midspan of beams for the specimens with small w/t ratios (case 1 of Groups W, Z, S, and K). The locations of strain gages, numbered from 1 to 6, are shown in Figure 3.10. For the beam specimens with medium and large w/t ratios, additional four strain gages were mounted along the longitudinal centerline of stiffened flange (Groups W and S) and stiffened plate (Groups Z and K). These two paired strain gages were placed at a distance equal to the overall width of the stiffened compression flange of hat sections for Groups W and S. For Groups Z and K, spacing of strain gages was equal to the plate width (BP) minus the unstiffened flange width (BL) on each side of the midspan of specimens. The arrangement of strain gages are shown in Figure 3.11.

The paired strain gages placed along the centerline of compression element of beams were used to determine the tested local buckling load by means of the modified strain reversal method, which is discussed in Reference 25. The strain gages placed along two sides of compression and tension elements at the midspan of beams were used to measure the tested yield and maximum strains of specimens.

3. Instrumentation and Test Procedure. All beam tests were performed by using the 880 Material Test System with a capacity of 110 kips located in the Engineering Research Laboratory at University of Missouri-Rolla. As shown in Figure 3.12, the MTS 880 automated test system consists of three components : the load frame, the control console, and the CAMAC (Computer Automated Measurement and Control) data acquisition. The main data acquisition module used in this system is a Kinetic System Model 4022 Transient Recorder. The unit has 64 simultaneously sampling input channels. The maximum rate to acquire test data for this unit is 25,000 sets of reading per second. For all tests, the maximum load range of 10 kips and the maximum stroke ranges of 2.5 or 1.0 inches were selected for the function generator of the test machine. The ramp time was programmed to have a constant speed in accordance with the calculated strain rate for each beam specimen.

The beam was simply supported and the load was applied from the lower compression platen to the specimen. C-shaped clamps were used in the tests to clamp both sides of beam specimens to 4-inch wide bearing plates. Two LVDT (Linear Variable Differential Transformer) were used at midspan to measure the beam deflections and to check any rotation of

beam specimens during the test. The applied load, actuator displacement, strains from 10 strain gage outputs, and the deflections from two LVDT outputs were recorded and stored in the CAMAC memory. After the data were acquired, it was downloaded to the Data General MV-10000 Computer for analysis purpose.

4. Test Results. The failure mode of the beam specimens varies with the width-to-thickness ratio of the compression stiffened flange (Groups W and S) and stiffened plate (Groups Z and K). The local buckling load was detected based on the load-strain diagram obtained from the paired strain gages attached back to back along the longitudinal centerline of the stiffened flange (Groups W and S) and stiffened plate (Groups Z and K). As shown in Figure 3.13, no local buckling occurred in specimens with small w/t ratios. Local buckling occurred in the elastic range for the specimens having large w/t ratios. After local buckling occurred in the test specimen, the stresses in the compression flange redistributed across the compression flange until edge stresses reached to the maximum. A typical failure pattern of the stiffened compression flange with a large w/t ratio under maximum load is shown in Figure 3.14. For the specimen having loacl buckled compression flange, the typical load-strain relationship is shown in Figure 3.15.

Three typical load-displacement relationships are shown in Figures 3.16 to 3.18 for Group W specimens with various w/t ratios tested under different strain rates. The average w/t ratios of stiffened compression flanges and the strain rates used in the tests are indicated in each

figure. Similarly, Figures 3.19 to 3.21 show typical load-displacement diagrams for Group Z specimens. Figures 3.22 to 3.24 and Figures 3.25 to 3.27 show the load-displacement diagrams for Group S specimens and Group K specimens, respectively. A constant speed was applied to the test specimen during the test. Because strain rate could not be retained constant after the yield moment was reached in the specimen, therefore, the value of strain rate was defined by a linear portion of the slope of the strain-time curve. A typical strain-time diagram is shown in Figure 3.28. The tested critical local buckling moment, yield moment, and ultimate moment for each beam specimen are evaluated and presented in Chapter IV.

IV. EVALUATION OF EXPERIMENTAL DATA

A. GENERAL

Hat-shaped beam specimens fabricated from two different sheet steels (25AK and 50SK) were tested to study the postbuckling strength of stiffened compression elements subjected to dynamic loads. The width-to-thickness ratio of stiffened elements controls the failure mode of the beam. In the previous phase of study[4], two types of hybrid stub column specimens, box-shaped and hat-shaped stub columns, fabricated from 25AK and 50SK sheet steels were tested under different strain rates to study the behavior of stiffened compression elements. It was concluded that the predicted ultimate loads of stub columns can be improved by using the dynamic yield stresses. The present phase of research was concentrated on a study of the structural strength of hybrid beams using two different sheet steels. Since the material properties and stress-strain relationships can be influenced by strain rate, comparisons between the experimental results and the ultimate loads predicted by the current AISI Automotive Steel Design Manual[1] using dynamic material properties are presented in this chapter.

All beam specimens were subjected to pure moments between two loading points located at one-fourth of span length from end supports. The uniformly distributed weight of tested beam specimen and the cross beam placed on the top of the specimen are light enough (approximately 80 lbs.) to be neglected in the evaluation of the test results. The dynamic yield stresses obtained from material tests was used for

calculating the critical local buckling moment (M_{cr}), the yield moment (M_y), and the ultimate moment (M_u) for all beam specimens.

B. CRITICAL LOCAL BUCKLING MOMENTS

The compression element of beam specimens may buckle locally in the elastic or inelastic range, depending on the w/t ratio of the compression element. The elastic critical local buckling stress, $(f_{cr})_E$, of stiffened compression elements subjected to a uniform compression can be calculated by using the following equation which is derived from Bryan's differential equation based on small deflection:

$$(f_{cr})_E = \frac{k\pi^2 E}{12(1-\mu^2)(w/t)^2} \tag{4.1}$$

Where E = modulus of elasticity

μ = Poisson's ratio = 0.3 for steel

k = buckling coefficient

t = thickness of element

w = width of element

The buckling coefficient used in Equation 4.1 is equal to 4.0 for stiffened compression elements supported along both longitudinal edges. If the elastic critical buckling stress exceeds the proportional limit, the compression element buckles in the inelastic range. Therefore, the concept of tangent modulus[26] can be applied to calculate the inelastic buckling stress, $(f_{cr})_I$, by using Equation 4.2.

$$(f_{cr})_I = F_y - \frac{F_{pr}(F_y - F_{pr})}{(f_{cr})_E} \tag{4.2}$$

Where F_y = compressive yield stress of steel

F_{pr} = proportional limit of steel

$(f_{cr})_E$ = elastic critical local buckling stress

The above equation is applicable for the stress between the proportional limit and yield stress. Once the critical local buckling stress ($(f_{cr})_E$ or $(f_{cr})_I$) was calculated, the computed critical local buckling moment of a homogeneous beam corresponding to the initiation of local buckling of its controlling compression element can be calculated as follows:

$$M_{cr} = S_x f_{cr} \tag{4.3}$$

Where S_x = elastic section modulus of the full cross section relative to the compression element

f_{cr} = critical local buckling stress

Based on the dimensions of full cross section of a beam and the mechanical properties of sheet steel, the critical local buckling loads of a homogeneous beam can be obtained according to the equation shown above. However, Equation 4.3 does not apply directly to hybrid beams fabricated from two different sheet steels because it is based on the assumption that the beam is homogeneous. To deal with the nonhomogeneous beam, the critical local buckling stress of a compression element of beam specimens needs to be calculated differently. The computed critical local buckling moment of a hybrid beam corresponding to the initiation of local buckling of its controlling compression element can be calculated by using the following steps:

(1) The section is subdivided into a number of elements (a total of 12 segments were used in the calculation as shown in Figure 4.1).

(2) A position of the neutral axis is assumed and the strain in the top fiber is computed based on the critical local buckling stress. According to these two values, the average strains in various elements are calculated.

(3) From the tested stress-strain relationships derived from material tests (Equations 4.4 through 4.6), the average stresses (σ) in various elements corresponding to such computed strains are found.

(4) Compute the area (A) for each element.

(5) The neutral axis can be obtained by iteration based on the condition $\Sigma A\sigma = 0$.

(6) The computed critical local buckling moment of a hybrid beam can be calculated by multiplying the force ($A\sigma$) and the distance for each element and summing up these values ($\Sigma A\sigma y$), in which y is the distance measured from the neutral axis to the centroid of each element.

The types of stress-strain relationship for 25AK and 50SK sheet steels are different. The stress-strain relationship for 25AK sheet steel is the gradual-yielding type. It is the sharp-yielding type for 50SK sheet steel. Therefore, in order to obtain the stresses for each element from the calculated strains, the following empirical equations were derived from material tests and used to compute the stresses for 25AK and 50SK sheet steels under different strain rates:

For 25AK sheet steel $$\sigma = A + \frac{B}{\varepsilon} + \frac{C}{\varepsilon^2} \tag{4.4}$$

For 50SK sheet steel $$\sigma = D + E\varepsilon + F\varepsilon^2 \tag{4.5}$$

where σ = compressive stress from proportional limit to yield point

ε = compressive strain from proportional limit to yield point

when strain rate = 10^{-4} in./in./sec.:

A = 23.64 B = -0.525 C = -0.008

D = 1.403 E = 334.7 F = -454.7

$(\varepsilon_{pr})_{25AK}$ = 0.00081 in./in. $(\varepsilon_{y})_{25AK}$ = 0.00275 in./in.

$(\varepsilon_{pr})_{50SK}$ = 0.00153 in./in. $(\varepsilon_{y})_{50SK}$ = 0.00222 in./in.

when strain rate = 10^{-3} in./in./sec.:

A = 24.17 B = -0.137 C = -0.044

D = 1.378 E = 331.7 F = -431.2

$(\varepsilon_{pr})_{25AK}$ = 0.00094 in./in. $(\varepsilon_{y})_{25AK}$ = 0.00290 in./in.

$(\varepsilon_{pr})_{50SK}$ = 0.00154 in./in. $(\varepsilon_{y})_{50SK}$ = 0.00228 in./in.

when strain rate = 10^{-2} in./in./sec.:

A = 24.71 B = 0.251 C = -0.080

D = 1.350 E = 328.6 F = -407.6

$(\varepsilon_{pr})_{25AK}$ = 0.00102 in./in. $(\varepsilon_{y})_{25AK}$ = 0.00316 in./in.

$(\varepsilon_{pr})_{50SK}$ = 0.00155 in./in. $(\varepsilon_{y})_{50SK}$ = 0.00234 in./in.

The strains used for calculating the stresses in the above equations were selected from the proportional limit to the yield point of steel. The values of ε_{pr} and ε_{y} represent the strains at the proportion limit and yield point, respectively. For the stresses beyond the yield point of the material, the following empirical equations were derived from material tests for the stress-strain relationships of 25AK sheet steel :

$$\sigma = a + b\varepsilon + \frac{c}{\varepsilon} \tag{4.6}$$

where σ = compressive stress beyond the yield point

ε = compressive strain beyond the yield point

when strain rate = 10^{-4} in./in./sec.:

for strain from the yield strain to 0.02 in./in.

a = 21.59 b = 3.454 c = -0.249

for strain from 0.02 to 0.05 in./in.

a = 28.66 b = 1.207 c = -5.400

when strain rate = 10^{-3} in./in./sec.:

for strain from the yield strain to 0.02 in./in.

a = 22.89 b = 3.481 c = -0.218

for strain from 0.02 to 0.05 in./in.

a = 30.38 b = 1.139 c = -5.831

when strain rate = 10^{-2} in./in./sec.:

for strain from the yield strain to 0.02 in./in.

a = 24.20 b = 3.509 c = -0.188

for strain from 0.02 to 0.05 in./in.

a = 32.11 b = 1.070 c = -6.261

Since 50SK sheet steel is a sharp-yielding type of material, the stress beyond the yield point is assumed to be equal to the value of yield point.

From Equations 4.4 and 4.5, it can be seen that these two empirical equations derived from material tests were used to compute the stress from proportional limit to yield point for 25AK and 50SK sheet steels, and Equation 4.6 which is used to compute the stress beyond the yield point for 25AK sheet steel is quite different from Equation 4.4. For

the practical purpose, it is better to find a simplified equation to represent the stress-strain relationship for both materials. According to Reference 30, a constitutive equation is given by

$$\sigma = K\varepsilon^{n}\dot{\varepsilon}^{m} \tag{4.7}$$

where k = constant

m = strain rate hardening exponent

n = strain hardening exponent

The symbols σ and ε shown in Equation 4.7 represent the true stress and true strain, respectively. However, the engineering stress and strain derived from material tests were adopted in the calculation of structural strength of hybrid beams in this report. Extended study is needed to find out whether or not Equation 4.7 gives a better fit than Equations 4.4 through 4.6.

The tested critical local buckling moments of beam specimens were determined from the product of the bending arm (L/4) and one half of the tested critical local buckling load ($P_{cr}/2$) as follows:

$$(M_{cr})_{test} = \frac{P_{cr}L}{8} \tag{4.8}$$

where P_{cr} = tested critical local buckling load

L = span length of beam specimen

The predicted and tested critical local buckling moments are presented in Tables 4.1 and 4.2 for the beam specimens, for which the hat sections were fabricated from 25AK sheet steel and the plates were

fabricated from 50SK sheet steel (Groups W and Z). In Tables 4.3 and 4.4, the hat section of the beam specimens were fabricated from 50SK sheet steel and the plates were fabricated from 25AK sheet steel (Groups S and K). On the basis of dynamic material properties, the predicted critical local buckling stresses and moments are shown in columns (2) and (4) of Tables 4.1 through 4.4, respectively. The tested critical local buckling loads listed in column (3) of these tables were determined from load-strain relationships by using the modified strain reversal method[25]. Based on the tested critical local buckling loads, the tested critical local buckling moments were obtained by applying Equation 4.8 and listed in column (5) of these tables.

From the tested load-strain relationships of beam specimens, it can be observed that no local buckling occurred in each group of specimens with small w/t ratios. For Groups W and K specimens, no buckling was observed even for the beams with medium w/t ratios, for which the 25AK steel was in compression. Comparisons of the computed and tested critical local buckling moments are listed in column (6) of these tables. The mean values of $(M_{cr})_{test}/(M_{cr})_{comp}$ ratios from Tables 4.1 through 4.4 seem to indicate that a good agreement can be achieved between the tested and computed critical local buckling moments. It is also noted that the number of half-sine waves developed in the stiffened compression elements of the specimens having large w/t ratios is the same for the same specimens regardless of the strain rate used for the

C. YIELD MOMENT

According to the AISI Manual[1] and Specification[24], two methods can be used to calculate the section strength of beams. One is based on the initiation of yielding using the effective section and the other is based on the inelastic reserve capacity. In these methods, it is assumed that the beam reaches its yield moment when the maximum edge stress in the extreme fiber reaches the yield stress of steel. In addition, the compression elements of thin-walled structural members with relatively large w/t ratios can continue to carry additional loads after the attainment of elastic buckling. However, the stresses in the compression elements will redistribute until the stresses along the supported edges reach the yield stress of steel. For design purpose, the concept of the effective width design can be used to calculate the effective section properties. According to the AISI Automotive Steel Design Manual[1], the effective design width of compression elements can be used for determining the load-carrying capacity of the member when the slenderness factor λ computed according to Equation 4.9 exceeds a value of 0.673.

$$\lambda = 1.052\left(\frac{w}{t}\right)\frac{\sqrt{f/E}}{\sqrt{k}} \tag{4.9}$$

where f = stress in the element

E = modulus of elasticity of the steel, 29500 ksi

k = buckling coefficient for the flat plate

w = flat width of the element

t = thickness of the element

Equation 4.9 is valid for materials with yield strengths up to F_y = 80 ksi. For the stiffened compression elements with a yield strength higher than 80 ksi, Reference 27 suggests that a reduced yield strength be substituted for the limiting value of f in Equation 4.9 and in all subsequent calculations to determine the bending capacity of the member. The reduced yield strength for a stiffened compression element, F_{yrs}, is obtained as follows:

$$F_{yrs} = \left(1.0 - 0.2\sqrt{\frac{w}{t}}\sqrt{\frac{F_y}{E}}\right)F_y \qquad (4.10)$$

The above expression was obtained from the tests with w/t ratios ranging from 18 to 137. F_y values ranged from 84 to 153 ksi, and $\sqrt{w/t}\sqrt{F_y/E}$ values varied from 0.27 to 0.84.

When λ = 0.673, the limiting width-to-thickness ratio (at which full capacity is achievable) can be evaluated as

$$\left[\frac{w}{t}\right]_{\lim} = 0.64\sqrt{\frac{kE}{f}} \qquad (4.11)$$

For fully stiffened compression elements under a uniform stress, k = 4. Equation 4.11 gives a limiting w/t value as follows:

$$\left[\frac{w}{t}\right]_{\lim} = S = 1.28\sqrt{\frac{E}{f}} \qquad (4.12)$$

When the w/t ratio exceeds the values of S, the effective width, b, is less than the actual width w. For the purpose of calculating the sectional properties, the effective width is divided into two equal parts and each half is positioned adjacent to the longitudinal support. Thus, the width (w-b) is considered to be removed at the center of the flat width when evaluating the section properties. The effective width b can be calculated from the 1991 AISI Automotive Steel Design Manual[1] given in Equation 4.13:

$$b = w\left(\frac{1-0.22/\lambda}{\lambda}\right) \tag{4.13}$$

Based on the initiation of yielding, the computed yield moment $(M_y)_{comp}$ of a homogeneous beam can be calculated by using the following equation:

$$\left(M_y\right)_{comp} = F_y S_e \tag{4.14}$$

where F_y = yield stress of steel

S_e = elastic section modulus of effective section

It should be noted that Equation 4.14 is valid only for the beams fabricated from one material because it is based on the assumption that the material is homogeneous. The same procedure used for calculating the critical local buckling moment was adopted for the calculation of the load-carrying capacity of beams fabricated from two different sheet steels. Based on this approach, the yield moment of the hybrid beam can be estimated by assuming that the strains of plane sections in the beam varied directly with their distance from the neutral axis.

Two similar steps were used to determine the yield moment of the hybrid beams:

(I) For the case of initiation of yielding occurring in the top compression flange of the beam such as cases A, B, and C of Groups W and S, and case C of Group Z, the yield moment can be computed by the following steps:

(1) The section is subdivided into a number of elements (a total of 12 segments were used in the calculation as shown in Figure 4.1).

(2) A position of the neutral axis is assumed and the strain in the top fiber of the compression flange is assumed to be the yield strain of the steel. According to these two values, the average strains in various elements are calculated.

(3) From the tested stress-strain relationships obtained from material tests, the average stresses σ in various elements corresponding to such computed strains are found.

(4) Calculate the effective width of the compression flange according to the yield stress of the steel in the compression flange.

(5) Compute the area A, including the effective section of compression flange, for each element.

(6) The neutral axis can be obtained by iteration based on the condition $\Sigma A\sigma=0$.

(7) The computed yield moment of a hybrid beam can be calculated by multiplying the force ($A\sigma$) and the distance for each element

and summing up these values ($\Sigma A\sigma y$), in which y is the distance measured from the neutral axis to the centroid of each element.

(II) For the case of initiation of yielding occurring in the bottom tension flange of the beam such as cases A, B, and C of Groups K and cases A and B of Group Z, the computed yield moment can be obtained by using the same steps discussed previously for the initiation of yielding occurred in the top compression flange except that steps (2) and (4) are changed as follows:

* A position of the neutral axis is assumed and the strain in the bottom fiber of the tension flange is assumed to be the yield strain of the steel. According to these two values, the average strains in various elements are calculated.
* Calculate the effective width of the stiffened compression flange for the compression stress obtained from the yield strain of the steel in the tension flange and the assumed neutral axis.

The tested yield moments of beam specimens were determined from the product of bending arm (L/4) and one half of the yield load ($P_y/2$) as follows:

$$\left(M_y\right)_{test} = \frac{P_y L}{8} \tag{4.15}$$

The tested yield load (P_y) shown above was determined from the load-strain relationships for each individual specimen. The computed and tested yield moments are presented in Tables 4.5 and 4.6 for Groups W and Z specimens, for which the hat sections were fabricated from 25AK

sheet steel and the plates were fabricated from 50SK sheet steel. Tables 4.7 and 4.8 are for Groups S and K specimens, for which the hat sections were fabricated from 50SK sheet steel and the plates were fabricated from 25AK sheet steel. The computed yield moments listed in column (4) of these tables are based on the dynamic compressive yield stresses corresponding to the strain rates used in the tests. Tables 4.9 through 4.12 show the similar data for Groups W, Z, S, and K specimens except that the computed yield moments were calculated based on the dynamic tensile stresses. The computed yield moments were also calculated based on the dynamic compressive and tensile stresses, that is, the compressive stresses were calculated for the element above the neutral axis and the tensile stresses were calculated for the element below the neutral axis, as shown in Tables 4.13 through 4.16. The tested yield loads corresponding to the initiation of yielding are listed in column (3) of these tables, and the tested yield moments are listed in column (5) of these tables. It is noted from these tables that the tested yield moment increases with increasing strain rate for specimens having the similar w/t ratios.

Comparisons of the computed and tested yield moments are listed in column (6) of these tables. By observing the values of $(M_y)_{test}/(M_y)_{comp}$ ratios, it can be seen that the difference between the tested and predicted yield moments is within 10 percent for most specimens. It is noted that the values of $(M_y)_{test}/(M_y)_{comp}$ ratios are quite close for the same case of beam specimens having similar dimensions but tested under different strain rates. Therefore, it seems

that the dynamic material properties factor can be considered in the calculation of yield moment of hybrid beams.

It was also observed from these tables that the ratios of tested-to-computed yield moments for case C of Groups W and Z specimens with large w/t ratios are slightly less than the values for cases A and B. There are two reasons to cause the discrepancies between the tested and computed values. One is because the imperfections of the compression elements with large w/t ratios may affect the strength of the specimen, and the other is because the strain gages used to measure the yield strains were not close to the edges of stiffened compression element and the local buckling occurred in the compression element may affect the readings of strain gages. The ratios of tested-to-computed yield moments for case A of Groups W and Z are larger than the values for cases B and C. This is possibly due to the cold work of forming. It is also noted that the ratios of tested-to-computed yield moments for all cases of Group K are slightly less than the values for all cases of Group S, it is possibly due to the initial deformation of beam specimens which were caused by welding during the fabrication. The direction of initial deformation of entire beams is upward for Group S specimens and is downward for Group K specimens as shown in Figure 4.2. The initial deformation between the middle line and the end of beam specimens ranged from 0.05 to 0.25 in. depending on the length of beams. Similar observations were found for Groups W and Z specimens. However, by comparing the ratios of tested-to-computed yield moments, it seems that the influence of initial deformation on Groups W and Z specimens is not significant.

Tables 4.5 through 4.16 present the comparison of tested yield moments and computed yield moments calculated based on the stress-strain relationships (Figure 4.3) obtained from the material tests for different group specimens. Since the types of stress-strain relationships for these two sheet steels (25AK and 50SK) are different, in order to simplify the calculating procedure, the idealized stress-strain relationships were adopted to calculate the computed yield moments as shown in Figure 4.4. Table 4.17 shows the comparison of tested yield moments and computed values calculated on the basis of the idealized stress-strain relationships for Group W specimens. From column (6) of the table, it can be seen that the computed yield moment can not provide a good prediction as compared with Table 4.9. The use of idealized stress-strain relationships as given in Figure 4.4 would result in conservative yield moments particularily for the beams with small w/t ratios.

The procedures mentioned previously give the reasonable results for critical local buckling moment and yield moment of hybrid beams. However, this method can not be easily used to calculate the moment capacity of hybrid beams from the practical point of view. The equivalent section concept may be applied to deal with the hybrid beams. Because the tested beam specimens in this phase of study consist of four groups (Groups W, Z, S, and K) which were fabricated from two different sheet steels, the structural strength can be calculated by transforming these hybrid beams into the equivalent homogeneous beams. Future study can be used to verify the feasibility of equivalent section method.

D. ULTIMATE MOMENT

It is well known that flexural members may continuously carry additional moment after the attainment of yielding in the compression flange or tension flange of the member. The inelastic reserve capacity of flexural members, which allows partial plastification of a cross section, is recognized in the current AISI Automotive Steel Design Manual[1]. It can be used to predict the ultimate moments of flexural members provided that such members satisfy the specific requirements. Even though the ultimate bending strengths of hat sections or track sections may be calculated on the basis of the inelastic reserve capacity, however, the design procedures recommended in the AISI Manual[1] can not be used to compute the ultimate flexural strength for the specimens studied in this investigation, because the tested specimens were fabricated from two different sheet steels with different types of stress-strain curves, see Figure 4.3.

Table 4.18 lists the average ratios of the tested ultimate moment to tested yield moment for Groups W and S specimens with stiffened flanges of the hat sections on the compression side. Table 4.19 lists the similar data for Groups Z and K specimens with stiffened plate on the compression side. It should be noted that all values listed in Tables 4.18 and 4.19 are the average of six tests using the specimens with similar w/t ratios. From these two tables it can be seen that the ratio of the tested ultimate moment to tested yield moment decreases with increasing w/t ratio. It was found that the reducing rate for

Group W and Group S specimens are quite similar. Similar results were found for Group Z and Group K specimens.

The tested ultimate moments of beam specimens were determined from the product of bending arm (L/4) and one half of the ultimate load ($P_u/2$) as follows:

$$(M_u)_{test} = \frac{P_u L}{8} \tag{4.16}$$

It was observed from the tests that the deflection of the beam specimen under the ultimate load is quite large comparing with the deflection under yield load particularily for Group Z and K specimens. Because the strains on the extreme compression and tension fibers are different depending on the section configuration and the material composition of a hybrid beam, the smaller strain (either compressive strain or tensile strain) under the tested ultimate load was chosen to be the reference strain for each individual beam specimen. By using the reference strain and the same procedure for computing the yield moment (page 32), the ultimate moments were calculated. Figures 4.5 and 4.6 show the stress and strain diagrams for the typical cross sections of Groups W and Z specimens, respectively. Similar plots are shown in Figures 4.7 and 4.8 for Groups S and K specimens.

The comparisons of the tested and computed ultimate moments for Groups W and Z specimens are presented in Tables 4.20 and 4.21, respectively. Tables 4.22 and 4.23 present the similar data for Groups S and K specimens. The computed ultimate moments are listed in column

(4) of Tables 4.20 through 4.23, and the tested ultimate moments calculated according to Equation 4.16 are listed in column (5). In these tables, the computed yield moments listed in column (2) are based on the procedure reported in Section C of this chapter with dynamic material properties corresponding to the actual strain rate used in the tests. It is noted from Tables 4.20 through 4.23 that the tested ultimate moment increases with increasing strain rate for specimens having the similar w/t ratios.

The tested and predicted ultimate moments are compared in column (6) of Tables 4.20 through 4.23. The mean value of the (Mu)test/(Mu)comp ratios for Groups W and Z specimens are 1.090 and 0.997 with standard deviations of 0.098 and 0.065, respectively. The mean values and standard deviations of the (Mu)test/(Mu)comp ratios are (0.935 and 0.040) for Group S specimens and (0.924 and 0.033) for Group K specimens. It can be seen that the difference between the tested and predicted ultimate moments is within 10 percent for most specimens. Tables 4.24 through 4.27 present the measured deflections under yield moments and ultimate moments for Groups W, Z, S, and K. It can be seen from these tables that the deflections under ultimate moments are larger than the deflections under yield moments except for the case C of Group W specimens. It is also noted that the measured deflections under yield moments are between Length/50 and Length/100.

V. CONCLUSIONS

In order to investigate the effect of strain rate on the structural strength of cold-formed steel hybrid sections, and to study the postbuckling strength of stiffened compression elements, four groups of beam specimens were tested under different strain rates. The materials used in the fabrication of hybrid beams were 25AK and 50SK sheet steels. A total of 72 hat-shaped beams were tested in this phase of study. Based on the available test results, the following conclusions can be drawn for the hybrid beams fabricated from 25AK and 50SK sheet steels:

1. For most cases, the yield moment and ultimate moment of hybrid beams increase with increasing strain rate for specimens having the similar w/t ratios.
2. The differences between the tested and computed yield moments is within 10 percent for most specimens. It seems that the dynamic material properties can be used for the calculation of yield moment of hybrid beams.
3. The computed yield moments calculated based on the dynamic tensile stresses are less conservative than those calculated on the basis of the dynamic compressive stresses.
4. The initial out-of-straightness of beam specimens caused by welding during the fabrication may affect the strength of hybrid beams.
5. The procedures listed in Chapter IV give the reasonable results for the critical local buckling moment, yield moment, and ultimate moment of hybrid beams.
6. The computed yield moment calculated on the basis of the actual stress-strain relationships (Figure 4.3) can provide a better

prediction than the value calculated from the idealized stress-strain relationship (Figure 4.4). The difference was found to be approximately 27 percent.

7. Same as the computed yield moment, the dynamic stress-strain relationship can be used for calculating the ultimate moment of hybrid beams, however, the measured strain under the ultimate load is needed for computing the ultimate moment of hybrid beams.
8. The effective cross-sectional area determined according to AISI Design Manual[1] can also be employed in the calculation of yield moment and ultimate moment for hybrid sections.
9. For hybrid beams fabricated from the gradual-yielding type of material, the calculation of ultimate moments may use a stress higher than the yield point in order to consider the inelastic reserve capacity.

In summary, the yield moment and ultimate moment of cold-formed steel hybrid beams increase with increasing strain rates. The dynamic stress-strain relationship can be used in the calculation of yield moment and ultimate moment of hybrid beams. The procedures discussed in Chapter IV can provide a reasonable approach for calculating the critical local buckling moment, the yield moment, and the ultimate moment for hybrid beams. For the same group of specimens, the ratios of tested ultimate moment to tested yield moment for the beams with small w/t ratios are much larger than those beams with large w/t ratios. The same is true for the values of $(d)_{mu}/(d)_{my}$ ratios. Because of the complexity for the calculation of ultimate moment and the excessive deflection, it is suggested that for the practical design, the yield

moment be used for the load-carrying capacity of hybrid beams. This approach is particularly appropriate for the beams having medium and large w/t ratios. Future beam tests can be used to verify and improve the findings.

ACKNOWLEDGMENTS

The research work reported herein was conducted in the Department of Civil Engineering at the University of Missouri-Rolla under the sponsorship of the American Iron and Steel Institute.

The financial assistance granted by the Institute and the technical guidance provided by members of the AISI Task Force on Automotive Structural Design and the AISI Automotive Applications Committee and the AISI staff (S.J. Errera, D.C. Martin, and L.A. Rysdrop) are gratefully acknowledged. Members of the Task Force are: Messrs. G.A. Beecher, J. Borchelt, T. Khalil, R.W. Lautensleger, H.F. Mahmood, D. Malen, E.C. Oren (chairperson), M.Y. Sheh, and M.T. Vecchio. Former members of the Task Force included Messrs. C. Haddad, C.M. Kim, J.G. Schroth, and T.N. Seel.

All materials used in the experimental study were donated by Inland Steel Company and National Steel Corporation.

Appreciation is also expressed to J. Bradshaw, J. McCracken, and S. Gabel, staff of the Department of Civil Engineering, for their technical support and to Mr. D. Morris for his valuable assistance in the preparation and performance of the tests.

REFERENCES

1. American Iron and Steel Institute, "Automotive Steel Design Manual," 1986 Edition, Revision 4.1 - August 1993.

2. Pan, C.L. and W.W. Yu, "Design of Automotive Structural Components Using High Strength Sheet Steels: Influence of Strain Rate on the Mechanical Properties of Sheet Steels and Structural Performance of Cold-Formed Steel Members," Eighteenth Progress Report, Civil Engineering Study 92-3, University of Missouri-Rolla, Dec., 1992.

3. Pan, C.L. and W.W. Yu, "Design of Automotive Structural Components Using High Strength Sheet Steels: Mechanical Properties of Materials," Seventeenth Progress Report, Civil Engineering Study 92-2, University of Missouri-Rolla, May, 1992.

4. Pan, C.L. and W.W. Yu, "Design of Automotive Structural Components Using High Strength Sheet Steels: Effect of Strain Rate on the Structural Strength and Crushing Behavior of Cold-Formed Steel Stub Columns," Nineteenth Progress Report, Civil Engineering Study 93-1, University of Missouri-Rolla, July, 1993.

5. Parkes, E.W., "The Permanent Deformation of a Cantilevel Struck Transversely at Its Tip," Proceeding of the Royal Society, London, England, Series A, Vol. 228, 1955, p.462.

6. Parkes, E.W., "The Permanent Deformation of an Encastre Beam Struck Transversely at any Point in Its Span," Proc. Inst. Civil Eng., July 1958.

7. Ezra, A.A., "The Plastic Response of a Simply Supported Beam to Impact Load at the Center," Proc. III U.S. Nat. Cong. Appl. Mech., 1958.

8. Ting, T.C.T. and P.S. Symonds, "Impact of a Cantilevel Beam with Strain Rate Sensitivity," Proceeding of Fourth U.S. National Congress of Apllied Mechanics, 1962.

9. Bonder, S.R. and P.S. Symonds, "Experimental and Theoretical Investigation of the Plastic Deformation of Cantilevel Beams Subjected to Impulsive Loading," Journal of Applied Mechanics, Volume 29., December 1962.

10. Rawlings, B., "The Dynamic Behavior of Steel in Pure Flexure," Proceeding of Royal Society, Series A, Volume 275, 1963.

11. Ting, T.C.T., "Large Deformation of a Rigid-Ideally-Plastic Cantilevel Beam," Journal of Applied Mechanics, June 1965.

12. Florence, A.L. and R.D. Firth, "Rigid-Plastic Beams under Uniformly Distributed Impulses," Journal of Applied Mechanics, Volume 32, 1965, p.481.

13. Jones, N., "Influence of Strain-Hardening and Strain-Rate Sensitivity on the Permanent Deformation of Impulsively Loaded Rigid-Plastic Beam," Int. J. Mech. Sci., Volume 9, 1967, p.777.

14. Aspden, R.J. and J.D. Campbell, "The Effect of Loading Rate on the Elasto-Plastic Flexure of Steel Beams," Proceedings of Royal Society, Volume A290, 1966.

15. Culver, C.G., E.A. Zanoni, and A.H. Osgood, "Response of Thin-Walled Beams to Impact Loading," Proceedings of the First Specialty Conference on Cold-Formed Steel Structures, University of Missouri-Rolla, August 1971.

16. Symonds, P.S. and N. Jones, "Impulsive Loading of Fully Clamped Beams with Finite Plastic Deflection and Strain-Rate Sensitivity," Int. J. Mech. Sci., Volume 14, 1972.

17. Forrestal, M.J. and M.J. Sagartz, "Elastic-Plastic Response of 304 Stainless Steel Beams to Impulse Loads," Journal of Applied Mechanics, Volume 45., September 1978.

18. Forrestal, M.J. and D.L. Wesenberg, "Elastic Plastic Response of Simply Supported 1018 Steel Beams to Impulse Loads," Journal of Applied Mechanics, December 1977.

19. Kassar, M, "Effect of Strain Rate on Material Properties of Sheet Steels and Structural Strengths of Cold-Formed Steel Members," Ph.D. Thesis, Also Published as "Design of Automotive Structural Components Using High Strength Sheet Steels: Effect of Strain Rate on Material Properties of Sheet Steels and Structural Strengths of Cold-Formed Steel Members," Fourteenth Progress Report, Civil Engineering Study 90-2, University of Missouri-Rolla, May, 1990.

20. Geerhard Haaijer, "Economy of High Strength Steel Structural Members," Journal of Structural Division, Proceeding of the American Society of Civil Engineers, Vol. 128, 1963.

21. Frost, R.W. and C.G. Schilling, "Behavior of Hybrid Beams Subjected to Static Loads," Journal of Structural Division, Proceeding of the American Society of Civil Engineers, Vol. 90, No. ST3, 1964.

22. Report of the Subcommittee on Hybrid Beams and Girders, Joint ASCE-AASHO Committee on Flexural Members, "Design of Hybrid Steel Beams," Journal of Structural Division, Proceeding of the American Society of Civil Engineers, Vol. 94, No. ST6, 1968.

23. Lew, H.S., M. Natarajan, A.A. Toprac, "Static Tests on Hybrid Plate Girders," Welding Research Supplement, Welding Journal, Vol. 48, No. 2, Feb 1969.

24. American Iron and Institute, "Specification for the Design of Cold-Formed Steel Structural Members," Cold-Formed Steel Design Manual, Pare I, 1986 Edition with the 1989 Addendum.

25. Johnson, A.L. and G. Winter, "The Structural Performance of Austenitic Stainless Steel Members," Report No. 327, Cornell University, November 1966.

26. Bleich, F., Buckling Strength of Metal Structures, New York: Mcgraw-Hill Book Company, 1952.

27. Pan, L.C., "Effective Design Widths of High Strength Cold-Formed Steel Members," Ph.D. Thesis, University of Missouri-Rolla, 1987.

28. Pan, C.L. and W.W. Yu, "Influence of Strain Rate on the Structural Strength of Cold-Formed Steel Automotive Components," Proceeding of International Body Engineering Conference, edited by M. Nasim Uddin, September 1993.

29. Pan, C.L., W.W. Yu, B.C. Schell, and M.Y. Sheh, "Effect of Strain Rate on the Structural Strength and Crushing Behavior of Hybrid Stub Columns," Proceeding of International Body Engineering Conference, edited by M. Nasim Uddin, September 1994.

30. Keeler, S.P., "Automotive Sheet Metal Formability," Report SG 79-1, American Iron and Steel Institute, July 1979.

Table 3.1

Designation of Beam Specimens Used in This Study

1st Digit	1st Letter	2nd Digit	2nd Letter	3rd Letter
Test Type	w/t Ratio (Case)	Strain-Rate (in./in./sec.)	Test No.	Section Type (Group)
3: Beam Test	A: Small	0: 0.0001	A: 1st Test	W:Hat Sec.-25AK Plate -50SK
	B: Medium	1: 0.001	B: 2nd Test	Z:Hat Sec.-25AK Plate -50SK
	C: Large	2: 0.01		S:Hat Sec.-50SK Plate -25AK
				K:Hat Sec.-50SK Plate -25AK

Note: (1) For the specimens with the section types of "W" or "S", the stiffened plate is tested on the tension side.

(2) For the specimens with the section types of "Z" or "K", the stiffened plate is tested on the compression side.

(3) See Figure 3.2

Table 3.2

Number of Performed Beam Tests
Hat-Shaped Specimens Assembled from Hat Section
(25AK Sheet Steel) and Plate (50SK Sheet Steel)
Beam Specimen - **Group W**

Spec.	Test Speed (in./min.)	Strain Rate (in./in./sec.)	w/t (25AK)	w/t (50SK)	No. of Tests Performed
3A1AW	0.010	0.0001	9.33	25.57	1
3A1BW	0.010	0.0001	9.26	25.64	1
3A2AW	0.100	0.001	9.35	25.55	1
3A2BW	0.100	0.001	9.63	25.58	1
3A3AW	1.000	0.01	9.30	25.69	1
3A3BW	1.000	0.01	9.51	25.76	1
3B1AW	0.0125	0.0001	28.56	46.07	1
3B1BW	0.0125	0.0001	28.70	45.76	1
3B2AW	0.125	0.001	28.72	45.93	1
3B2BW	0.125	0.001	28.83	46.18	1
3B3AW	1.250	0.01	28.60	45.82	1
3B3BW	1.250	0.01	28.62	45.93	1
3C1AW	0.0167	0.0001	63.28	82.42	1
3C1BW	0.0167	0.0001	63.29	82.43	1
3C2AW	0.167	0.001	63.25	82.35	1
3C2BW	0.167	0.001	63.21	82.24	1
3C3AW	1.670	0.01	63.30	82.46	1
3C3BW	1.670	0.01	63.33	82.39	1
Subtotal					18

Table 3.3

Number of Performed Beam Tests
Hat-Shaped Specimens Assembled from Hat Section
(25AK Sheet Steel) and Plate (50SK Sheet Steel)
Beam Specimen - **Group Z**

Spec.	Test Speed (in./min.)	Strain Rate (in./in./sec.)	w/t (25AK)	w/t (50SK)	No. of Tests Performed
3A1AZ	0.010	0.0001	9.30	25.62	1
3A1BZ	0.010	0.0001	9.26	25.61	1
3A2AZ	0.100	0.001	9.29	25.73	1
3A2BZ	0.100	0.001	9.37	25.66	1
3A3AZ	1.000	0.01	9.53	25.65	1
3A3BZ	1.000	0.01	9.31	25.74	1
3B1AZ	0.0125	0.0001	28.48	45.95	1
3B1BZ	0.0125	0.0001	28.62	45.89	1
3B2AZ	0.125	0.001	28.66	45.73	1
3B2BZ	0.125	0.001	28.53	45.82	1
3B3AZ	1.250	0.01	28.65	45.73	1
3B3BZ	1.250	0.01	28.60	45.78	1
3C1AZ	0.0167	0.0001	63.29	82.32	1
3C1BZ	0.0167	0.0001	63.26	82.38	1
3C2AZ	0.167	0.001	63.24	82.49	1
3C2BZ	0.167	0.001	63.17	82.11	1
3C3AZ	1.670	0.01	63.26	82.41	1
3C3BZ	1.670	0.01	63.24	82.35	1
Subtotal					18

Table 3.4

Number of Performed Beam Tests
Hat-Shaped Specimens Assembled from Hat Section
(50SK Sheet Steel) and Plate (25AK Sheet Steel)
Beam Specimen - **Group S**

Spec.	Test Speed (in./min.)	Strain Rate (in./in./sec.)	w/t (50SK)	w/t (25AK)	No. of Tests Performed
3A1AS	0.010	0.0001	24.83	37.50	1
3A1BS	0.010	0.0001	24.89	37.26	1
3A2AS	0.100	0.001	24.91	37.36	1
3A2BS	0.100	0.001	24.83	37.14	1
3A3AS	1.000	0.01	24.97	37.31	1
3A3BS	1.000	0.01	24.78	37.29	1
3B1AS	0.0125	0.0001	42.30	53.94	1
3B1BS	0.0125	0.0001	42.53	53.79	1
3B2AS	0.125	0.001	42.45	53.82	1
3B2BS	0.125	0.001	42.24	53.73	1
3B3AS	1.250	0.01	42.47	53.78	1
3B3BS	1.250	0.01	42.49	53.82	1
3C1AS	0.0167	0.0001	69.55	79.45	1
3C1BS	0.0167	0.0001	69.60	79.38	1
3C2AS	0.167	0.001	69.57	79.45	1
3C2BS	0.167	0.001	69.69	79.38	1
3C3AS	1.670	0.01	69.29	79.33	1
3C3BS	1.670	0.01	69.52	79.45	1
Subtotal					18

Table 3.5

Number of Performed Beam Tests
Hat-Shaped Specimens Assembled from Hat Section
(50SK Sheet Steel) and Plate (25AK Sheet Steel)
Beam Specimen - **Group K**

Spec.	Test Speed (in./min.)	Strain Rate (in./in./sec.)	w/t (50SK)	w/t (25AK)	No. of Tests Performed
3A1AK	0.010	0.0001	24.95	37.22	1
3A1BK	0.010	0.0001	24.76	37.21	1
3A2AK	0.100	0.001	24.89	37.28	1
3A2BK	0.100	0.001	24.67	37.09	1
3A3AK	1.000	0.01	24.86	37.29	1
3A3BK	1.000	0.01	24.83	37.21	1
3B1AK	0.0125	0.0001	42.33	53.74	1
3B1BK	0.0125	0.0001	42.26	53.81	1
3B2AK	0.125	0.001	42.28	53.74	1
3B2BK	0.125	0.001	42.14	53.74	1
3B3AK	1.250	0.01	42.43	53.76	1
3B3BK	1.250	0.01	42.40	53.82	1
3C1AK	0.0167	0.0001	69.34	79.42	1
3C1BK	0.0167	0.0001	69.53	79.40	1
3C2AK	0.167	0.001	69.30	79.28	1
3C2BK	0.167	0.001	69.53	79.46	1
3C3AK	1.670	0.01	69.68	79.45	1
3C3BK	1.670	0.01	69.60	79.46	1
Subtotal					18

Table 3.6

Average Mechanical Properties of 25AK Sheet Steel Used in the Experimental Study under Different Strain Rate

Strain Rate in./in./sec.	$(F_y)_c$ (ksi)	$(F_{pr})_c$ (ksi)	$(F_y)_t$ (ksi)	$(F_u)_t$ (ksi)	Elongation (%)
0.0001	21.66	15.93	24.60	42.76	-----
0.01	24.77	19.55	27.86	44.44	49.31
0.1	29.80	22.81	31.72	47.35	50.98
1.0	38.14	*****	35.13	51.25	58.18

Table 3.7

Average Mechanical Properties of 50SK Sheet Steel Used in the Experimental Study under Different Strain Rate

Strain Rate in./in./sec.	$(F_y)_c$ (ksi)	$(F_{pr})_c$ (ksi)	$(F_y)_t$ (ksi)	$(F_u)_t$ (ksi)	Elongation (%)
0.0001	53.55	41.89	54.97	67.07	36.09
0.01	55.91	42.46	56.83	68.98	33.04
0.1	56.96	44.36	58.06	71.04	34.45
1.0	59.41	*****	60.73	76.50	40.13

Note: (1) $(F_y)_c$ and $(F_{pr})_c$ are based on longitudinal compression coupon tests.
(2) $(F_y)_t$, $(F_u)_t$, and Elongation are determined from longitudinal tension coupon tests.
(3) Elongation was measured by using a 2-in. gage length.

Table 3.8

Dimensions of Hat-Shaped Beams Assembled from Hat Section (25AK Sheet Steel) and Plate (50SK Sheet Steel) Beam Specimens - **Group W**

(a) Dimensions of Hat Sections (25AK Sheet Steel)

Spec.	BF (in.)	BW (in.)	BL (in.)	t (in.)	w/t	Length (in.)
3A1AW	1.196	1.088	0.904	0.078	9.33	35.0
3A1BW	1.191	1.090	0.901	0.078	9.26	35.0
3A2AW	1.198	1.087	0.904	0.078	9.35	35.0
3A2BW	1.220	1.069	0.898	0.078	9.63	35.0
3A3AW	1.194	1.093	0.893	0.078	9.30	35.0
3A3BW	1.210	1.083	0.895	0.078	9.51	35.0
3B1AW	2.696	1.577	0.888	0.078	28.56	60.0
3B1BW	2.707	1.577	0.911	0.078	28.70	60.0
3B2AW	2.709	1.580	0.912	0.078	28.72	60.0
3B2BW	2.717	1.577	0.910	0.078	28.83	60.0
3B3AW	2.699	1.574	0.905	0.078	28.60	60.0
3B3BW	2.701	1.573	0.903	0.078	28.62	60.0
3C1AW	5.404	2.061	0.911	0.078	63.28	72.0
3C1BW	5.405	2.064	0.903	0.078	63.29	72.0
3C2AW	5.402	2.068	0.912	0.078	63.25	72.0
3C2BW	5.399	2.059	0.915	0.078	63.21	72.0
3C3AW	5.406	2.052	0.903	0.078	63.30	72.0
3C3BW	5.408	2.051	0.906	0.078	63.33	72.0

Note: For symbols of dimensions, see Figure 3.1.

Table 3.8 (cont'd)

Dimensions of Hat-Shaped Beams Assembled from Hat Section (25AK Sheet Steel) and Plate (50SK Sheet Steel) Beam Specimens - **Group W**

(b) Dimensions of Plate (50SK Sheet Steel)

Spec.	BP (in.)	t (in.)	w/t	Length (in.)
3A1AW	2.796	0.074	25.57	35.0
3A1BW	2.798	0.074	25.64	35.0
3A2AW	2.795	0.074	25.55	35.0
3A2BW	2.791	0.074	25.58	35.0
3A3AW	2.794	0.074	25.69	35.0
3A3BW	2.801	0.074	25.76	35.0
3B1AW	4.297	0.074	46.07	60.0
3B1BW	4.297	0.074	45.76	60.0
3B2AW	4.311	0.074	45.93	60.0
3B2BW	4.327	0.074	46.18	60.0
3B3AW	4.296	0.074	45.82	60.0
3B3BW	4.302	0.074	45.93	60.0
3C1AW	7.010	0.074	82.42	72.0
3C1BW	7.003	0.074	82.43	72.0
3C2AW	7.006	0.074	82.35	72.0
3C2BW	7.001	0.074	82.24	72.0
3C3AW	7.005	0.074	82.46	72.0
3C3BW	7.003	0.074	82.39	72.0

Note: For symbols of dimensions, see Figure 3.1.

Table 3.9

Dimensions of Hat-Shaped Beams Assembled from Hat Section (25AK Sheet Steel) and Plate (50SK Sheet Steel) Beam Specimens - **Group Z**

(a) Dimensions of Hat Sections (25AK Sheet Steel)

Spec.	BF (in.)	BW (in.)	BL (in.)	t (in.)	w/t	Length (in.)
3A1AZ	1.194	1.092	0.900	0.078	9.30	35.0
3A1BZ	1.191	1.092	0.903	0.078	9.26	35.0
3A2AZ	1.193	1.091	0.931	0.078	9.29	35.0
3A2BZ	1.199	1.088	0.900	0.078	9.37	35.0
3A3AZ	1.212	1.079	0.901	0.078	9.53	35.0
3A3BZ	1.195	1.090	0.898	0.078	9.31	35.0
3B1AZ	2.690	1.589	0.900	0.078	28.48	60.0
3B1BZ	2.701	1.579	0.903	0.078	28.62	60.0
3B2AZ	2.704	1.577	0.910	0.078	28.66	60.0
3B2BZ	2.694	1.582	0.906	0.078	28.53	60.0
3B3AZ	2.703	1.575	0.918	0.078	28.65	60.0
3B3BZ	2.699	1.578	0.910	0.078	28.60	60.0
3C1AZ	5.405	2.058	0.909	0.078	63.29	72.0
3C1BZ	5.403	2.071	0.907	0.078	63.26	72.0
3C2AZ	5.401	2.068	0.903	0.078	63.24	72.0
3C2BZ	5.396	2.062	0.907	0.078	63.17	72.0
3C3AZ	5.403	2.057	0.906	0.078	63.26	72.0
3C3BZ	5.401	2.058	0.908	0.078	63.24	72.0

Note: For symbols of dimensions, see Figure 3.1.

Table 3.9 (cont'd)

Dimensions of Hat-Shaped Beams Assembled from Hat Section (25AK Sheet Steel) and Plate (50SK Sheet Steel) Beam Specimens - **Group Z**

(b) Dimensions of Plate (50SK Sheet Steel)

Spec.	BP (in.)	t (in.)	w/t	Length (in.)
3A1AZ	2.796	0.074	25.62	35.0
3A1BZ	2.798	0.074	25.61	35.0
3A2AZ	2.805	0.074	25.73	35.0
3A2BZ	2.799	0.074	25.66	35.0
3A3AZ	2.799	0.074	25.65	35.0
3A3BZ	2.803	0.074	25.74	35.0
3B1AZ	4.300	0.074	45.95	60.0
3B1BZ	4.299	0.074	45.89	60.0
3B2AZ	4.294	0.074	45.73	60.0
3B2BZ	4.297	0.074	45.82	60.0
3B3AZ	4.302	0.074	45.73	60.0
3B3BZ	4.298	0.074	45.78	60.0
3C1AZ	7.001	0.074	82.32	72.0
3C1BZ	7.003	0.074	82.38	72.0
3C2AZ	7.007	0.074	82.49	72.0
3C2BZ	6.983	0.074	82.11	72.0
3C3AZ	7.004	0.074	82.41	72.0
3C3BZ	7.002	0.074	82.35	72.0

Note: For symbols of dimensions, see Figure 3.1.

Table 3.10

Dimensions of Hat-Shaped Beams Assembled from Hat Section (50SK Sheet Steel) and Plate (25AK Sheet Steel) Beam Specimens - **Group S**

(a) Dimensions of Hat Sections (50SK Sheet Steel)

Spec.	BF (in.)	BW (in.)	BL (in.)	t (in.)	w/t	Length (in.)
3A1AS	2.298	1.045	0.781	0.074	24.83	50.0
3A1BS	2.302	1.042	0.797	0.074	24.89	50.0
3A2AS	2.304	1.049	0.792	0.074	24.91	50.0
3A2BS	2.298	1.045	0.807	0.074	24.83	50.0
3A3AS	2.308	1.047	0.794	0.074	24.97	50.0
3A3BS	2.294	1.043	0.797	0.074	24.78	50.0
3B1AS	3.591	1.560	0.794	0.074	42.30	65.0
3B1BS	3.608	1.540	0.801	0.074	42.53	65.0
3B2AS	3.602	1.541	0.805	0.074	42.45	65.0
3B2BS	3.586	1.549	0.813	0.074	42.24	65.0
3B3AS	3.603	1.545	0.808	0.074	42.47	65.0
3B3BS	3.305	1.546	0.803	0.074	42.49	65.0
3C1AS	5.607	2.047	0.804	0.074	69.55	72.0
3C1BS	5.611	2.036	0.807	0.074	69.60	72.0
3C2AS	5.609	2.053	0.807	0.074	69.57	72.0
3C2BS	5.618	2.050	0.812	0.074	69.70	72.0
3C3AS	5.588	2.019	0.810	0.074	69.29	72.0
3C3BS	5.605	2.045	0.804	0.074	69.52	72.0

Note: For symbols of dimensions, see Figure 3.1.

Table 3.10 (cont'd)

Dimensions of Hat-Shaped Beams Assembled from Hat Section
(50SK Sheet teel) and Plate (25AK Sheet Steel)
Beam Specimens - **Group S**

(b) Dimensions of Plate (25AK Sheet Steel)

Spec.	BP (in.)	t (in.)	w/t	Length (in.)
3A1AS	3.706	0.078	37.50	50.0
3A1BS	3.703	0.078	37.26	50.0
3A2AS	3.706	0.078	37.36	50.0
3A2BS	3.704	0.078	37.14	50.0
3A3AS	3.704	0.078	37.31	50.0
3A3BS	3.706	0.078	37.29	50.0
3B1AS	5.001	0.078	53.94	65.0
3B1BS	4.997	0.078	53.79	65.0
3B2AS	5.003	0.078	53.82	65.0
3B2BS	5.004	0.078	53.73	65.0
3B3AS	5.003	0.078	53.78	65.0
3B3BS	5.001	0.078	53.82	65.0
3C1AS	7.000	0.078	79.44	72.0
3C1BS	6.999	0.078	79.38	72.0
3C2AS	7.004	0.078	79.45	72.0
3C2BS	7.007	0.078	79.38	72.0
3C3AS	6.998	0.078	79.33	72.0
3C3BS	7.001	0.078	79.45	72.0

Note: For symbols of dimensions, see Figure 3.1.

Table 3.11

Dimensions of Hat-Shaped Beams Assembled from Hat Section (50SK Sheet Steel) and Plate (25AK Sheet Steel) Beam Specimens - **Group K**

(a) Dimensions of Hat Sections (50SK Sheet Steel)

Spec.	BF (in.)	BW (in.)	BL (in.)	t (in.)	w/t	Length (in.)
3A1AK	2.307	1.034	0.798	0.074	24.95	50.0
3A1BK	2.293	1.146	0.796	0.074	24.76	50.0
3A2AK	2.302	1.042	0.794	0.074	24.89	50.0
3A2BK	2.286	1.051	0.805	0.074	24.67	50.0
3A3AK	2.300	1.049	0.794	0.074	24.86	50.0
3A3BK	2.298	1.045	0.797	0.074	24.83	50.0
3B1AK	3.593	1.546	0.805	0.074	42.33	65.0
3B1BK	3.588	1.551	0.804	0.074	42.26	65.0
3B2AK	3.589	1.535	0.803	0.074	42.28	65.0
3B2BK	3.579	1.545	0.803	0.074	42.14	65.0
3B3AK	3.600	1.535	0.798	0.074	42.43	65.0
3B3BK	3.598	1.537	0.800	0.074	42.40	65.0
3C1AK	5.592	2.045	0.808	0.074	69.34	72.0
3C1BK	5.606	2.048	0.809	0.074	69.53	72.0
3C2AK	5.589	2.054	0.814	0.074	69.30	72.0
3C2BK	5.606	2.049	0.806	0.074	69.53	72.0
3C3AK	5.617	2.038	0.803	0.074	69.68	72.0
3C3BK	5.611	2.041	0.803	0.074	69.60	72.0

Note: For symbols of dimensions, see Figure 3.1.

Table 3.11 (cont'd)

Dimensions of Hat-Shaped Beams Assembled from Hat Section
(50SK Sheet Steel) and Plate (25AK Sheet Steel)
Beam Specimens - **Group K**

(b) Dimensions of Plate (25AK Sheet Steel)

Spec.	BP (in.)	t (in.)	w/t	Length (in.)
3A1AK	3.701	0.078	37.22	50.0
3A1BK	3.698	0.078	37.21	50.0
3A2AK	3.702	0.078	37.28	50.0
3A2BK	3.698	0.078	37.09	50.0
3A3AK	3.703	0.078	37.30	50.0
3A3BK	3.699	0.078	37.21	50.0
3B1AK	4.997	0.078	53.74	65.0
3B1BK	5.001	0.078	53.81	65.0
3B2AK	4.995	0.078	53.74	65.0
3B2BK	4.995	0.078	53.74	65.0
3B3AK	4.991	0.078	53.76	65.0
3B3BK	4.998	0.078	53.82	65.0
3C1AK	7.003	0.078	79.42	72.0
3C1BK	7.002	0.078	79.40	72.0
3C2AK	6.998	0.078	79.28	72.0
3C2BK	7.004	0.078	79.46	72.0
3C3AK	7.000	0.078	79.45	72.0
3C3BK	7.001	0.078	79.46	72.0

Note: For symbols of dimensions, see Figure 3.1.

Table 4.1

Comparison of Computed and Tested Critical Local Buckling Moments
Beam Specimens - **Group W**
(Based on Dynamic Compressive Stresses)

Specimen	w/t (25AK) (1)	f_{cr} (ksi.) (2)	$(P_{cr})_{test}$ (kips) (3)	$(M_{cr})_{comp}$ (in.-kips) (4)	$(M_{cr})_{test}$ (in.-kips) (5)	(5)/(4) (6)
3A1AW	9.33	21.56	N/A	3.98	N/A	N/A
3A1BW	9.26	21.56	N/A	3.97	N/A	N/A
3A2AW	9.35	23.09	N/A	4.17	N/A	N/A
3A2BW	9.63	23.09	N/A	4.11	N/A	N/A
3A3AW	9.30	23.63	N/A	4.48	N/A	N/A
3A3BW	9.51	23.62	N/A	4.46	N/A	N/A
3B1AW	28.56	20.94	N/A	9.44	N/A	N/A
3B1BW	28.70	20.93	N/A	9.48	N/A	N/A
3B2AW	28.72	22.42	N/A	9.72	N/A	N/A
3B2BW	28.83	22.42	N/A	9.72	N/A	N/A
3B3AW	28.60	23.93	N/A	9.95	N/A	N/A
3B3BW	28.62	23.93	N/A	9.95	N/A	N/A
3C1AW	63.28	18.23	N/A	16.78	N/A	N/A
3C1BW	63.29	18.22	2.023	16.81	17.19	1.023
3C2AW	63.25	19.55	2.333	17.71	19.83	1.119
3C2BW	63.21	19.56	2.308	17.62	19.62	1.114
3C3AW	63.30	20.90	2.489	18.40	21.16	1.150
3C3BW	63.33	20.90	2.369	18.39	20.14	1.095
Mean						1.093
Standard Deviation						0.040

Note: The dynamic compressive stresses were used for calculating the critical local buckling moments ($(M_{cr})_{comp}$).

Table 4.2

Comparison of Computed and Tested Critical Local Buckling Moments
Beam Specimens - **Group Z**
(Based on Dynamic Compressive Stresses)

Specimen	w/t (50SK) (1)	f_{cr} (ksi.) (2)	$(P_{cr})_{test}$ (kips) (3)	$(M_{cr})_{comp}$ (in.-kips) (4)	$(M_{cr})_{test}$ (in.-kips) (5)	(5)/(4) (6)
3A1AZ	25.62	50.37	N/A	5.60	N/A	N/A
3A1BZ	25.61	50.38	N/A	5.59	N/A	N/A
3A2AZ	25.73	51.37	N/A	5.86	N/A	N/A
3A2BZ	25.66	51.38	N/A	5.84	N/A	N/A
3A3AZ	25.65	52.40	N/A	6.06	N/A	N/A
3A3BZ	25.74	52.37	N/A	6.11	N/A	N/A
3B1AZ	45.95	43.89	1.752	13.29	12.26	0.923
3B1BZ	45.89	43.91	1.768	13.21	12.38	0.937
3B2AZ	45.73	44.36	1.825	13.82	12.78	0.924
3B2BZ	45.82	44.32	1.837	13.85	12.86	0.928
3B3AZ	45.73	44.73	1.910	14.41	13.37	0.928
3B3BZ	45.78	44.70	1.881	14.42	13.17	0.913
3C1AZ	82.32	15.74	2.264	18.78	19.25	1.025
3C1BZ	82.38	15.72	2.194	18.91	18.65	0.986
3C2AZ	82.49	15.68	2.223	19.68	18.90	0.960
3C2BZ	82.11	15.82	2.528	19.77	21.49	1.087
3C3AZ	82.41	15.71	2.565	20.51	21.80	1.063
3C3BZ	82.35	15.73	2.516	20.51	21.39	1.043
Mean						0.976
Standard Deviation						0.062

Note: The dynamic compressive stresses were used for calculating the critical local buckling moments ($(M_{cr})_{comp}$).

Table 4.3

Comparison of Computed and Tested Critical Local Buckling Moments
Beam Specimens - **Group S**
(Based on Dynamic Compressive Stresses)

Specimen	w/t (50SK) (1)	f_{cr} (ksi.) (2)	$(P_{cr})_{test}$ (kips) (3)	$(M_{cr})_{comp}$ (in.-kips) (4)	$(M_{cr})_{test}$ (in.-kips) (5)	(5)/(4) (6)
3A1AS	24.83	50.55	N/A	8.92	N/A	N/A
3A1BS	24.89	50.54	N/A	8.91	N/A	N/A
3A2AS	24.91	51.57	N/A	9.54	N/A	N/A
3A2BS	24.83	52.59	N/A	9.49	N/A	N/A
3A3AS	24.97	52.59	N/A	9.58	N/A	N/A
3A3BS	24.78	52.64	N/A	9.53	N/A	N/A
3B1AS	42.30	45.32	2.510	19.42	19.14	0.986
3B1BS	42.53	45.23	2.487	19.13	18.96	0.991
3B2AS	42.45	45.78	2.535	20.33	19.33	0.951
3B2BS	42.24	45.87	2.552	20.42	19.46	0.953
3B3AS	42.47	46.27	2.648	20.46	20.19	0.987
3B3BS	42.49	46.26	2.775	20.47	21.16	1.034
3C1AS	69.55	22.05	2.448	22.12	20.80	0.940
3C1BS	69.60	22.02	2.438	21.96	20.72	0.943
3C2AS	69.57	22.03	2.457	22.16	20.89	0.942
3C2BS	69.70	21.96	2.528	22.07	21.49	0.974
3C3AS	69.29	22.21	2.492	22.01	21.18	0.962
3C3BS	69.52	22.07	2.452	22.22	20.85	0.938
Mean						0.967
Standard Deviation						0.029

Note: The dynamic compressive stresses were used for calculating the critical local buckling moments ($(M_{cr})_{comp}$).

Table 4.4

Comparison of Computed and Tested Critical Local Buckling Moments
Beam Specimens - **Group K**
(Based on Dynamic Compressive Stresses)

Specimen	w/t (25AK) (1)	f_{cr} (ksi.) (2)	$(P_{cr})_{test}$ (kips) (3)	$(M_{cr})_{comp}$ (in.-kips) (4)	$(M_{cr})_{test}$ (in.-kips) (5)	(5)/(4) (6)
3A1AK	37.22	20.45	N/A	9.98	N/A	N/A
3A1BK	37.21	20.45	N/A	10.08	N/A	N/A
3A2AK	37.28	21.91	N/A	10.48	N/A	N/A
3A2BK	37.09	21.93	N/A	10.58	N/A	N/A
3A3AK	37.30	23.39	N/A	10.57	N/A	N/A
3A3BK	37.21	23.39	N/A	10.54	N/A	N/A
3B1AK	53.74	19.17	N/A	16.12	N/A	N/A
3B1BK	53.81	19.17	N/A	16.18	N/A	N/A
3B2AK	53.74	20.56	N/A	17.01	N/A	N/A
3B2BK	53.74	20.56	N/A	17.13	N/A	N/A
3B3AK	53.76	21.96	N/A	16.73	N/A	N/A
3B3BK	53.82	21.96	N/A	16.77	N/A	N/A
3C1AK	79.42	16.27	2.259	20.69	19.20	0.928
3C1BK	79.40	16.27	2.308	20.74	19.62	0.946
3C2AK	79.28	16.97	2.506	20.90	21.30	1.019
3C2BK	79.46	16.89	2.364	20.83	20.10	0.965
3C3AK	79.45	16.90	2.291	20.81	19.48	0.936
3C3BK	79.46	16.89	2.372	20.84	20.16	0.967
Mean						0.960
Standard Deviation						0.033

Note: The dynamic compressive stresses were used for calculating the critical local buckling moments ($(M_{cr})_{comp}$).

Table 4.5

Comparison of Computed and Tested Yield Moments
Beam Specimens - **Group W**
(Based on Dynamic Compressive Stresses)

Specimen	w/t (25AK) (1)	F_y (Comp.) (ksi.) (2)	$(P_y)_{test}$ (kips) (3)	$(M_y)_{comp}$ (in.-kips) (4)	$(M_y)_{test}$ (in.-kips) (5)	(5)/(4) (6)
3A1AW	9.33	21.63	1.082	3.34	4.19	1.254
3A1BW	9.26	21.63	1.117	3.34	4.33	1.296
3A2AW	9.35	23.17	1.130	3.58	4.38	1.223
3A2BW	9.63	23.17	1.135	3.53	4.40	1.246
3A3AW	9.30	24.71	1.241	3.88	4.81	1.240
3A3BW	9.51	24.71	1.264	3.87	4.90	1.266
3B1AW	28.56	21.63	1.570	9.87	10.99	1.117
3B1BW	28.70	21.63	1.531	9.88	10.72	1.085
3B2AW	28.72	23.17	1.650	10.69	11.55	1.080
3B2BW	28.83	23.17	1.583	10.69	11.08	1.036
3B3AW	28.60	24.71	1.766	11.44	12.36	1.080
3B3BW	28.62	24.71	1.785	11.44	12.49	1.092
3C1AW	63.28	21.63	2.432	21.00	20.67	0.984
3C1BW	63.29	21.63	2.450	21.04	20.83	0.990
3C2AW	63.25	23.17	2.677	22.34	22.75	1.018
3C2BW	63.21	23.17	2.648	22.22	22.51	1.013
3C3AW	63.30	24.71	2.789	23.30	23.71	1.018
3C3BW	63.33	24.71	2.731	23.29	23.21	0.997
Mean						1.113
Standard Deviation						0.110

Note: The dynamic compressive stresses were used for calculating the yield moments ($(M_y)_{comp}$).

Table 4.6

Comparison of Computed and Tested Yield Moments
Beam Specimens - **Group Z**
(Based on Dynamic Compressive Stresses)

Specimen	w/t (50SK) (1)	F_y (Comp.) (ksi.) (2)	$(P_y)_{test}$ (kips) (3)	$(M_y)_{comp}$ (in.-kips) (4)	$(M_y)_{test}$ (in.-kips) (5)	(5)/(4) (6)
3A1AZ	25.62	53.30	1.070	3.35	4.14	1.236
3A1BZ	25.61	53.30	1.111	3.35	4.31	1.287
3A2AZ	25.73	54.61	1.180	3.59	4.57	1.273
3A2BZ	25.66	54.61	1.164	3.58	4.51	1.260
3A3AZ	25.65	55.92	1.238	3.85	4.80	1.247
3A3BZ	25.74	55.92	1.278	3.87	4.95	1.279
3B1AZ	45.95	53.30	1.492	9.93	10.44	1.051
3B1BZ	45.89	53.30	1.550	9.88	10.85	1.098
3B2AZ	45.73	54.61	1.605	10.63	11.24	1.057
3B2BZ	45.82	54.61	1.611	10.65	11.27	1.058
3B3AZ	45.73	55.92	1.728	11.35	12.10	1.066
3B3BZ	45.78	55.92	1.680	11.37	11.76	1.034
3C1AZ	82.32	53.30	2.800	23.17	23.80	1.027
3C1BZ	82.38	53.30	2.870	23.34	24.40	1.045
3C2AZ	82.49	54.61	3.012	25.02	25.60	1.023
3C2BZ	82.11	54.61	3.060	24.91	26.01	1.044
3C3AZ	82.41	55.92	3.158	26.64	26.84	1.088
3C3BZ	82.35	55.92	3.140	26.65	26.69	1.002
Mean						1.116
Standard Deviation						0.110

Note: The dynamic compressive stresses were used for calculating the yield moments ($(M_y)_{comp}$).

Table 4.7

Comparison of Computed and Tested Yield Moments
Beam Specimens - **Group S**
(Based on Dynamic Compressive Stresses)

Specimen	w/t (50SK) (1)	F_y (Comp.) (ksi.) (2)	$(P_y)_{test}$ (kips) (3)	$(M_y)_{comp}$ (in.-kips) (4)	$(M_y)_{test}$ (in.-kips) (5)	(5)/(4) (6)
3A1AS	24.83	53.30	1.590	9.71	9.14	0.941
3A1BS	24.89	53.30	1.613	9.70	9.27	0.956
3A2AS	24.91	54.61	1.650	10.16	9.49	0.934
3A2BS	24.83	54.61	1.645	10.11	9.46	0.936
3A3AS	24.97	55.92	1.686	10.30	9.69	0.941
3A3BS	24.78	55.92	1.739	10.21	10.00	0.979
3B1AS	42.30	53.30	2.617	19.89	19.95	1.003
3B1BS	42.53	53.30	2.610	19.62	19.90	1.014
3B2AS	42.45	54.61	2.752	20.35	20.98	1.031
3B2BS	42.24	54.61	2.741	20.48	20.90	1.021
3B3AS	42.47	55.92	2.798	20.78	21.33	1.026
3B3BS	42.49	55.92	2.875	20.79	21.92	1.054
3C1AS	69.55	53.30	3.425	30.91	29.11	0.942
3C1BS	69.60	53.30	3.371	30.72	28.65	0.933
3C2AS	69.57	54.61	3.620	32.20	30.77	0.956
3C2BS	69.70	54.61	3.582	32.15	30.45	0.947
3C3AS	69.29	55.92	3.653	31.98	31.05	0.971
3C3BS	69.52	55.92	3.599	32.37	30.59	0.945
Mean						0.974
Standard Deviation						0.040

Note: The dynamic compressive stresses were used for calculating the yield moments ($(M_y)_{comp}$).

Table 4.8

Comparison of Computed and Tested Yield Moments
Beam Specimens - **Group K**
(Based on Dynamic Compressive Stresses)

Specimen	w/t (25AK) (1)	F_y (Comp.) (ksi.) (2)	$(P_y)_{test}$ (kips) (3)	$(M_y)_{comp}$ (in.-kips) (4)	$(M_y)_{test}$ (in.-kips) (5)	(5)/(4) (6)
3A1AK	37.22	21.63	1.540	9.62	8.86	0.921
3A1BK	37.21	21.63	1.532	9.72	8.81	0.906
3A2AK	37.28	23.17	1.590	10.07	9.14	0.908
3A2BK	37.09	23.17	1.610	10.14	9.26	0.913
3A3AK	37.30	24.71	1.692	10.30	9.73	0.945
3A3BK	37.21	24.71	1.670	10.25	9.60	0.937
3B1AK	53.74	21.63	2.630	22.24	20.05	0.901
3B1BK	53.81	21.63	2.615	22.30	19.94	0.894
3B2AK	53.74	23.17	2.700	22.84	20.59	0.901
3B2BK	53.74	23.17	2.714	22.98	20.69	0.900
3B3AK	53.76	24.71	2.758	23.34	21.03	0.901
3B3BK	53.82	24.71	2.816	23.38	21.47	0.918
3C1AK	79.42	21.63	3.987	36.05	33.90	0.940
3C1BK	79.40	21.63	4.052	36.14	34.44	0.953
3C2AK	79.28	23.17	4.172	38.64	35.46	0.918
3C2BK	79.46	23.17	4.203	38.44	35.73	0.930
3C3AK	79.45	24.71	4.298	38.85	36.53	0.940
3C3BK	79.46	24.71	4.301	38.92	36.56	0.939
Mean						0.920
Standard Deviation						0.019

Note: The dynamic compressive stresses were used for calculating the yield moments ($(M_y)_{comp}$).

Table 4.9

Comparison of Computed and Tested Yield Moments
Beam Specimens - **Group W**
(Based on Dynamic Tensile Stresses)

Specimen	w/t (25AK) (1)	F_y (Ten.) (ksi.) (2)	$(P_y)_{test}$ (kips) (3)	$(M_y)_{comp}$ (in.-kips) (4)	$(M_y)_{test}$ (in.-kips) (5)	(5)/(4) (6)
3A1AW	9.33	24.57	1.082	3.81	4.19	1.100
3A1BW	9.26	24.57	1.117	3.81	4.33	1.136
3A2AW	9.35	26.18	1.130	4.05	4.38	1.081
3A2BW	9.63	26.18	1.135	3.99	4.40	1.103
3A3AW	9.30	27.80	1.241	4.37	4.81	1.101
3A3BW	9.51	27.80	1.264	4.35	4.90	1.126
3B1AW	28.56	24.57	1.570	11.25	10.99	0.977
3B1BW	28.70	24.57	1.531	11.29	10.72	0.950
3B2AW	28.72	26.18	1.650	12.13	11.55	0.952
3B2BW	28.83	26.18	1.583	12.12	11.08	0.914
3B3AW	28.60	27.80	1.766	12.78	12.36	0.967
3B3BW	28.62	27.80	1.785	12.77	12.49	0.978
3C1AW	63.28	24.57	2.432	23.13	20.67	0.894
3C1BW	63.29	24.57	2.450	23.17	20.83	0.900
3C2AW	63.25	26.18	2.677	24.46	22.75	0.930
3C2BW	63.21	26.18	2.648	24.32	22.51	0.926
3C3AW	63.30	27.80	2.789	25.57	23.71	0.927
3C3BW	63.33	27.80	2.731	25.56	23.21	0.908
Mean						0.993
Standard Deviation						0.088

Note: The dynamic tensile stresses were used for calculating the yield moments ($(M_y)_{comp}$).

Table 4.10

Comparison of Computed and Tested Yield Moments
Beam Specimens - **Group Z**
(Based on Dynamic Tensile Stresses)

Specimen	w/t (50SK) (1)	F_y (Ten.) (ksi.) (2)	$(P_y)_{test}$ (kips) (3)	$(M_y)_{comp}$ (in.-kips) (4)	$(M_y)_{test}$ (in.-kips) (5)	(5)/(4) (6)
3A1AZ	25.62	54.92	1.070	3.82	4.14	1.083
3A1BZ	25.61	54.92	1.111	3.82	4.31	1.128
3A2AZ	25.73	55.88	1.180	4.06	4.57	1.126
3A2BZ	25.66	55.88	1.164	4.05	4.51	1.114
3A3AZ	25.65	56.84	1.238	4.33	4.80	1.109
3A3BZ	25.74	56.84	1.278	4.33	4.95	1.138
3B1AZ	45.95	54.92	1.492	11.31	10.44	0.923
3B1BZ	45.89	54.92	1.550	11.25	10.85	0.964
3B2AZ	45.73	55.88	1.605	12.03	11.24	0.934
3B2BZ	45.82	55.88	1.611	12.04	11.27	0.936
3B3AZ	45.73	56.84	1.728	12.76	12.10	0.948
3B3BZ	45.78	56.84	1.680	12.78	11.76	0.920
3C1AZ	82.32	54.92	2.800	26.33	23.80	0.904
3C1BZ	82.38	54.92	2.870	26.53	24.40	0.920
3C2AZ	82.49	55.88	3.012	28.10	25.60	0.911
3C2BZ	82.11	55.88	3.060	27.99	26.01	0.929
3C3AZ	82.41	56.84	3.158	29.91	26.84	0.897
3C3BZ	82.35	56.84	3.140	29.93	26.69	0.892
Mean						0.988
Standard Deviation						0.096

Note: The dynamic tensile stresses were used for calculating the yield moments ($(M_y)_{comp}$).

Table 4.11

Comparison of Computed and Tested Yield Moments
Beam Specimens - **Group S**
(Based on Dynamic Tensile Stresses)

Specimen	w/t (50SK) (1)	F_y (Ten.) (ksi.) (2)	$(P_y)_{test}$ (kips) (3)	$(M_y)_{comp}$ (in.-kips) (4)	$(M_y)_{test}$ (in.-kips) (5)	(5)/(4) (6)
3A1AS	24.83	54.92	1.590	10.09	9.14	0.906
3A1BS	24.89	54.92	1.613	10.07	9.27	0.921
3A2AS	24.91	55.88	1.650	10.51	9.49	0.903
3A2BS	24.83	55.88	1.645	10.45	9.46	0.905
3A3AS	24.97	56.84	1.686	10.65	9.69	0.910
3A3BS	24.78	56.84	1.739	10.56	10.00	0.947
3B1AS	42.30	54.92	2.617	20.73	19.95	0.962
3B1BS	42.53	54.92	2.610	20.43	19.90	0.974
3B2AS	42.45	55.88	2.752	21.01	20.98	0.999
3B2BS	42.24	55.88	2.741	21.14	20.90	0.989
3B3AS	42.47	56.84	2.798	21.33	21.33	1.000
3B3BS	42.49	56.84	2.875	21.34	21.92	1.027
3C1AS	69.55	54.92	3.425	32.05	29.11	0.908
3C1BS	69.60	54.92	3.371	31.85	28.65	0.900
3C2AS	69.57	55.88	3.620	33.26	30.77	0.925
3C2BS	69.70	55.88	3.582	33.21	30.45	0.917
3C3AS	69.29	56.84	3.653	32.80	31.05	0.947
3C3BS	69.52	56.84	3.599	33.34	30.59	0.918
Mean						0.942
Standard Deviation						0.040

Note: The dynamic tensile stresses were used for calculating the yield moments ($(M_y)_{comp}$).

Table 4.12

Comparison of Computed and Tested Yield Moments
Beam Specimens - **Group K**
(Based on Dynamic Tensile Stresses)

Specimen	w/t (25AK) (1)	F_y (Ten.) (ksi.) (2)	$(P_y)_{test}$ (kips) (3)	$(M_y)_{comp}$ (in.-kips) (4)	$(M_y)_{test}$ (in.-kips) (5)	(5)/(4) (6)
3A1AK	37.22	24.57	1.540	9.99	8.86	0.887
3A1BK	37.21	24.57	1.532	10.09	8.81	0.873
3A2AK	37.28	26.18	1.590	10.42	9.14	0.877
3A2BK	37.09	26.18	1.610	10.48	9.26	0.884
3A3AK	37.30	27.80	1.692	10.65	9.73	0.914
3A3BK	37.21	27.80	1.670	10.60	9.60	0.906
3B1AK	53.74	24.57	2.630	23.14	20.05	0.866
3B1BK	53.81	24.57	2.615	23.21	19.94	0.859
3B2AK	53.74	26.18	2.700	23.63	20.59	0.871
3B2BK	53.74	26.18	2.714	23.77	20.69	0.870
3B3AK	53.76	27.80	2.758	24.01	21.03	0.876
3B3BK	53.82	27.80	2.816	24.05	21.47	0.893
3C1AK	79.42	24.57	3.987	38.21	33.90	0.887
3C1BK	79.40	24.57	4.052	38.31	34.44	0.899
3C2AK	79.28	26.18	4.172	40.64	35.46	0.873
3C2BK	79.46	26.18	4.203	40.41	35.73	0.884
3C3AK	79.45	27.80	4.298	40.87	36.53	0.894
3C3BK	79.46	27.80	4.301	40.93	36.56	0.893
Mean						0.884
Standard Deviation						0.014

Note: The dynamic tensile stresses were used for calculating the yield moments ($(M_y)_{comp}$).

Table 4.13

Comparison of Computed and Tested Yield Moments
Beam Specimens - **Group W**
(Based on Dynamic Compressive and Tensile Stresses)

Specimen	w/t (25AK) (1)	F_y (Ten.) (ksi.) (2)	F_y (Comp.) (ksi.) (3)	$(P_y)_{test}$ (kips) (4)	$(M_y)_{comp}$ (in.-kips) (5)	$(M_y)_{test}$ (in.-kips) (6)	(6)/(5) (7)
3A1AW	9.33	24.57	21.63	1.082	3.33	4.19	1.258
3A1BW	9.26	24.57	21.63	1.117	3.33	4.33	1.300
3A2AW	9.35	26.18	23.17	1.130	3.56	4.38	1.230
3A2BW	9.63	26.18	23.17	1.135	3.52	4.40	1.250
3A3AW	9.30	27.80	24.71	1.241	3.86	4.81	1.246
3A3BW	9.51	27.80	24.71	1.264	3.85	4.90	1.273
3B1AW	28.56	24.57	21.63	1.570	9.89	10.99	1.111
3B1BW	28.70	24.57	21.63	1.531	9.92	10.72	1.081
3B2AW	28.72	26.18	23.17	1.650	10.72	11.55	1.077
3B2BW	28.83	26.18	23.17	1.583	10.71	11.08	1.035
3B3AW	28.60	27.80	24.71	1.766	11.33	12.36	1.091
3B3BW	28.62	27.80	24.71	1.785	11.33	12.49	1.102
3C1AW	63.28	24.57	21.63	2.432	20.97	20.67	0.986
3C1BW	63.29	24.57	21.63	2.450	21.01	20.83	0.991
3C2AW	63.25	26.18	23.17	2.677	22.27	22.75	1.022
3C2BW	63.21	26.18	23.17	2.648	22.14	22.51	1.017
3C3AW	63.30	27.80	24.71	2.789	23.34	23.71	1.016
3C3BW	63.33	27.80	24.71	2.731	23.33	23.21	0.995
Mean							1.116
Standard Deviation							0.112

Table 4.14

Comparison of Computed and Tested Yield Moments
Beam Specimens - **Group Z**
(Based on Dynamic Compressive and Tensile Stresses)

Specimen	w/t (50SK) (1)	F_y (Ten.) (ksi.) (2)	F_y (Comp.) (ksi.) (3)	$(P_y)_{test}$ (kips) (4)	$(M_y)_{comp}$ (in.-kips) (5)	$(M_y)_{test}$ (in.-kips) (6)	(6)/(5) (7)
3A1AZ	25.62	54.92	53.30	1.070	3.82	4.14	1.084
3A1BZ	25.61	54.92	53.30	1.111	3.82	4.31	1.128
3A2AZ	25.73	55.88	54.61	1.180	4.07	4.57	1.123
3A2BZ	25.66	55.88	54.61	1.164	4.06	4.51	1.111
3A3AZ	25.65	56.84	55.92	1.238	4.35	4.80	1.103
3A3BZ	25.74	56.84	55.92	1.278	4.37	4.95	1.133
3B1AZ	45.95	54.92	53.30	1.492	11.32	10.44	0.922
3B1BZ	45.89	54.92	53.30	1.550	11.26	10.85	0.964
3B2AZ	45.73	55.88	54.61	1.605	11.96	11.24	0.940
3B2BZ	45.82	55.88	54.61	1.611	11.98	11.27	0.941
3B3AZ	45.73	56.84	55.92	1.728	12.83	12.10	0.943
3B3BZ	45.78	56.84	55.92	1.680	12.84	11.76	0.916
3C1AZ	82.32	54.92	53.30	2.800	26.22	23.80	0.908
3C1BZ	82.38	54.92	53.30	2.870	26.41	24.40	0.924
3C2AZ	82.49	55.88	54.61	3.012	28.05	25.60	0.913
3C2BZ	82.11	55.88	54.61	3.060	27.94	26.01	0.931
3C3AZ	82.41	56.84	55.92	3.158	29.78	26.84	0.901
3C3BZ	82.35	56.84	55.92	3.140	29.79	26.69	0.896
Mean							0.988
Standard Deviation							0.093

Table 4.15

Comparison of Computed and Tested Yield Moments
Beam Specimens - **Group S**
(Based on Dynamic Compressive and Tensile Stresses)

Specimen	w/t (50SK) (1)	F_y (Ten.) (ksi.) (2)	F_y (Comp.) (ksi.) (3)	$(P_y)_{test}$ (kips) (4)	$(M_y)_{comp}$ (in.-kips) (5)	$(M_y)_{test}$ (in.-kips) (6)	(6)/(5) (7)
3A1AS	24.83	54.92	53.30	1.590	9.83	9.14	0.930
3A1BS	24.89	54.92	53.30	1.613	9.81	9.27	0.945
3A2AS	24.91	55.88	54.61	1.650	10.29	9.49	0.922
3A2BS	24.83	55.88	54.61	1.645	10.23	9.46	0.925
3A3AS	24.97	56.84	55.92	1.686	10.47	9.69	0.926
3A3BS	24.78	56.84	55.92	1.739	10.37	10.00	0.964
3B1AS	43.30	54.92	53.30	2.617	20.27	19.95	0.984
3B1BS	42.53	54.92	53.30	2.610	19.98	19.90	0.996
3B2AS	42.45	55.88	54.61	2.752	20.72	20.98	1.013
3B2BS	42.24	55.88	54.61	2.741	20.85	20.90	1.002
3B3AS	42.47	56.84	55.92	2.798	21.08	21.33	1.012
3B3BS	42.49	56.84	55.92	2.875	21.09	21.92	1.039
3C1AS	69.55	54.92	53.30	3.425	31.45	29.11	0.926
3C1BS	69.60	54.92	53.30	3.371	31.25	28.65	0.917
3C2AS	69.57	55.88	54.61	3.620	32.73	30.77	0.940
3C2BS	69.70	55.88	54.61	3.582	32.69	30.45	0.930
3C3AS	69.29	56.84	55.92	3.653	32.45	31.05	0.957
3C3BS	69.52	56.84	55.92	3.599	32.99	30.59	0.927
Mean							0.959
Standard Deviation							0.093

Table 4.16

Comparison of Computed and Tested Yield Moments
Beam Specimens - **Group K**
(Based on Dynamic Compressive and Tensile Stresses)

Specimen	w/t (25AK) (1)	F_y (Ten.) (ksi.) (2)	F_y (Comp.) (ksi.) (3)	$(P_y)_{test}$ (kips) (4)	$(M_y)_{comp}$ (in.-kips) (5)	$(M_y)_{test}$ (in.-kips) (6)	(6)/(5) (7)
3A1AK	37.22	24.57	21.63	1.540	9.88	8.86	0.897
3A1BK	37.21	24.57	21.63	1.532	9.98	8.81	0.883
3A2AK	37.28	26.18	23.17	1.590	10.29	9.14	0.888
3A2BK	37.09	26.18	23.17	1.610	10.36	9.26	0.894
3A3AK	37.30	27.80	24.71	1.692	10.49	9.73	0.928
3A3BK	37.21	27.80	24.71	1.670	10.43	9.60	0.920
3B1AK	53.74	24.57	21.63	3.630	22.77	20.05	0.881
3B1BK	53.81	24.57	21.63	3.615	22.84	19.94	0.873
3B2AK	53.74	26.18	23.17	2.700	23.29	20.59	0.884
3B2BK	53.74	26.18	23.17	2.714	23.43	20.69	0.883
3B3AK	53.76	27.80	24.71	2.758	23.64	21.03	0.890
3B3BK	53.82	27.80	24.71	2.816	23.68	21.47	0.907
3C1AK	79.42	24.57	21.63	3.987	36.15	33.90	0.938
3C1BK	79.40	24.57	21.63	4.052	36.25	34.44	0.950
3C2AK	79.28	26.18	23.17	4.172	38.66	35.46	0.917
3C2BK	79.46	26.18	23.17	4.203	38.43	35.73	0.930
3C3AK	79.45	27.80	24.71	4.298	39.13	36.53	0.934
3C3BK	79.46	27.80	24.71	4.301	39.20	36.56	0.933
Mean							0.907
Standard Deviation							0.024

Table 4.17

Comparison of Computed and Tested Yield Moments
Beam Specimens - **Group W**
(Based on Dynamic Tensile Stresses)

Specimen	w/t (25AK) (1)	F_y (Ten.) (ksi.) (2)	$(P_y)_{test}$ (kips) (3)	$(M_y)_{comp}$ (in.-kips) (4)	$(M_y)_{test}$ (in.-kips) (5)	(5)/(4) (6)
3A1AW	9.33	24.57	1.082	2.80	4.19	1.496
3A1BW	9.26	24.57	1.117	2.80	4.33	1.546
3A2AW	9.35	26.18	1.130	2.98	4.38	1.470
3A2BW	9.63	26.18	1.135	2.96	4.40	1.486
3A3AW	9.30	27.80	1.241	3.22	4.81	1.494
3A3BW	9.51	27.80	1.264	3.22	4.90	1.522
3B1AW	28.56	24.57	1.570	8.95	10.99	1.228
3B1BW	28.70	24.57	1.531	9.00	10.72	1.191
3B2AW	28.72	26.18	1.650	9.62	11.55	1.201
3B2BW	28.83	26.18	1.583	9.62	11.08	1.152
3B3AW	28.60	27.80	1.766	10.13	12.36	1.220
3B3BW	28.62	27.80	1.785	10.13	12.49	1.233
3C1AW	63.28	24.57	2.432	19.69	20.67	1.050
3C1BW	63.29	24.57	2.450	19.72	20.83	1.056
3C2AW	63.25	26.18	2.677	20.72	22.75	1.098
3C2BW	63.21	26.18	2.648	20.63	22.51	1.091
3C3AW	63.30	27.80	2.789	21.49	23.71	1.103
3C3BW	63.33	27.80	2.731	21.49	23.21	1.080
Mean						1.262
Standard Deviation						0.179

Table 4.18

Ratios of Tested Ultimate Loads to Tested Yield Loads
Plate Section is in Tension

(Group W)		(Group S)	
w/t	P_u/P_y	w/t	P_u/P_y
9.40	1.605	24.87	1.180
28.67	1.161	42.41	1.057
63.28	1.000	69.54	1.049

Table 4.19

Ratios of Tested Ultimate Loads to Tested Yield Loads
Plate Section is in Compression

(Group Z)		(Group K)	
w/t	P_u/P_y	w/t	P_u/P_y
25.67	1.355	37.22	1.234
45.82	1.221	53.77	1.147
82.34	1.100	79.41	1.077

Note: The w/t ratios listed in these two tables represent the average values of six similar specimens.

Table 4.20

Comparison of Computed and Tested Ultimate Mooments
Beam Specimens - **Group W**
(Based on Dynamic Compressive and Tensile Stresses)

Specimen	w/t (25AK) (1)	$(M_y)_{comp}$ (in.-kips) (2)	$(P_u)_{test}$ (kips) (3)	$(M_u)_{comp}$ (in.-kips) (4)	$(M_u)_{test}$ (in.-kips) (5)	(5)/(4) (6)
3A1AW	9.33	3.33	1.732	5.70	6.71	1.177
3A1BW	9.26	3.33	1.783	5.70	6.91	1.212
3A2AW	9.35	3.56	1.837	5.97	7.12	1.193
3A2BW	9.63	3.52	1.847	5.86	7.16	1.222
3A3AW	9.30	3.86	1.969	6.13	7.63	1.244
3A3BW	9.51	3.85	2.012	6.09	7.80	1.281
3B1AW	28.56	9.89	1.837	11.94	12.86	1.077
3B1BW	28.70	9.92	1.778	11.97	12.45	1.040
3B2AW	28.72	10.72	1.865	12.89	13.06	1.013
3B2BW	28.83	10.71	1.843	12.86	12.90	1.003
3B3AW	28.60	11.33	2.076	13.63	14.53	1.066
3B3BW	28.62	11.33	2.076	13.64	14.53	1.065
3C1AW	63.28	20.97	2.432	20.97	20.67	0.986
3C1BW	63.29	21.01	2.450	21.01	20.83	0.991
3C2AW	63.25	22.27	2.677	22.27	22.75	1.022
3C2BW	63.21	22.14	2.648	22.14	22.51	1.017
3C3AW	63.30	23.34	2.789	23.34	23.71	1.016
3C3BW	63.33	23.33	2.731	23.33	23.21	0.995
Mean						1.090
Standard Deviation						0.098

Table 4.21

Comparison of Computed and Tested Ultimate Mooments
Beam Specimens - **Group Z**
(Based on Dynamic Compressive and Tensile Stresses)

Specimen	w/t (50SK) (1)	(M_y) comp (in.-kips) (2)	(P_u) test (kips) (3)	(M_u) comp (in.-kips) (4)	(M_u) test (in.-kips) (5)	(5)/(4) (6)
3A1AZ	25.62	3.82	1.441	5.49	5.58	1.016
3A1BZ	25.61	3.82	1.475	5.48	5.72	1.044
3A2AZ	25.73	4.07	1.602	5.70	6.21	1.089
3A2BZ	25.66	4.06	1.593	5.69	6.17	1.084
3A3AZ	25.65	4.35	1.676	5.90	6.50	1.102
3A3BZ	25.74	4.37	1.753	5.95	6.79	1.141
3B1AZ	45.95	11.32	1.852	14.19	12.96	0.913
3B1BZ	45.89	11.26	1.912	14.15	13.38	0.946
3B2AZ	45.73	11.96	1.933	14.64	13.53	0.924
3B2BZ	45.82	11.98	1.953	14.68	13.67	0.931
3B3AZ	45.73	12.83	2.115	15.22	14.81	0.973
3B3BZ	45.78	12.84	2.034	15.20	14.24	0.937
3C1AZ	82.32	26.22	3.107	27.43	26.41	0.963
3C1BZ	82.38	26.41	3.170	27.63	26.95	0.975
3C2AZ	82.49	28.05	3.303	28.92	28.07	0.971
3C2BZ	82.11	27.94	3.317	28.84	28.20	0.978
3C3AZ	82.41	29.78	3.496	30.07	29.72	0.988
3C3BZ	82.35	29.79	3.444	30.09	29.27	0.973
Mean						0.997
Standard Deviation						0.065

Table 4.22

Comparison of Computed and Tested Ultimate Mooments
Beam Specimens - **Group S**
(Based on Dynamic Compressive and Tensile Stresses)

Specimen	w/t (50SK) (1)	$(M_y)_{comp}$ (in.-kips) (2)	$(P_u)_{test}$ (kips) (3)	$(M_u)_{comp}$ (in.-kips) (4)	$(M_u)_{test}$ (in.-kips) (5)	(5)/(4) (6)
3A1AS	24.83	9.83	1.831	11.22	10.53	0.939
3A1BS	24.89	9.81	1.934	11.22	11.12	0.991
3A2AS	24.91	10.29	1.949	11.94	11.21	0.939
3A2BS	24.83	10.23	1.940	11.90	11.16	0.938
3A3AS	24.97	10.47	1.950	12.12	11.21	0.925
3A3BS	24.78	10.37	2.106	12.04	12.11	1.006
3B1AS	42.30	20.27	2.756	22.34	21.02	0.941
3B1BS	42.53	19.98	2.762	22.05	21.06	0.955
3B2AS	42.45	20.72	2.913	23.08	22.21	0.962
3B2BS	42.24	20.85	2.892	23.24	22.05	0.949
3B3AS	42.47	21.08	2.983	23.41	22.75	0.972
3B3BS	42.49	21.09	3.021	23.40	23.04	0.985
3C1AS	69.55	31.45	3.631	34.16	30.86	0.903
3C1BS	69.60	31.25	3.558	33.96	30.24	0.890
3C2AS	69.57	32.73	3.744	36.39	31.82	0.874
3C2BS	69.70	32.69	3.697	36.33	31.43	0.865
3C3AS	69.29	32.45	3.837	36.02	32.62	0.906
3C3BS	69.52	32.99	3.815	36.52	32.43	0.888
Mean						0.935
Standard Deviation						0.040

Table 4.23

Comparison of Computed and Tested Ultimate Mooments
Beam Specimens - **Group K**
(Based on Dynamic Compressive and Tensile Stresses)

Specimen	w/t (25AK) (1)	$(M_y)_{comp}$ (in.-kips) (2)	$(P_u)_{test}$ (kips) (3)	$(M_u)_{comp}$ (in.-kips) (4)	$(M_u)_{test}$ (in.-kips) (5)	(5)/(4) (6)
3A1AK	37.22	9.88	1.886	11.66	10.85	0.931
3A1BK	37.21	9.98	1.873	11.79	10.77	0.913
3A2AK	37.28	10.29	1.979	12.08	11.38	0.942
3A2BK	37.09	10.36	1.983	12.18	11.40	0.936
3A3AK	37.30	10.49	2.062	12.48	11.86	0.950
3A3BK	37.21	10.43	2.110	12.42	12.13	0.977
3B1AK	53.74	22.77	2.965	24.56	22.61	0.921
3B1BK	53.81	22.84	2.987	24.63	22.78	0.925
3B2AK	53.74	23.29	3.123	24.96	23.81	0.954
3B2BK	53.74	23.43	3.015	25.12	22.99	0.915
3B3AK	53.76	23.64	3.221	25.55	24.56	0.961
3B3BK	53.82	23.68	3.315	25.59	25.28	0.988
3C1AK	79.42	36.15	4.284	41.81	36.41	0.871
3C1BK	79.40	36.25	4.358	41.94	37.04	0.883
3C2AK	79.28	38.66	4.483	43.32	38.11	0.880
3C2BK	79.46	38.43	4.594	43.16	39.05	0.905
3C3AK	79.45	39.13	4.604	43.96	39.13	0.890
3C3BK	79.46	39.20	4.623	44.03	39.30	0.893
Mean						0.924
Standard Deviation						0.033

Table 4.24

Measured Deflections under Yield Moments and Ultimate Moments
(Beam Specimens - **Group W**)

Specimen	w/t (25AK) (1)	$(d)_{My}$ (in.) (2)	$(d)_{My}/L$ (3)	$(d)_{Mu}$ (in.) (4)	$(d)_{Mu}/L$ (5)	L, Span Length (in.) (6)
3A1AW	9.33	0.352	0.011	--	--	31.0
3A1BW	9.26	0.334	0.011	2.794	0.090	31.0
3A2AW	9.35	--	--	--	--	31.0
3A2BW	9.63	0.364	0.012	2.849	0.092	31.0
3A3AW	9.30	0.385	0.012	--	--	31.0
3A3BW	9.51	0.393	0.013	2.705	0.087	31.0
3B1AW	28.56	0.772	0.014	1.784	0.032	56.0
3B1BW	28.70	0.788	0.014	1.736	0.031	56.0
3B2AW	28.72	--	--	1.736	0.031	56.0
3B2BW	28.83	--	--	--	--	56.0
3B3AW	28.60	0.882	0.016	1.903	0.034	56.0
3B3BW	28.62	0.903	0.016	1.986	0.035	56.0
3C1AW	63.28	0.646	0.010	0.646	0.010	68.0
3C1BW	63.29	0.659	0.010	0.659	0.010	68.0
3C2AW	63.25	0.720	0.011	0.720	0.011	68.0
3C2BW	63.21	0.720	0.011	0.720	0.011	68.0
3C3AW	63.30	0.715	0.011	0.715	0.011	68.0
3C3BW	63.33	0.703	0.010	0.703	0.010	68.0

Note: $(d)_{My}$ represents the measured deflection under yield moment.
$(d)_{Mu}$ represents the measured deflection under ultimate moment.

Table 4.25

Measured Deflections under Yield Moments and Ultimate Moments
(Beam Specimens - **Group Z**)

Specimen	w/t (50SK) (1)	$(d)_{My}$ (in.) (2)	$(d)_{My}/L$ (3)	$(d)_{Mu}$ (in.) (4)	$(d)_{Mu}/L$ (5)	Span Length (in.) (6)
3A1AZ	25.62	0.366	0.012	2.310	0.075	31.0
3A1BZ	25.61	0.362	0.012	2.358	0.076	31.0
3A2AZ	25.73	0.389	0.013	2.387	0.077	31.0
3A2BZ	25.66	0.372	0.012	2.360	0.076	31.0
3A3AZ	25.65	0.398	0.013	2.209	0.071	31.0
3A3BZ	25.74	0.392	0.013	2.223	0.072	31.0
3B1AZ	45.95	--	--	--	--	56.0
3B1BZ	45.89	0.780	0.014	4.283	0.076	56.0
3B2AZ	45.73	0.779	0.014	4.393	0.078	56.0
3B2BZ	45.82	0.791	0.014	4.430	0.079	56.0
3B3AZ	45.73	0.853	0.015	4.525	0.081	56.0
3B3BZ	45.78	0.846	0.015	4.608	0.082	56.0
3C1AZ	82.32	0.798	0.012	2.193	0.032	68.0
3C1BZ	82.38	0.823	0.012	2.026	0.030	68.0
3C2AZ	82.49	0.881	0.013	2.059	0.030	68.0
3C2BZ	82.11	0.901	0.013	2.114	0.031	68.0
3C3AZ	82.41	0.876	0.013	--	--	68.0
3C3BZ	82.35	0.931	0.014	2.127	0.031	68.0

Note: $(d)_{My}$ represents the measured deflection under yield moment.
$(d)_{Mu}$ represents the measured deflection under ultimate moment.

Table 4.26

Measured Deflections under Yield Moments and Ultimate Moments
(Beam Specimens - **Group S**)

Specimen	w/t (50SK) (1)	$(d)_{My}$ (in.) (2)	$(d)_{My}/L$ (3)	$(d)_{Mu}$ (in.) (4)	$(d)_{Mu}/L$ (5)	Span Length (in.) (6)
3A1AS	24.83	0.813	0.018	1.347	0.029	46.0
3A1BS	24.89	0.880	0.019	1.574	0.034	46.0
3A2AS	24.91	0.848	0.018	1.410	0.031	46.0
3A2BS	24.83	0.857	0.019	1.483	0.032	46.0
3A3AS	24.97	0.869	0.019	1.352	0.029	46.0
3A3BS	24.78	0.877	0.019	1.542	0.034	46.0
3B1AS	42.30	1.079	0.018	1.209	0.020	61.0
3B1BS	42.53	1.027	0.017	1.123	0.180	61.0
3B2AS	42.45	1.142	0.019	1.224	0.200	61.0
3B2BS	42.24	1.089	0.018	1.207	0.020	61.0
3B3AS	42.47	1.112	0.018	1.233	0.020	61.0
3B3BS	42.49	1.163	0.019	1.246	0.020	61.0
3C1AS	69.55	0.785	0.012	1.095	0.016	68.0
3C1BS	69.60	0.741	0.011	1.069	0.016	68.0
3C2AS	69.57	0.816	0.012	1.131	0.017	68.0
3C2BS	69.70	0.776	0.011	1.064	0.016	68.0
3C3AS	69.29	0.830	0.012	1.123	0.017	68.0
3C3BS	69.52	0.815	0.012	1.109	0.016	68.0

Note: $(d)_{My}$ represents the measured deflection under yield moment.
$(d)_{Mu}$ represents the measured deflection under ultimate moment.

Table 4.27

Measured Deflections under Yield Moments and Ultimate Moments
(Beam Specimens - **Group K**)

Specimen	w/t (25AK) (1)	$(d)_{My}$ (in.) (2)	$(d)_{My}/L$ (3)	$(d)_{Mu}$ (in.) (4)	$(d)_{Mu}/L$ (5)	Span Length (in.) (6)
3A1AK	37.22	0.909	0.020	2.576	0.056	46.0
3A1BK	37.21	0.861	0.019	2.539	0.055	46.0
3A2AK	37.28	0.873	0.019	2.614	0.057	46.0
3A2BK	37.09	0.890	0.019	2.413	0.052	46.0
3A3AK	37.30	0.888	0.019	2.438	0.053	46.0
3A3BK	37.21	0.902	0.020	2.549	0.055	46.0
3B1AK	53.74	1.165	0.019	1.931	0.032	61.0
3B1BK	53.81	1.140	0.019	1.894	0.031	61.0
3B2AK	53.74	1.184	0.019	1.951	0.032	61.0
3B2BK	53.74	1.171	0.019	2.046	0.034	61.0
3B3AK	53.76	1.165	0.019	1.996	0.033	61.0
3B3BK	53.82	1.173	0.019	2.122	0.035	61.0
3C1AK	79.42	0.993	0.015	1.758	0.026	68.0
3C1BK	79.40	1.135	0.017	1.764	0.026	68.0
3C2AK	79.28	1.196	0.018	1.864	0.027	68.0
3C2BK	79.46	1.158	0.017	1.884	0.028	68.0
3C3AK	79.45	--	--	--	--	68.0
3C3BK	79.46	--	--	--	--	68.0

Note: $(d)_{My}$ represents the measured deflection under yield moment.
$(d)_{Mu}$ represents the measured deflection under ultimate moment.

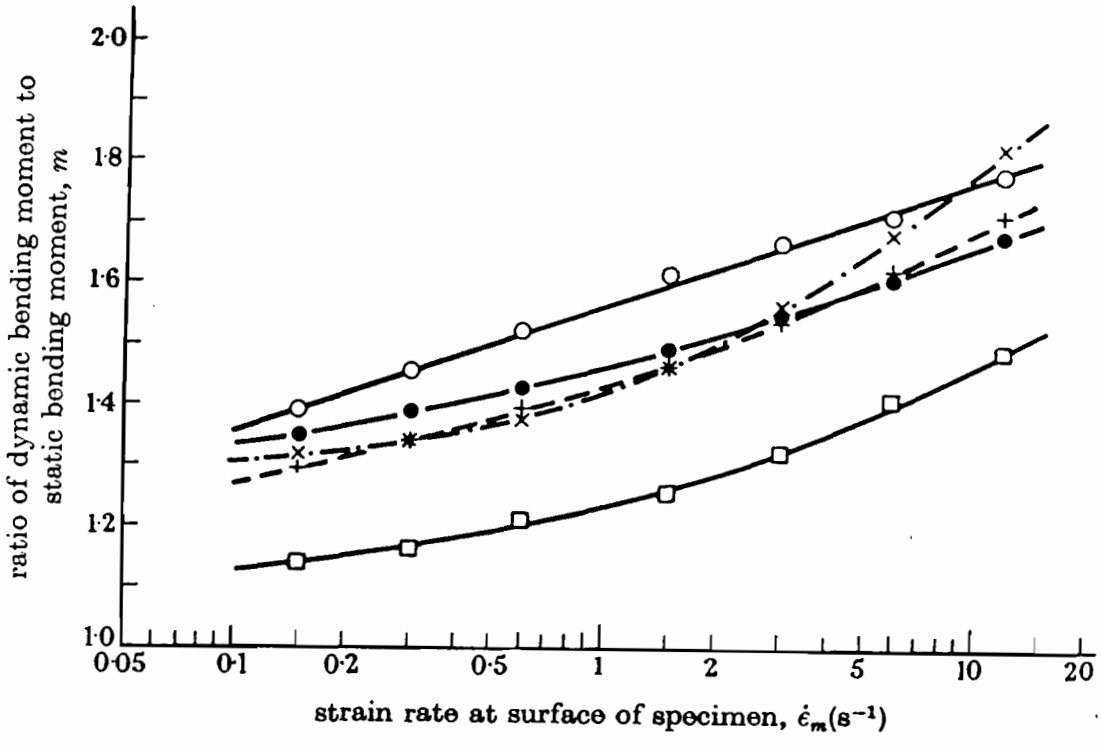

Figure 2.1 Variation of Upper and Lower Yield Moments with Strain Rate at Surface of a Specimen[14]

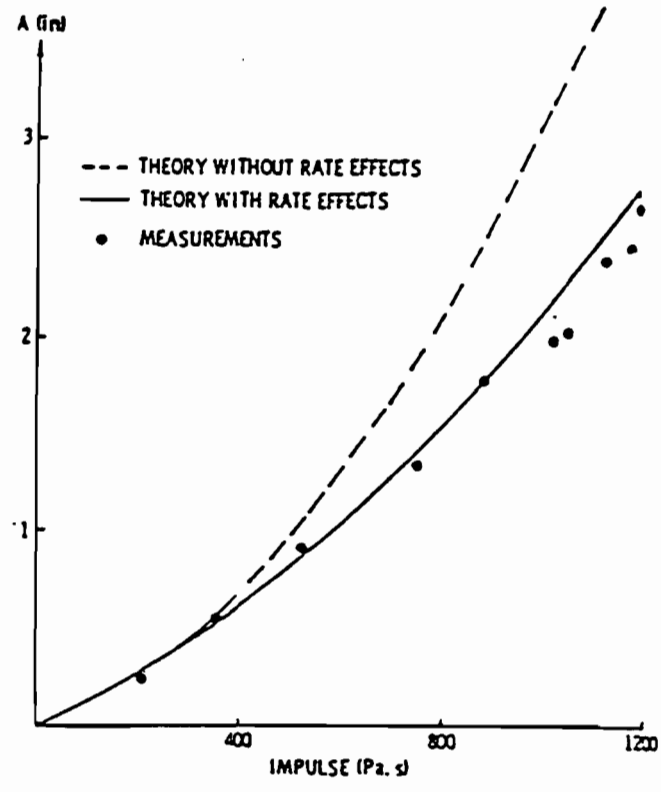

(a) AISI 1018 Steel Beams[80]

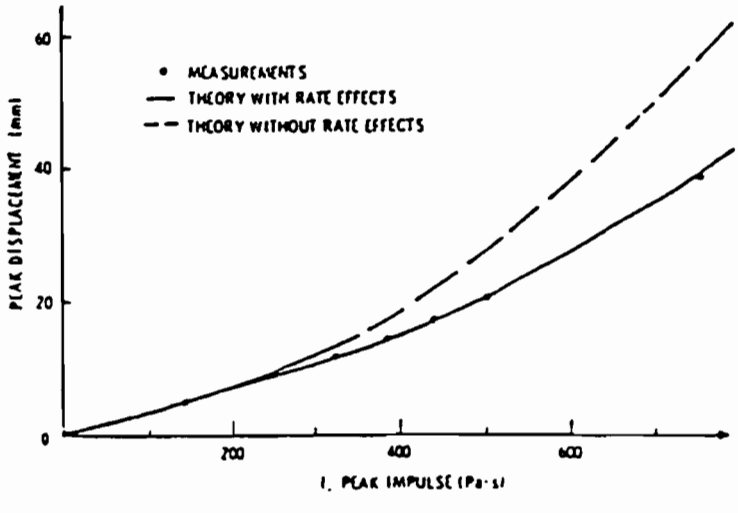

(b) Type 304 Stainless Steel Beams[79]

Figure 2.2 Peak Displacement Versus Impulse[17]

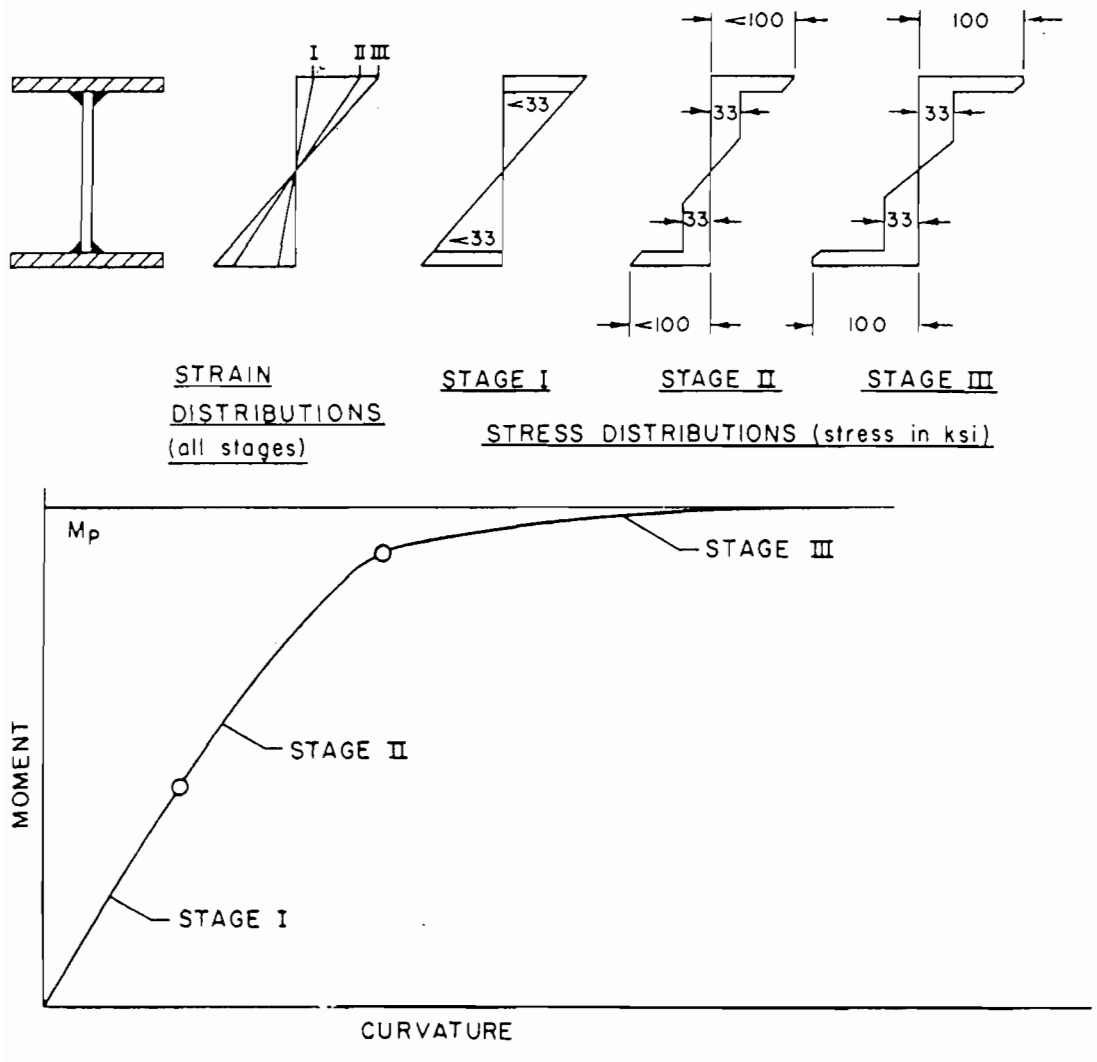

Figure 2.3 Structural Behavior of a Hybrid Steel Beam[20]

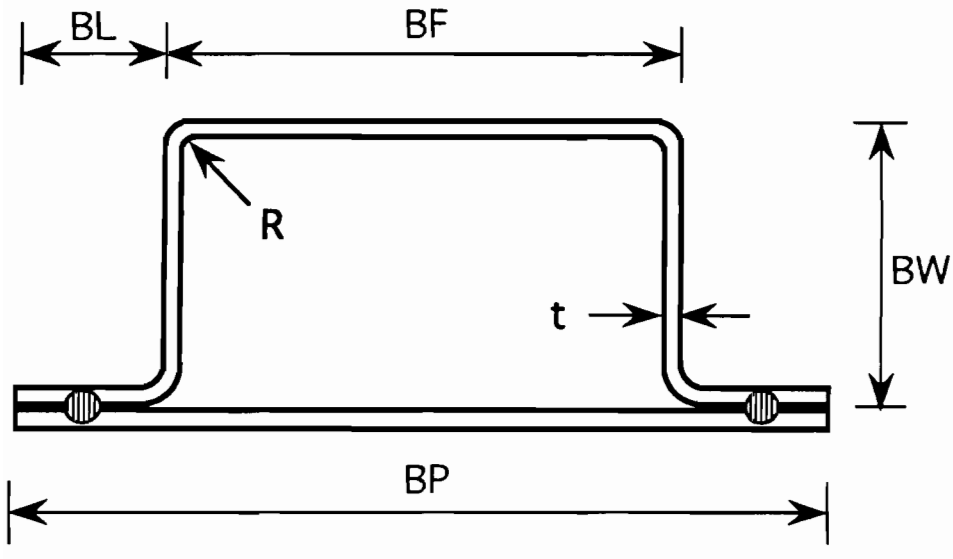

Specimen Configuration

Figure 3.1 Configuration of Beam Specimens

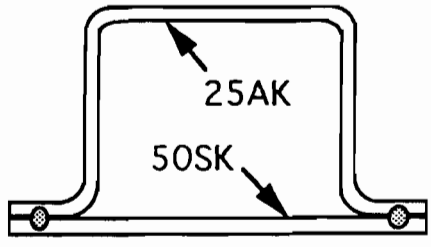

Group W

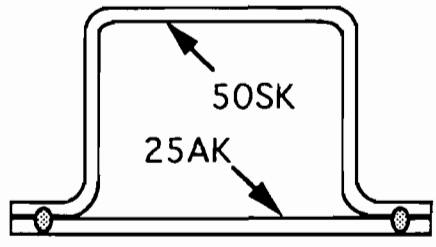

Group S

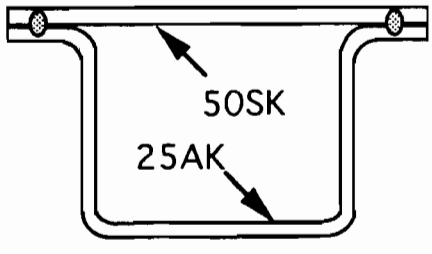

Group Z

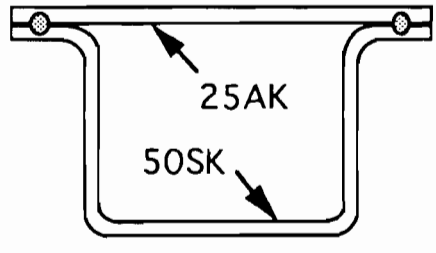

Group K

Figure 3.2 Cross Section of Beams Used in This Study

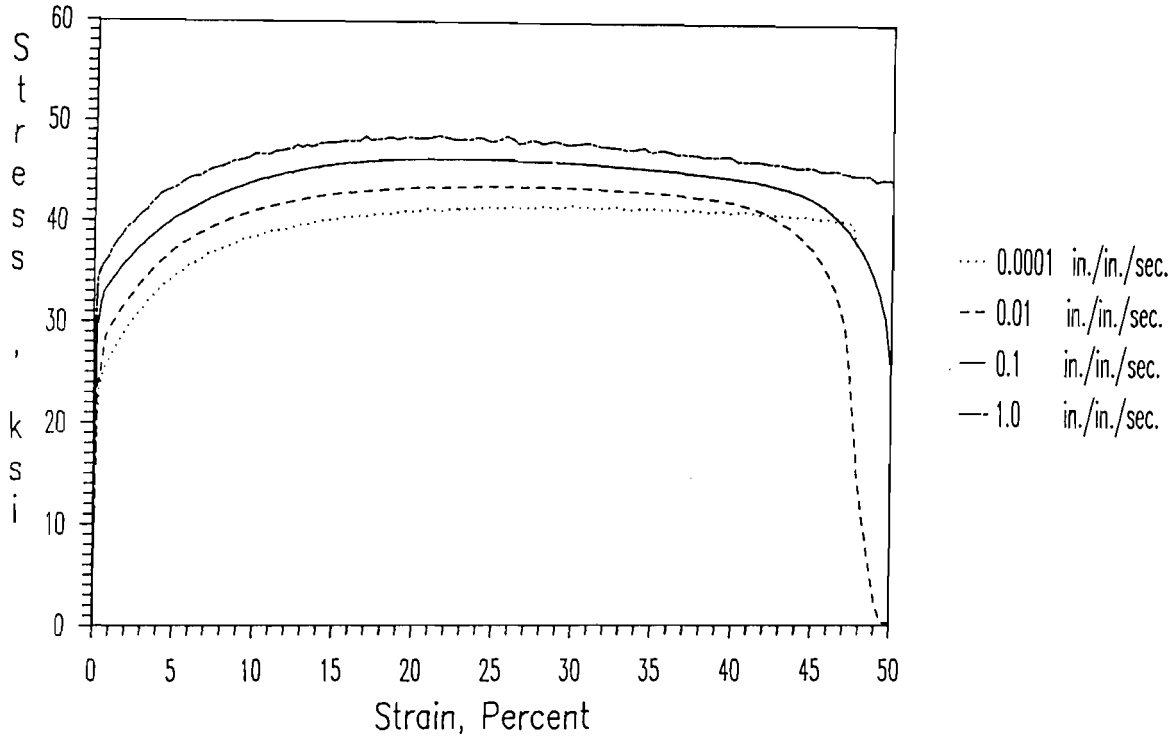

Figure 3.3 Stress-Strain Curves for 25AK Steel in Longitudinal Tension under Different Strain Rates

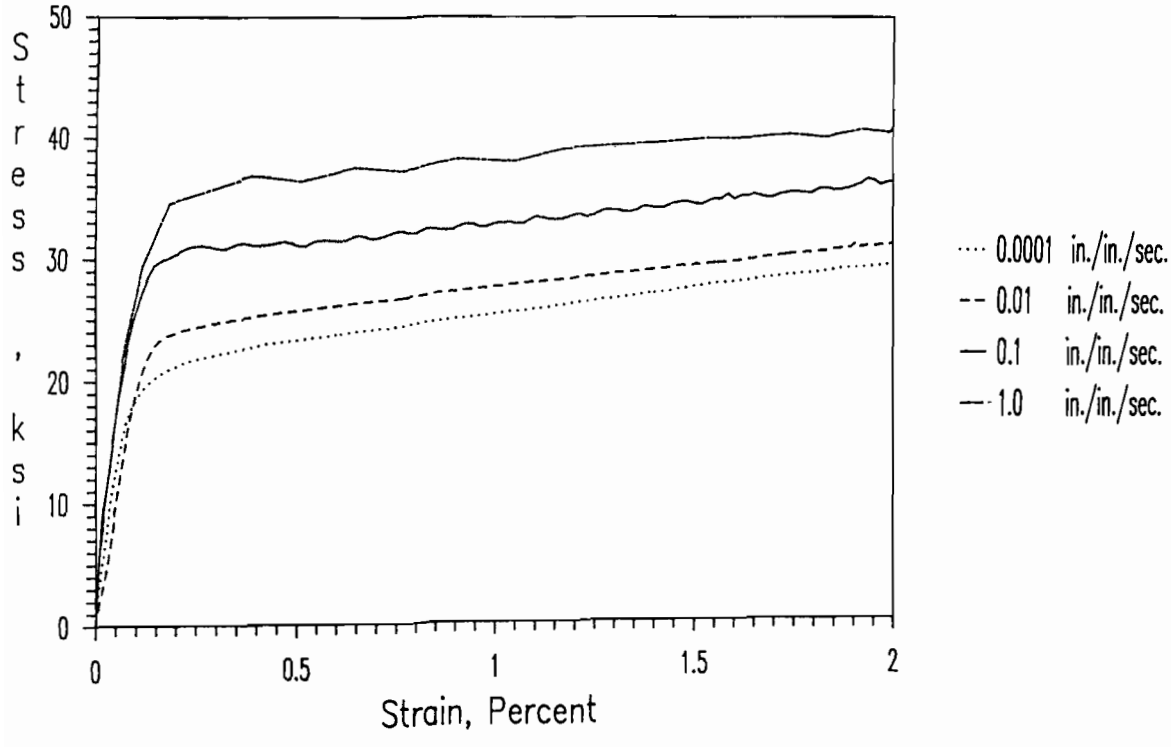

Figure 3.4 Stress-Strain Curves for 25AK Steel in Longitudinal Compression under Different Strain Rates

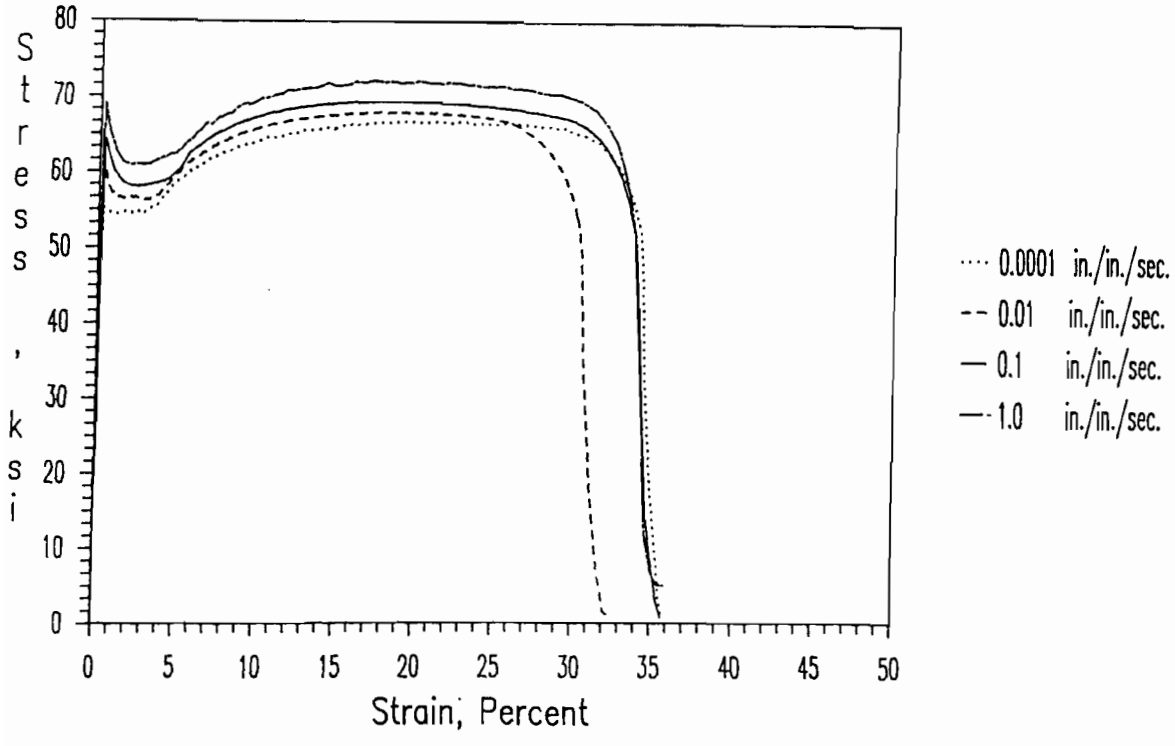

Figure 3.5 Stress-Strain Curves for 50SK Steel in Longitudinal Tension under Different Strain Rates

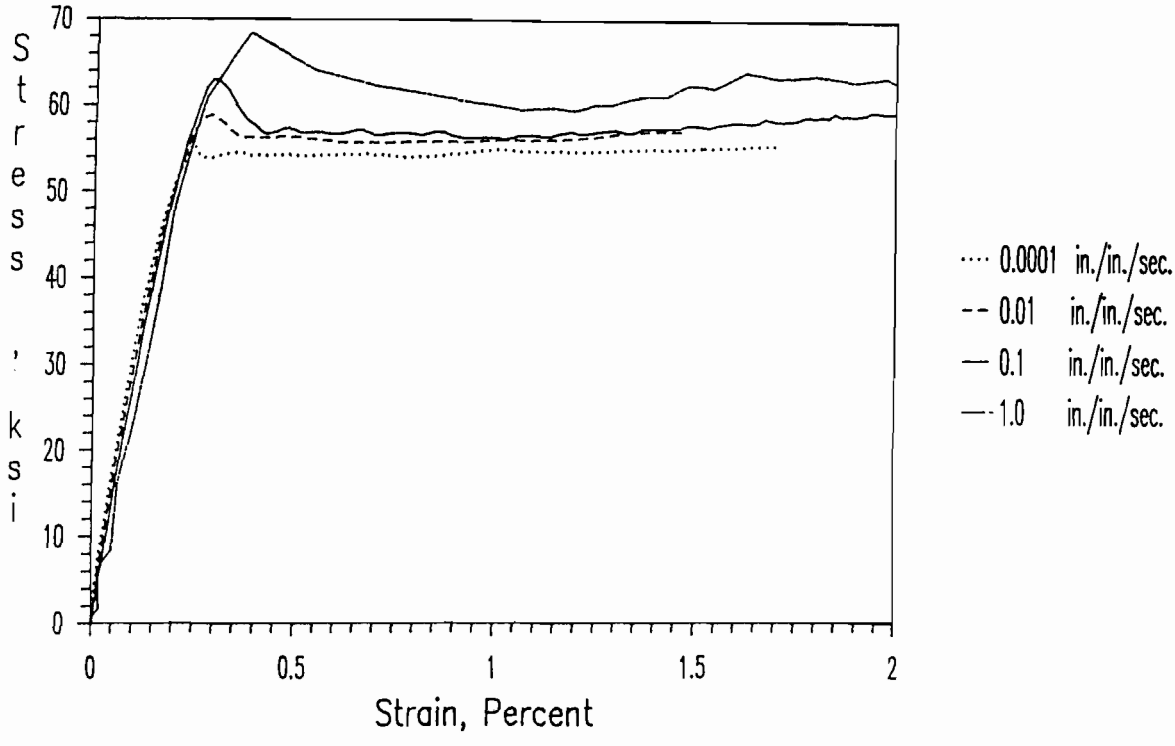

Figure 3.6 Stress-Strain Curves for 50SK Steel in Longitudinal Compression under Different Strain Rates

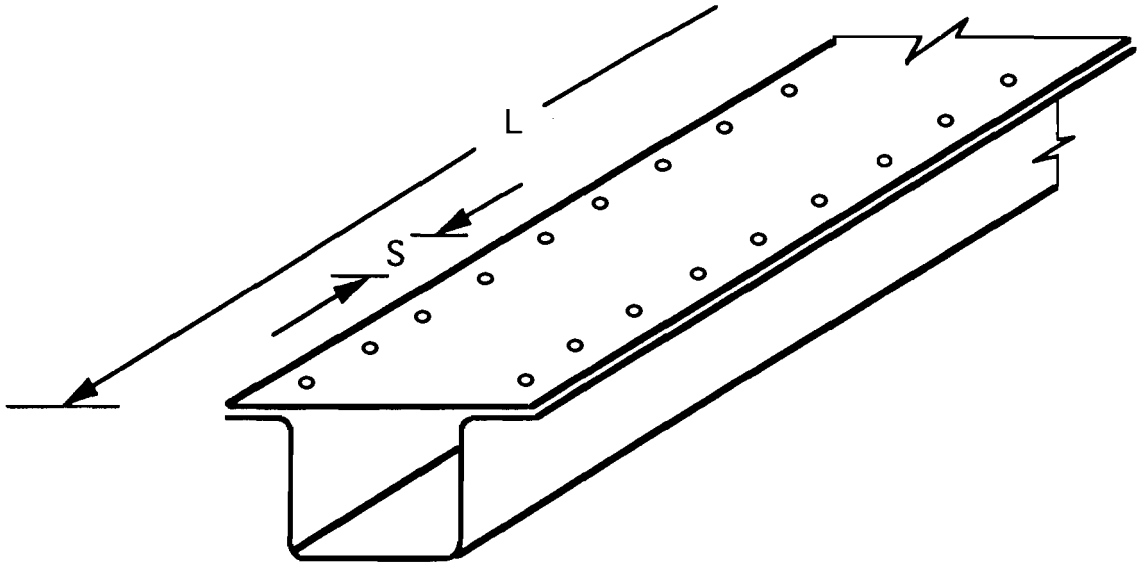

L : Length of Specimen (Ranged from 35" to 72")

S : Spacing of Spot Welding (Equal to 1 in. for All Specimens)

Figure 3.7 Location of Spot Welds for Beam Specimens

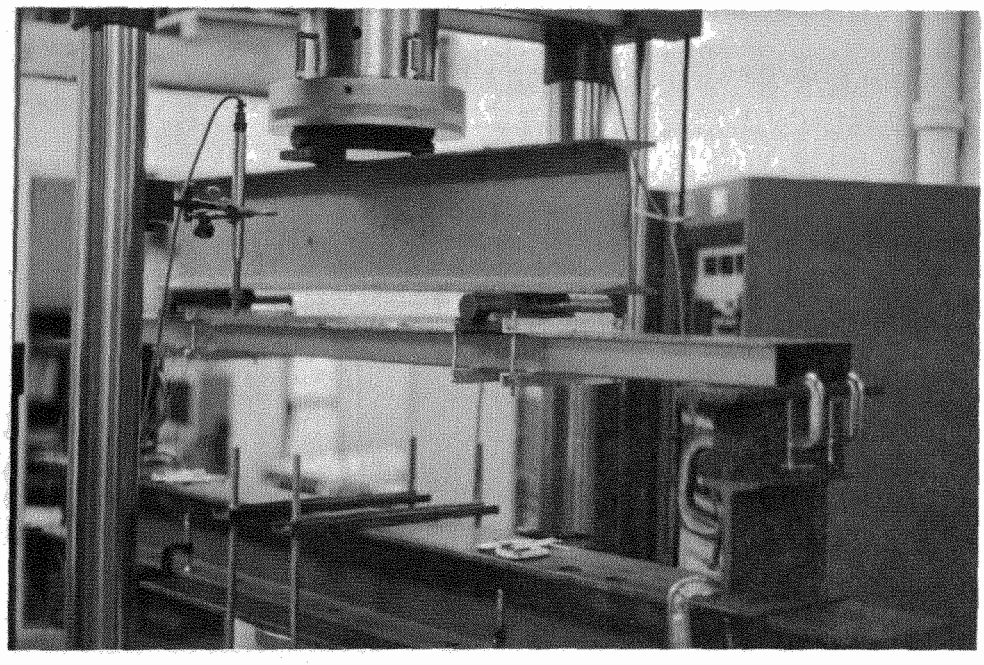

Figure 3.8 Test Setup for Groups Z and K Specimens

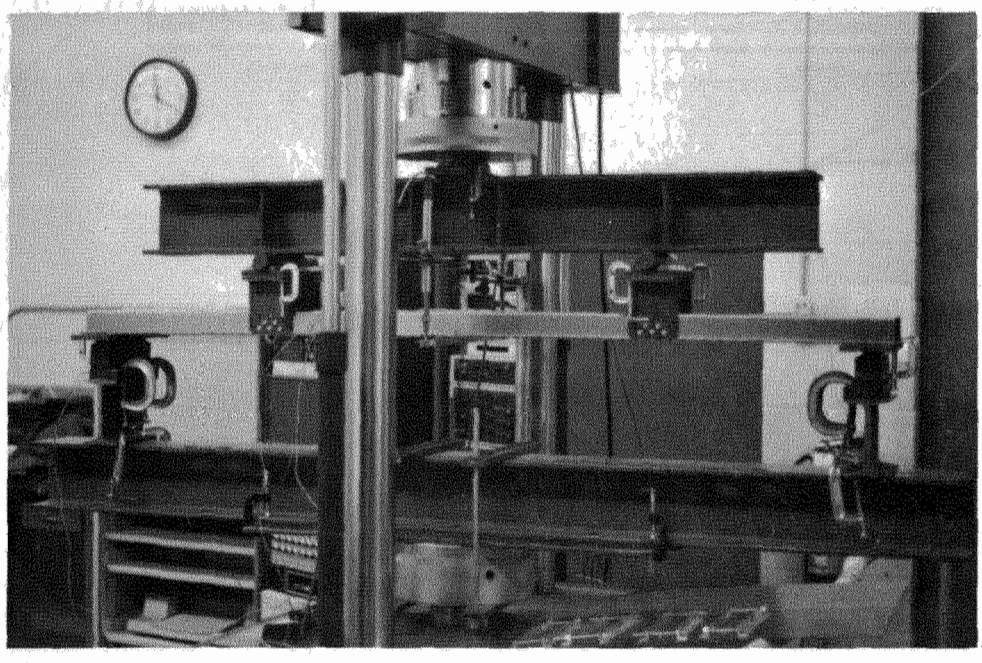

Figure 3.9 Test Setup for Groups W and S Specimens

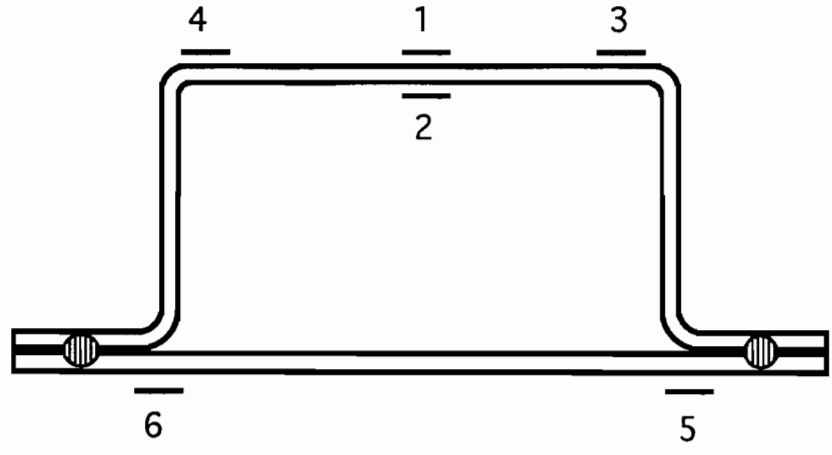

(a) Group W and Group S

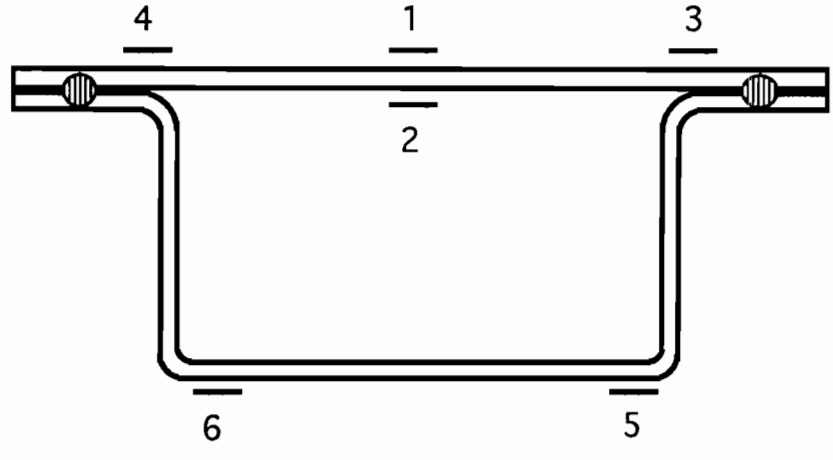

(b) Group Z and Group K

Figure 3.10 Locations of Strain Gages at Midspan Section of Beams

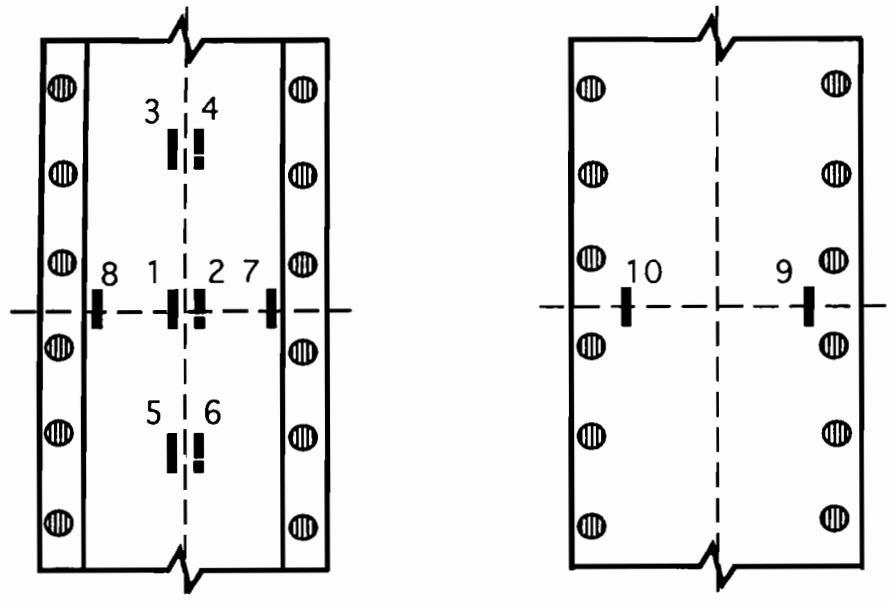

(Top View) (Bottom View)

(a) Group W and Group S

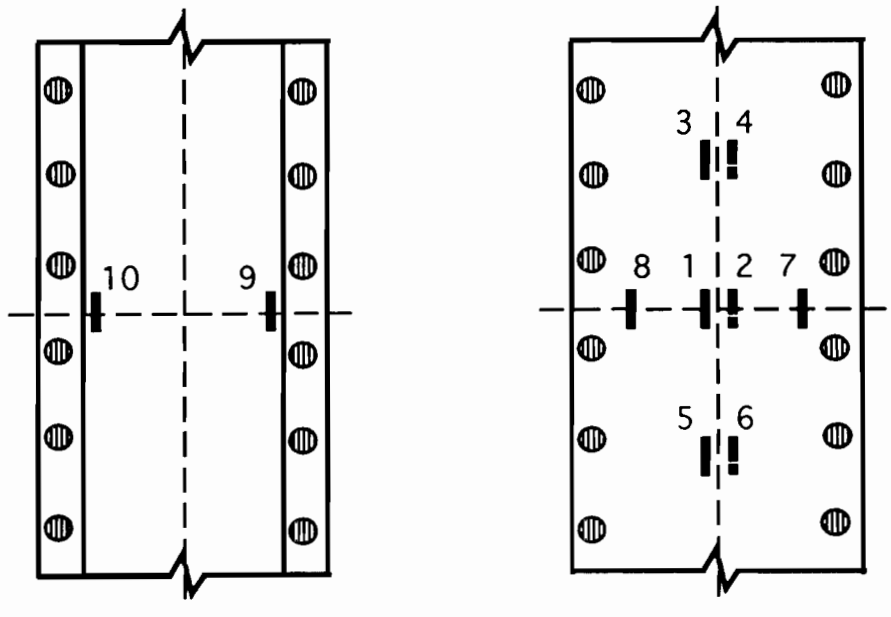

(Bottom View) (Top View)

(b) Group Z and Group K

Figure 3.11 Locations of Strain Gages on Beams Having Middle and Large w/t Ratios

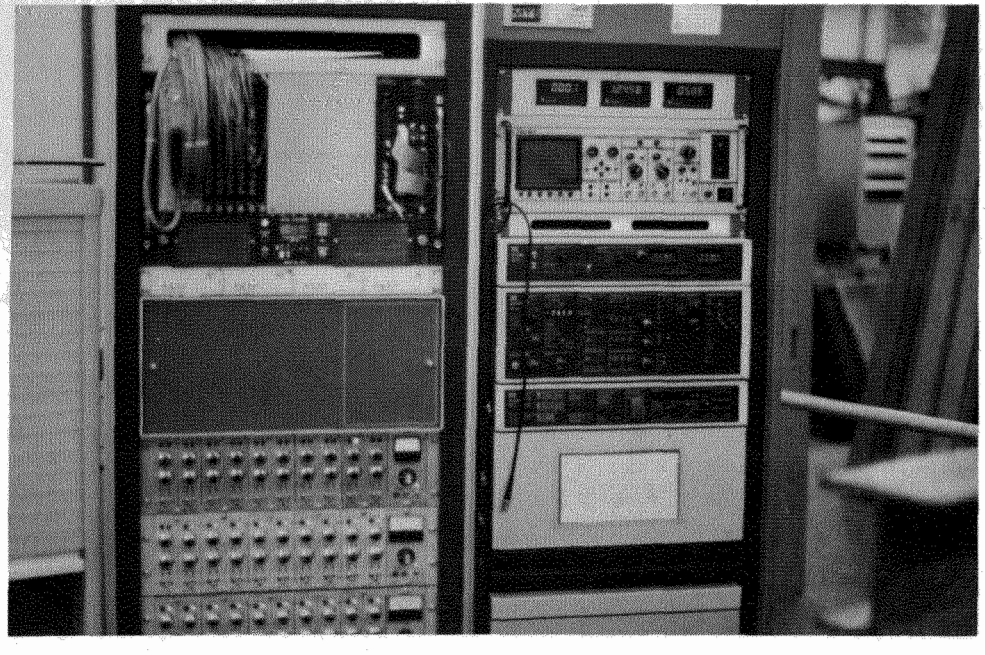

Figure 3.12 880 Material Test System and Data Acquisition System

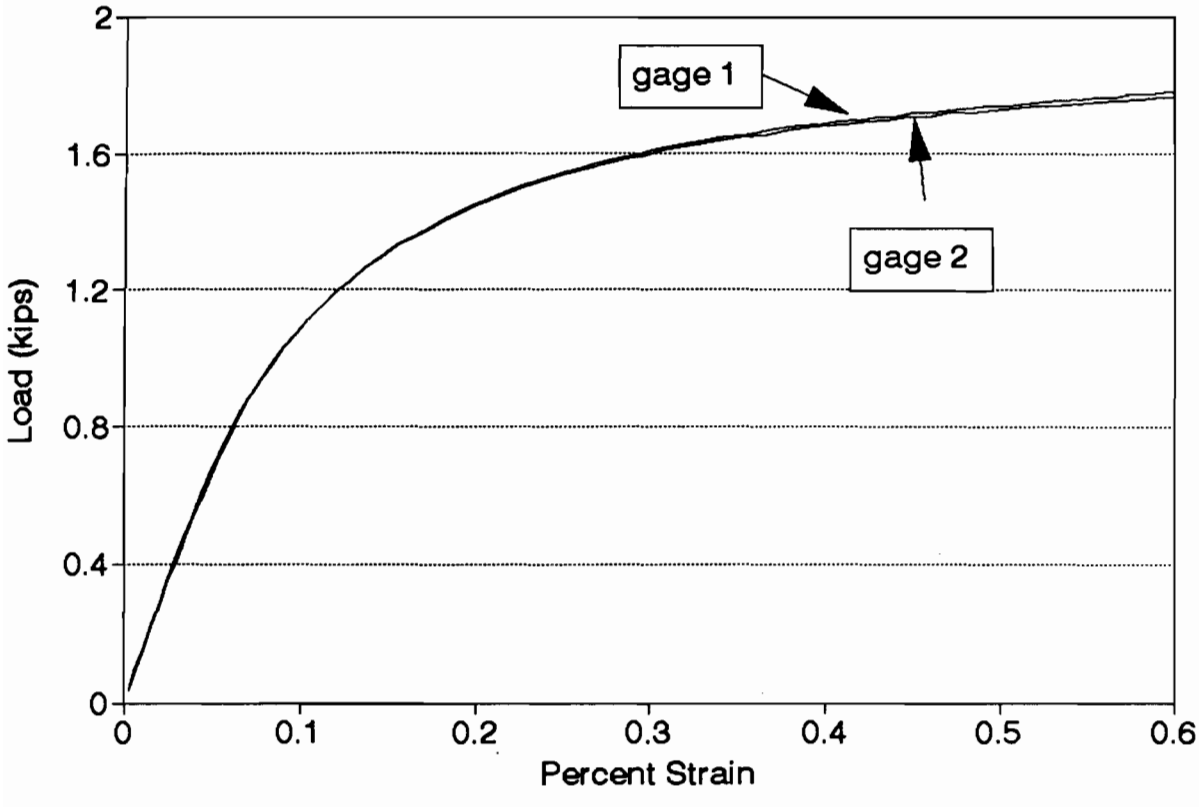

Figure 3.13 Load-Strain Curves of Strain Gages #1 and #2 Installed at the Center of Stiffened Elements (Spec. 1B1AW)

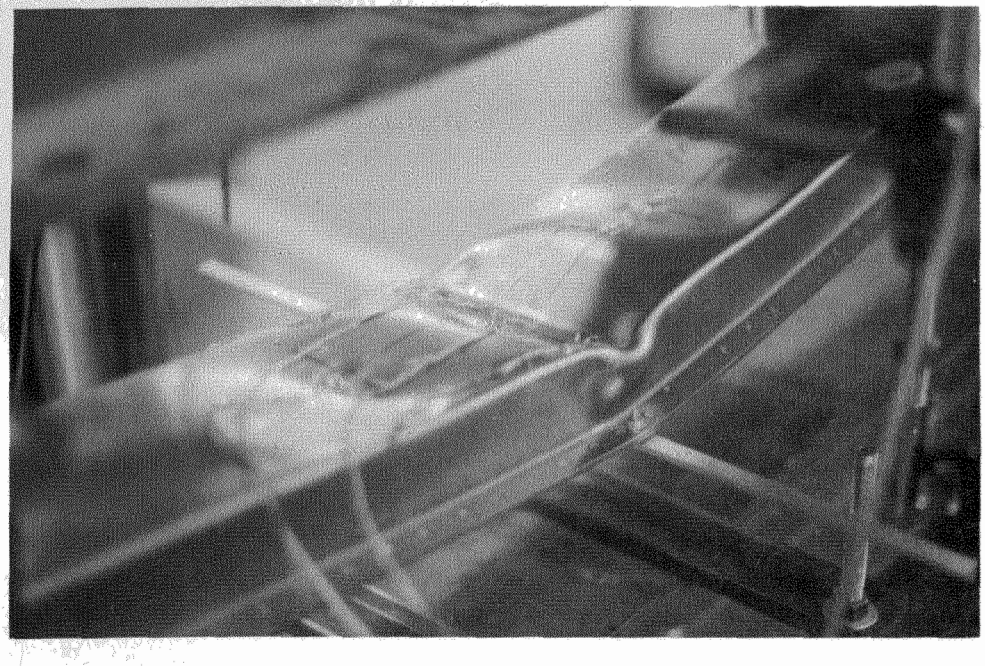

Figure 3.14 Typical Failure of a Beam with Large w/t Ratio (Spec. 3C3BW)

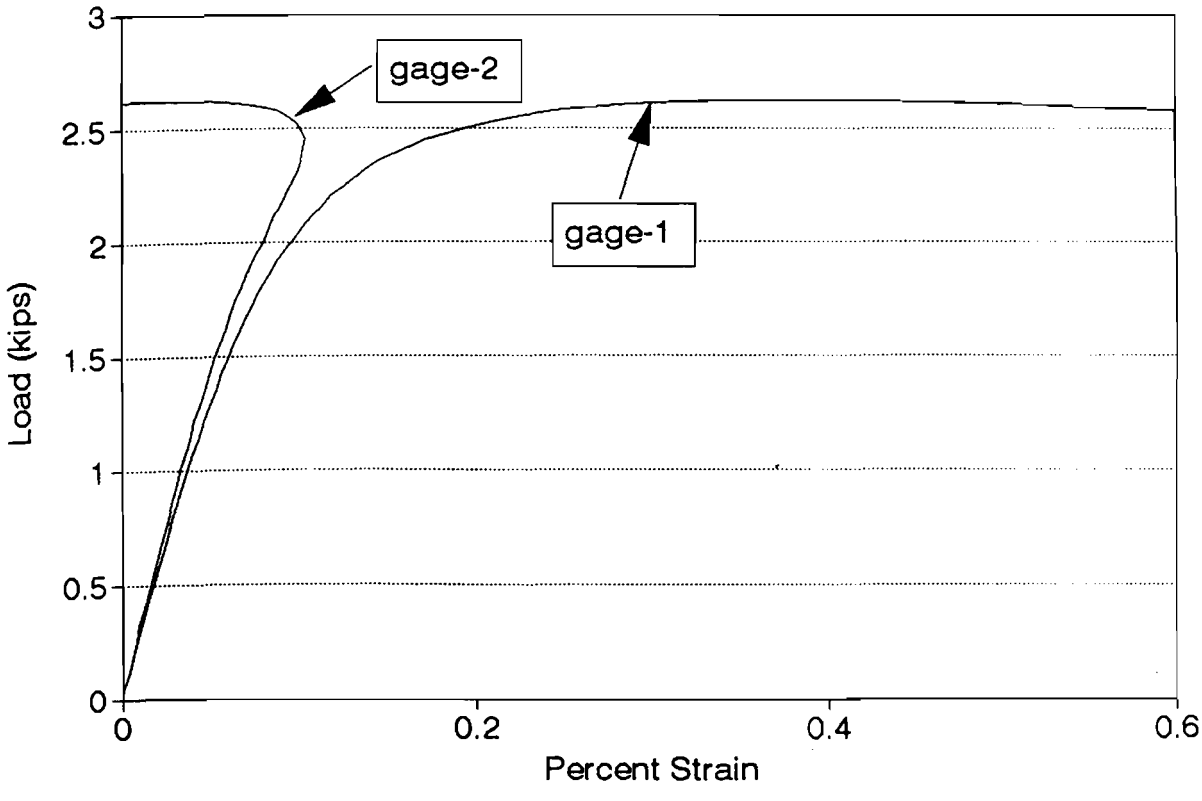

Figure 3.15 Load-Strain Curves of Strain Gages #1 and #2 Installed at the Center of Stiffened Elements (Spec. 3C2AW)

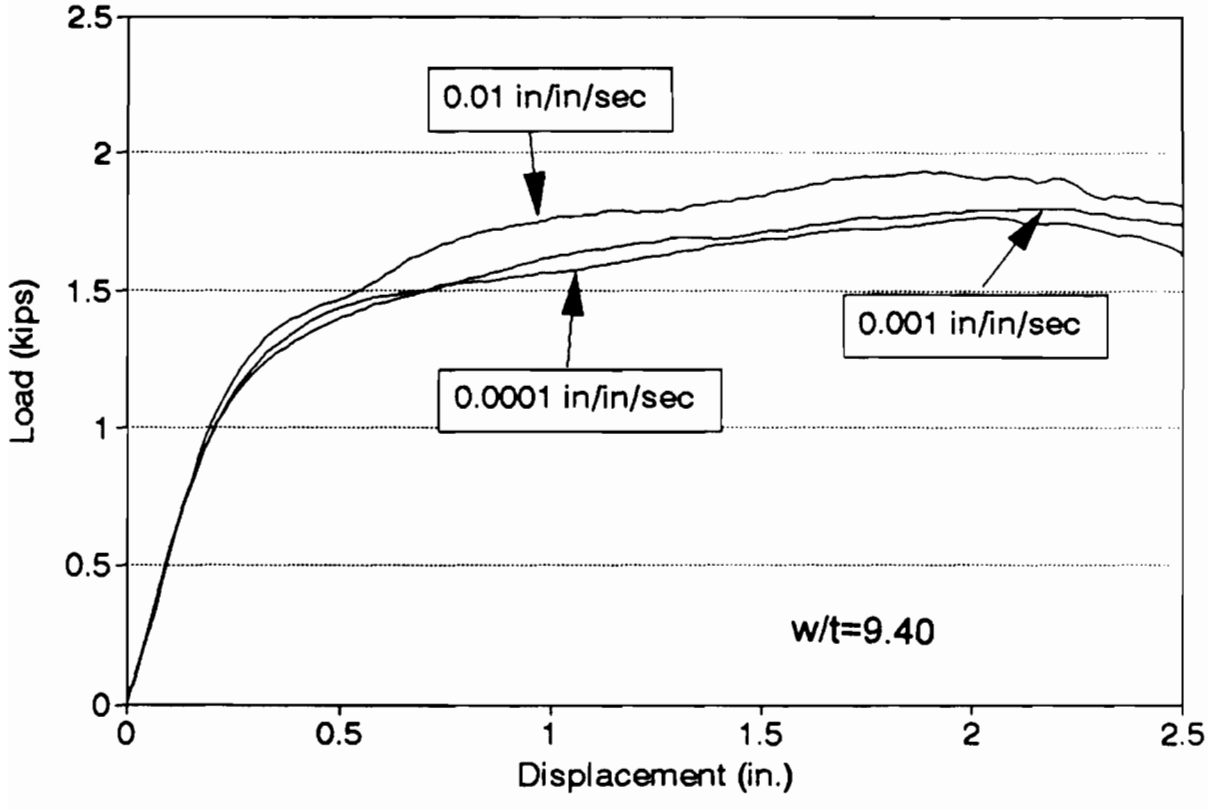

Figure 3.16 Load-Displacement Curves for Case 1 of Group W Secimens 3A1BW, 3A2BW, and 3A3BW

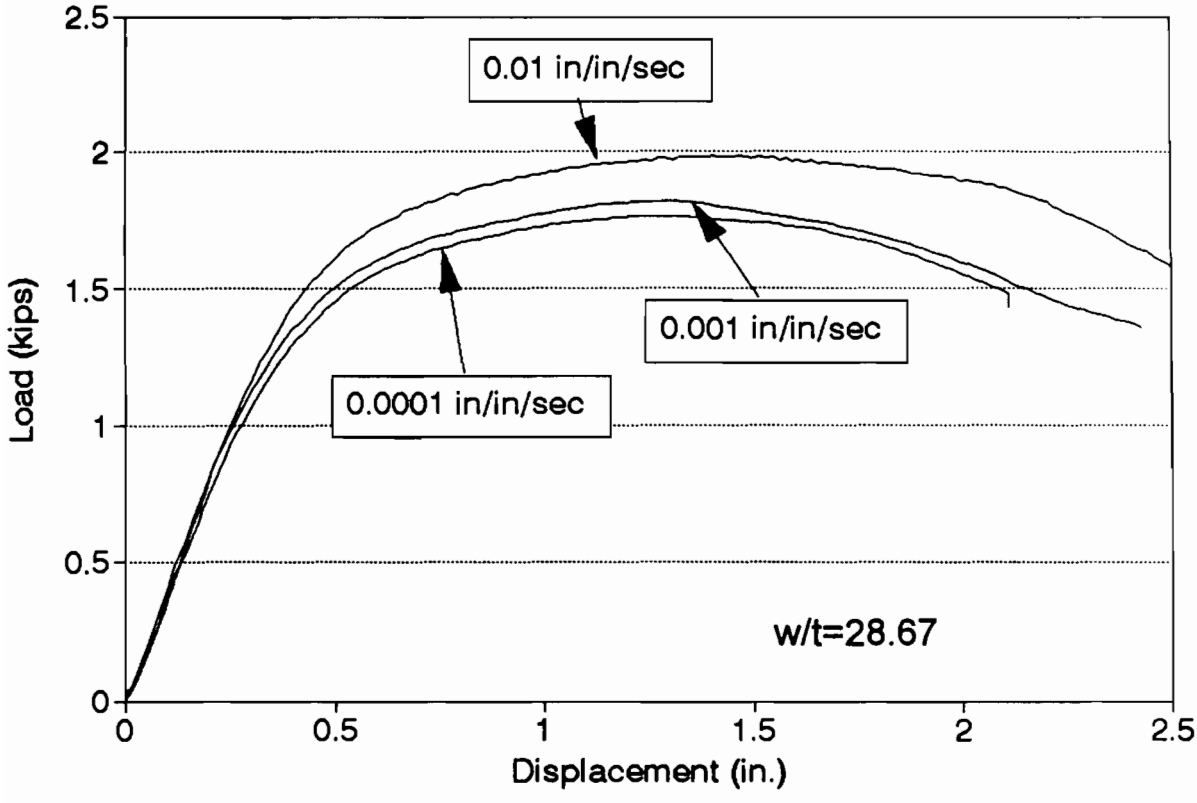

Figure 3.17 Load-Displacement Curves for Case 2 of Group W Secimens 3B1BW, 3B2AW, and 3B3AW

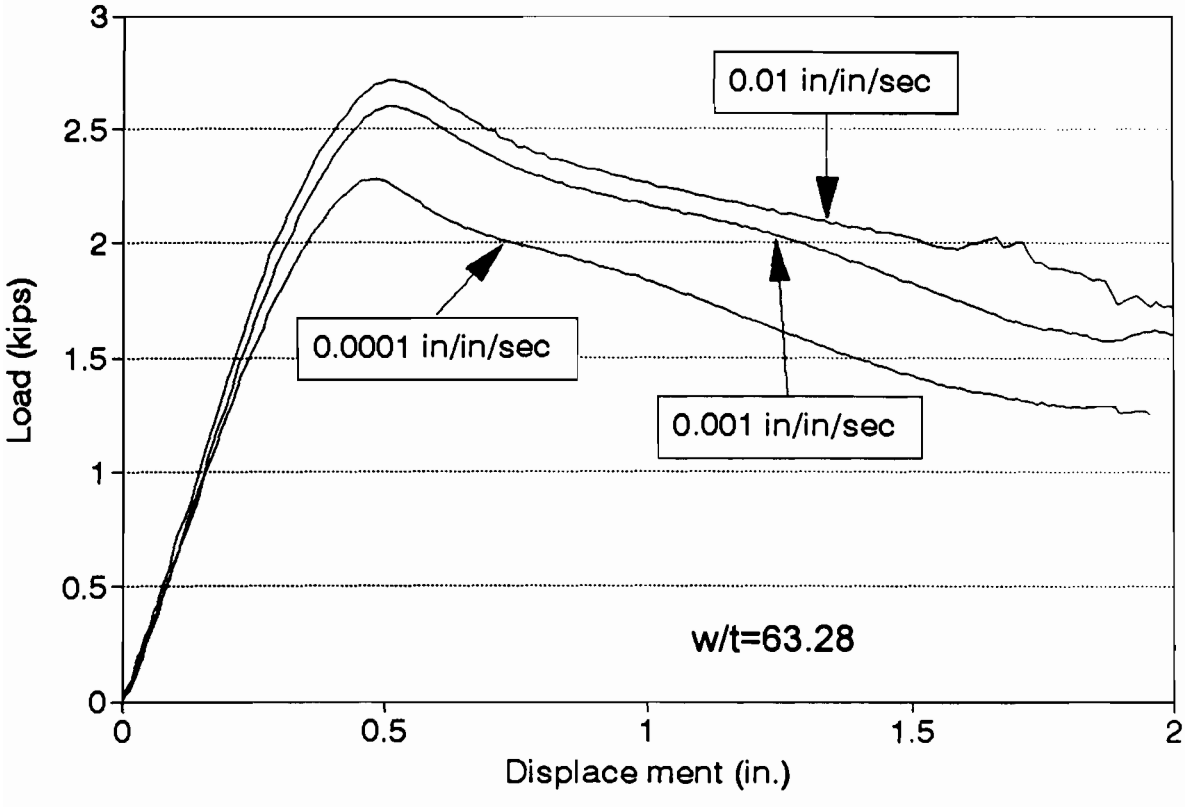

Figure 3.18 Load-Displacement Curves for Case 3 of Group W Secimens 3C1BW, 3C2AW, and 3C3AW

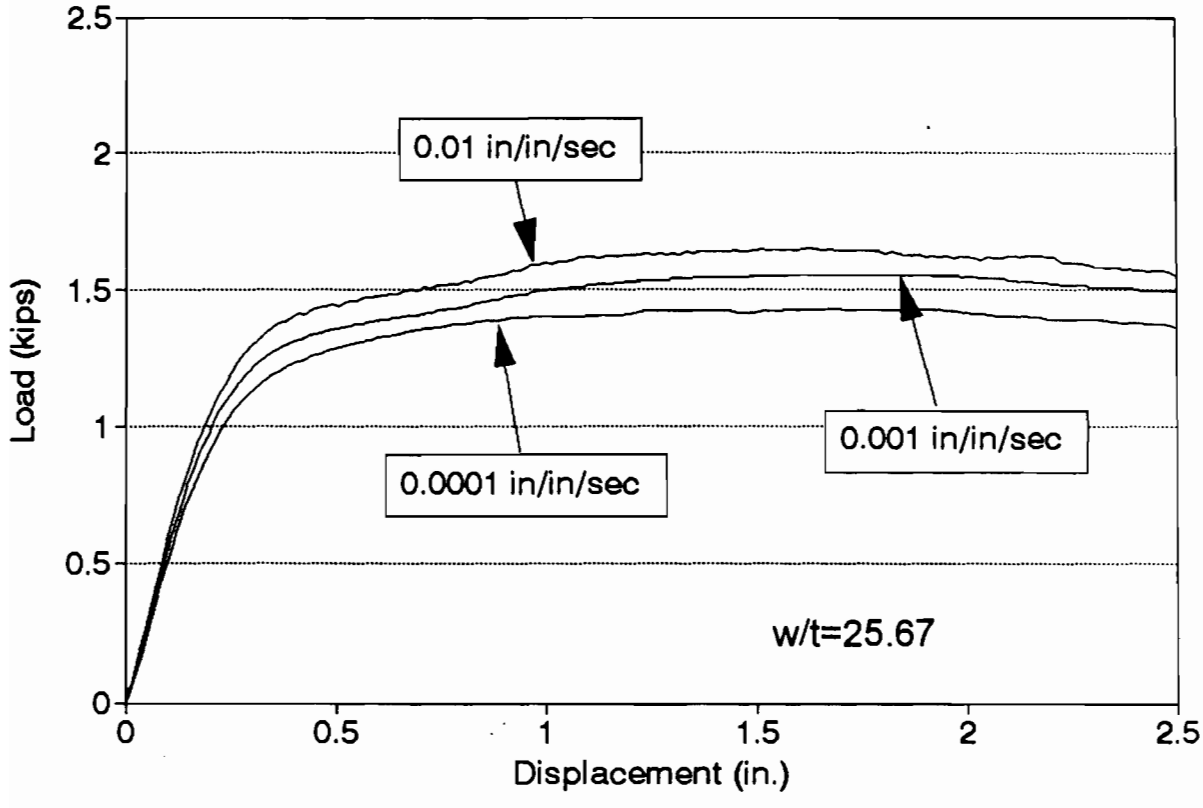

Figure 3.19 Load-Displacement Curves for Case 1 of Group Z Secimens 3A1AZ, 3A2BZ, and 3A3BZ

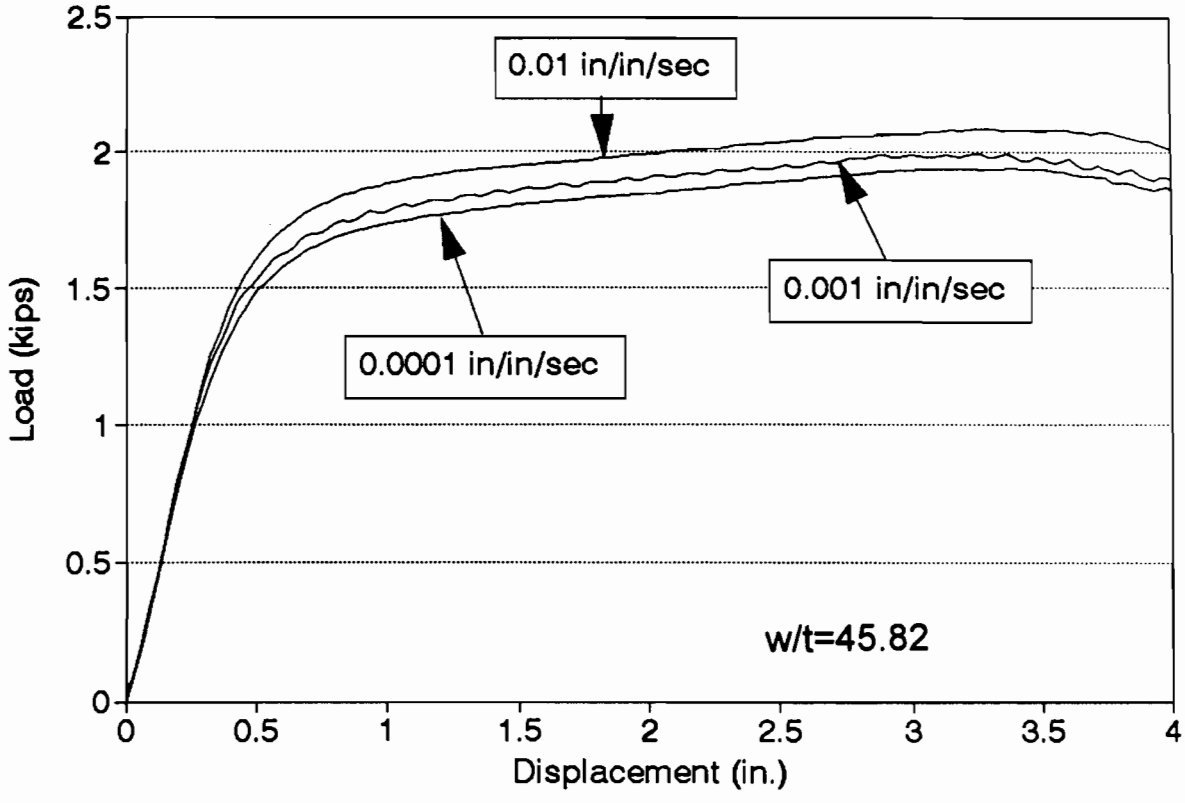

Figure 3.20 Load-Displacement Curves for Case 2 of Group Z Secimens 3B1BZ, 3B2BZ, and 3B3AZ

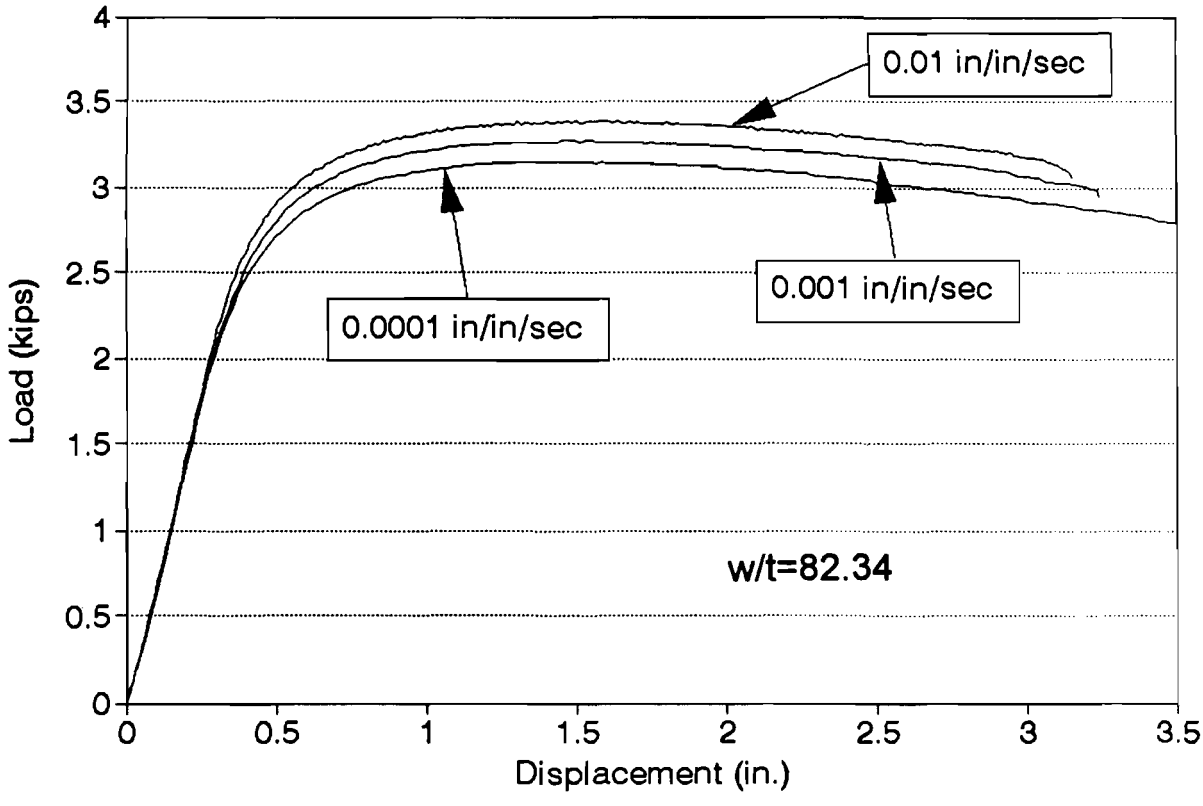

Figure 3.21 Load-Displacement Curves for Case 3 of Group Z Secimens 3C1BZ, 3C2AZ, and 3C3BZ

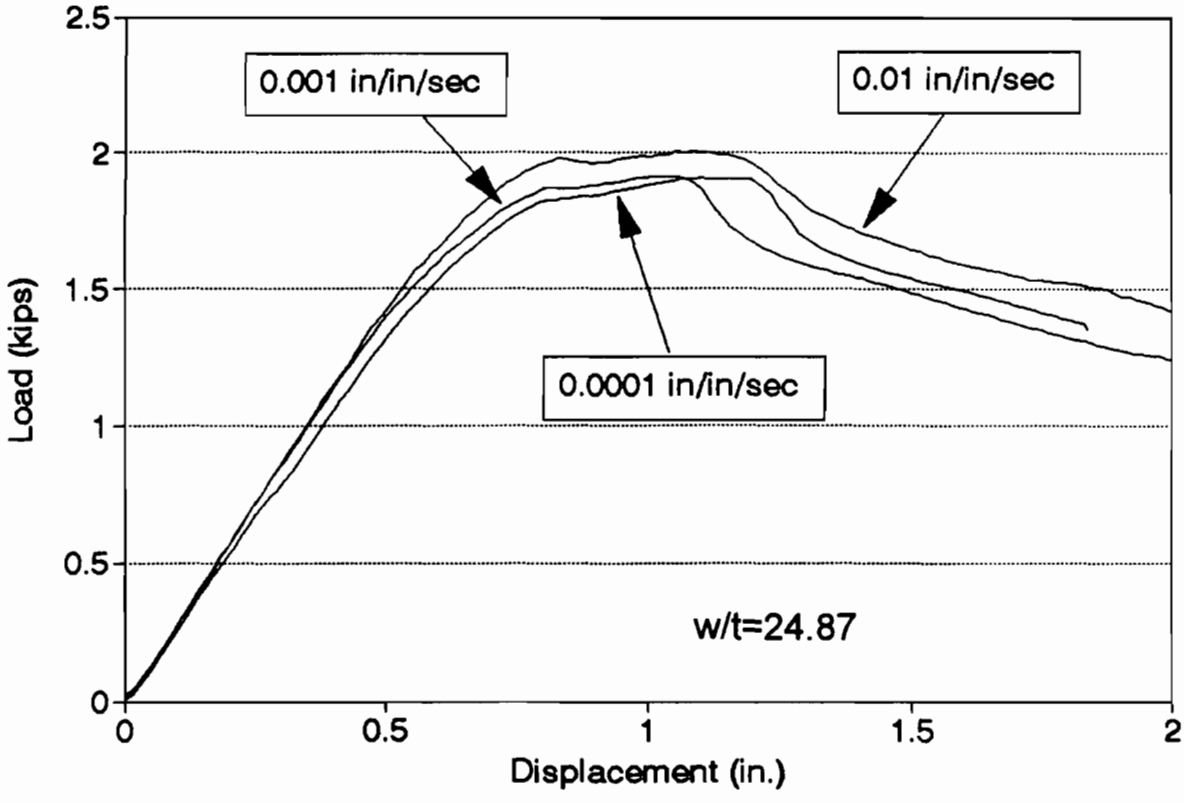

Figure 3.22 Load-Displacement Curves for Case 1 of Group S Secimens 3A1BS, 3A2AS, and 3A3BS

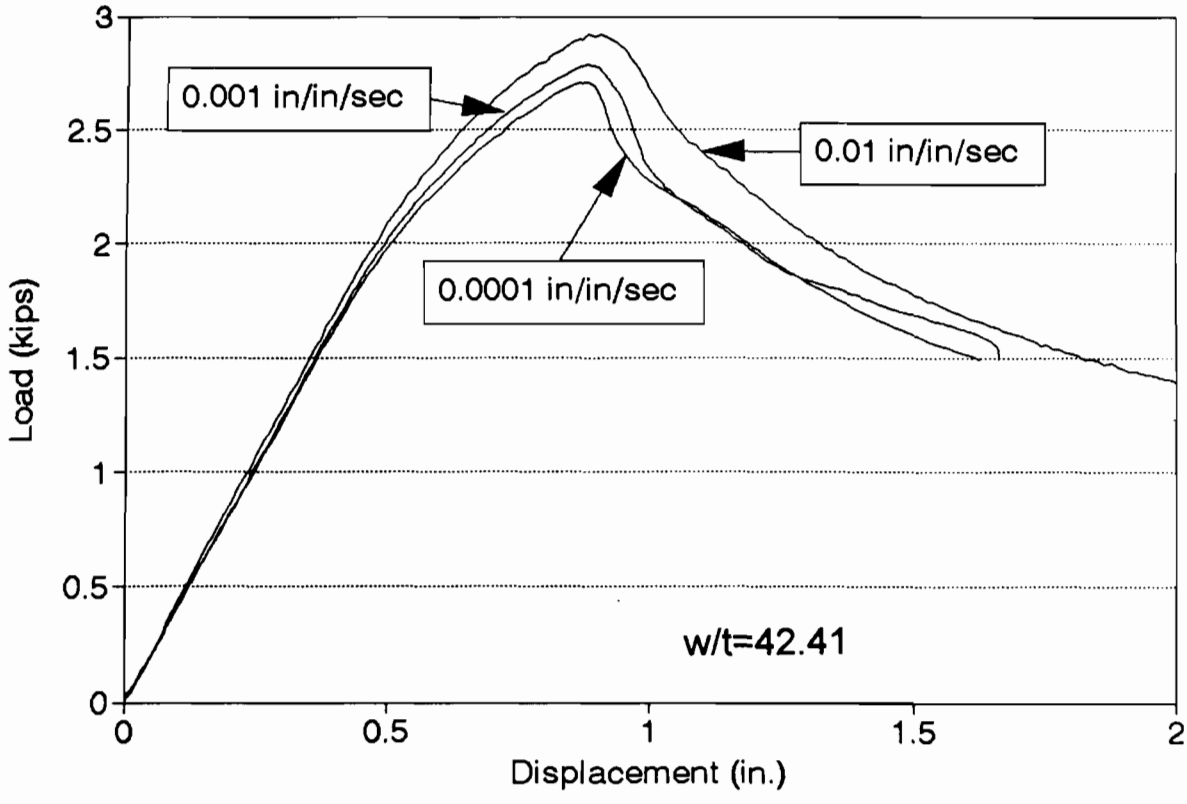

Figure 3.23 Load-Displacement Curves for Case 2 of Group S Secimens 3B1AS, 3B2AS, and 3B3BS

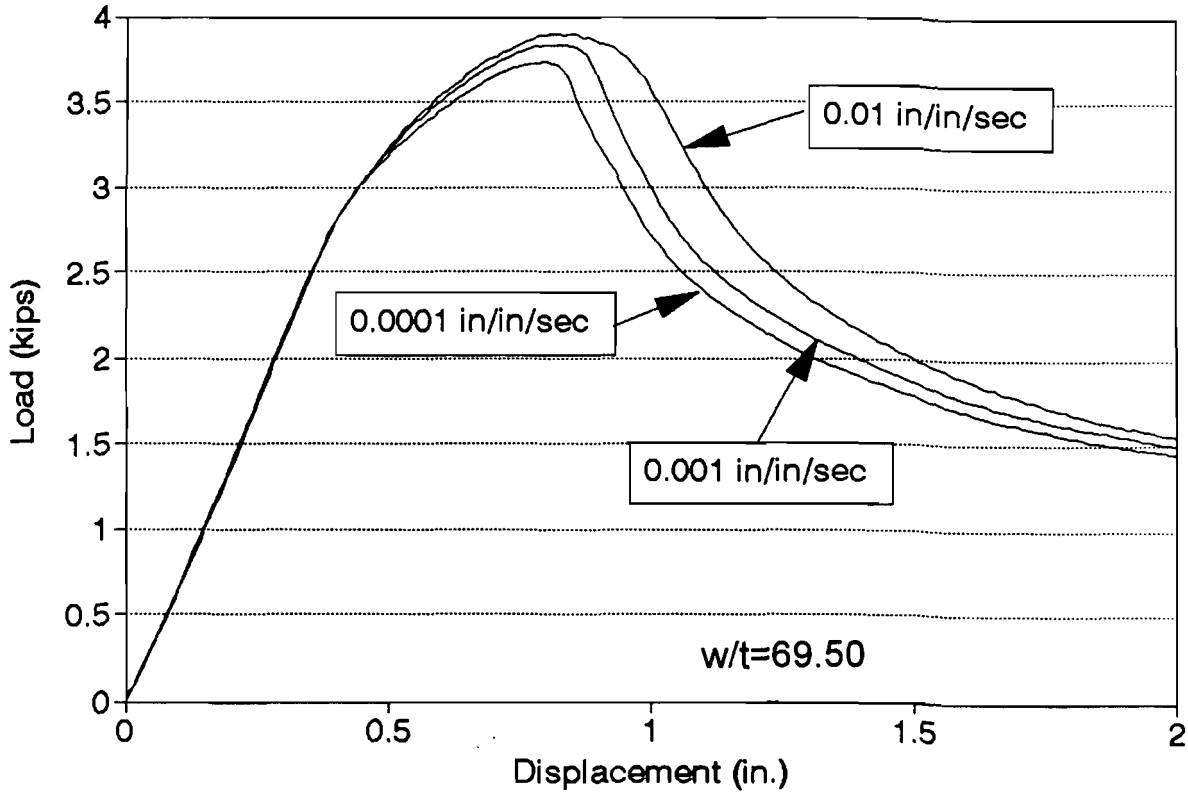

Figure 3.24 Load-Displacement Curves for Case 3 of Group S Secimens 3C1AS, 3C2AS, and 3C3AS

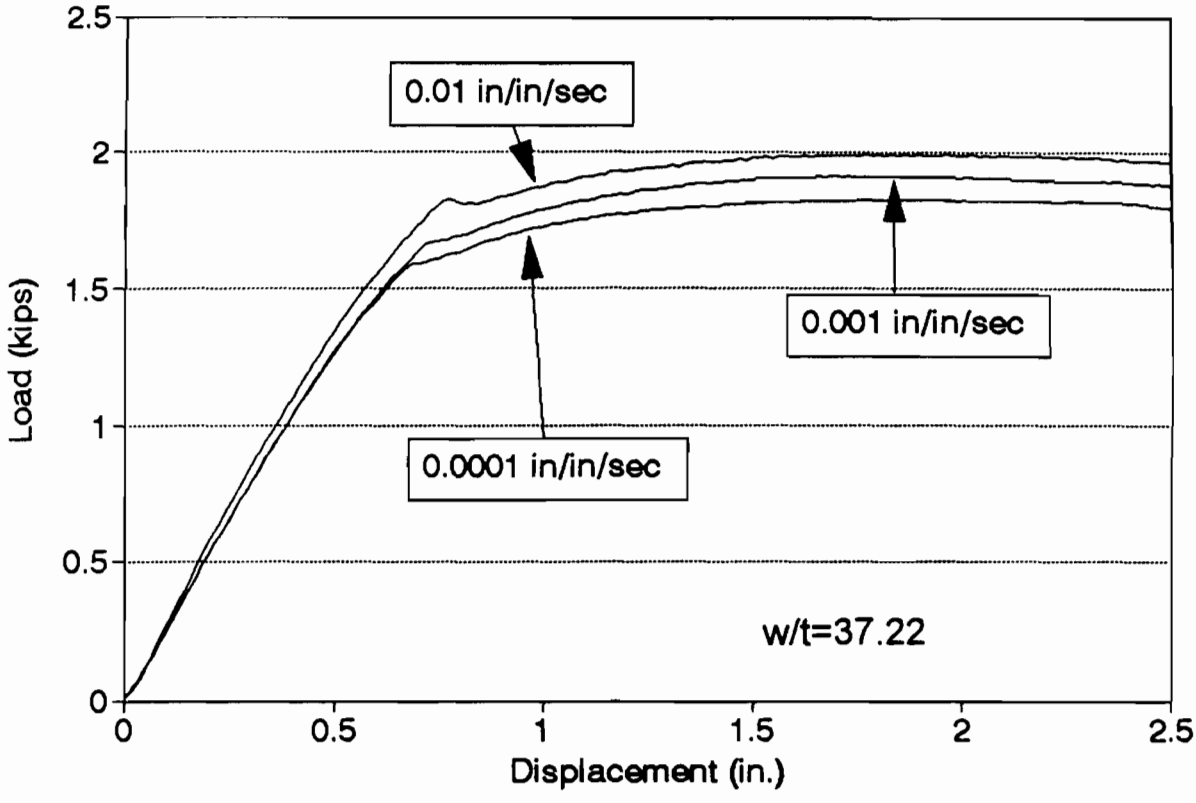

Figure 3.25 Load-Displacement Curves for Case 1 of Group K Secimens 3A1BK, 3A2BK, and 3A3BK

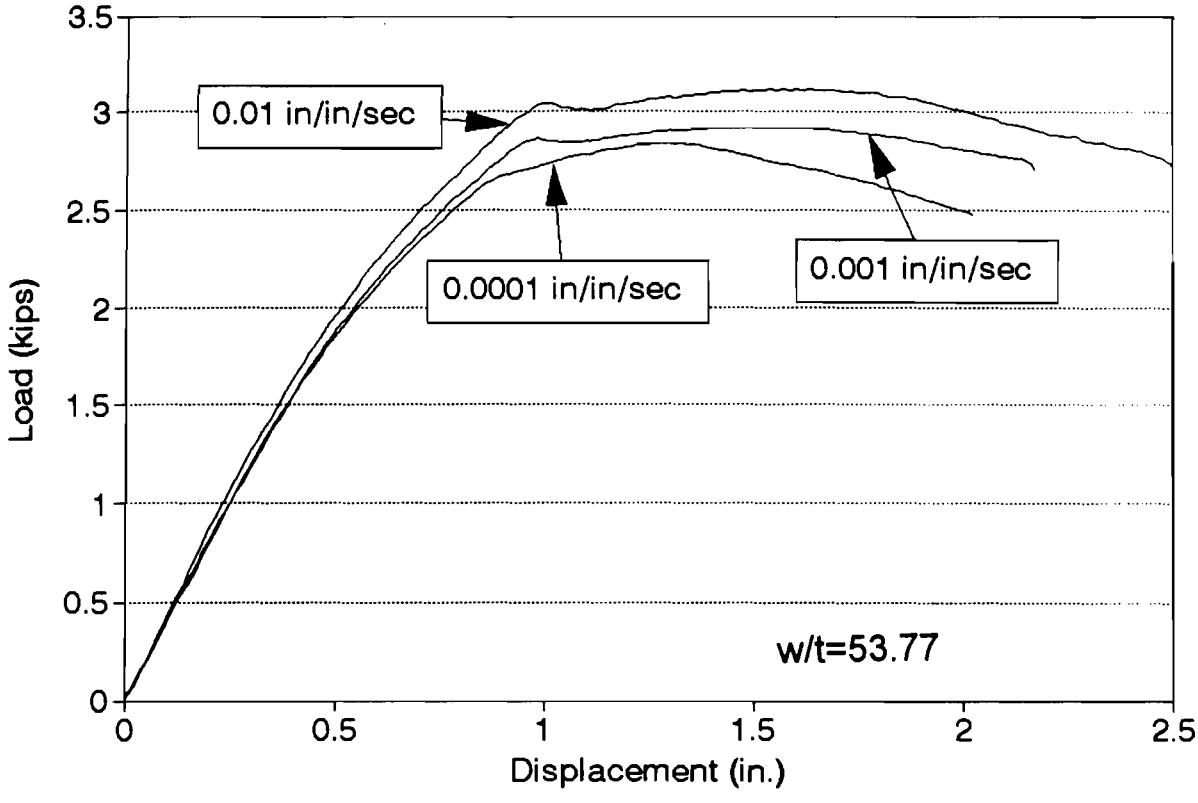

Figure 3.26 Load-Displacement Curves for Case 2 of Group K Secimens 3B1BK, 3B2BK, and 3B3BK

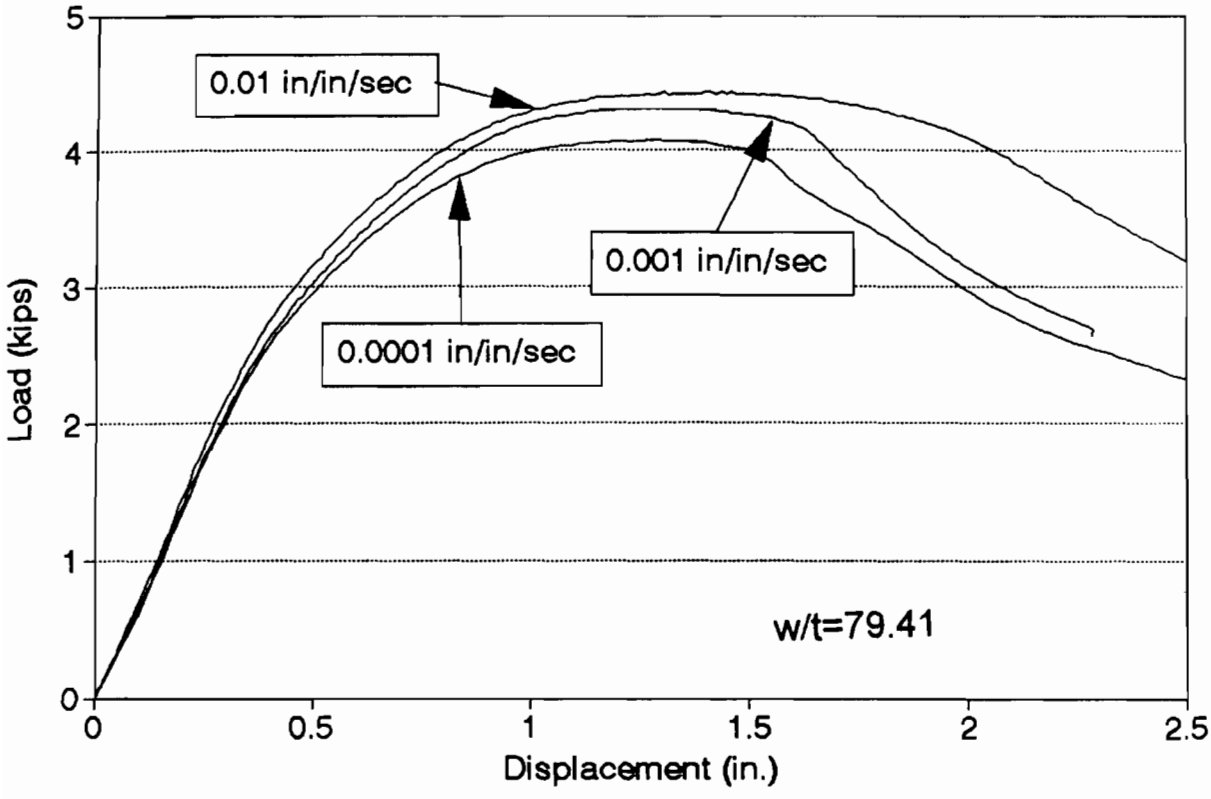

Figure 3.27 Load-Displacement Curves for Case 3 of Group K Secimens 3C1BK, 3C2BK, and 3C3BK

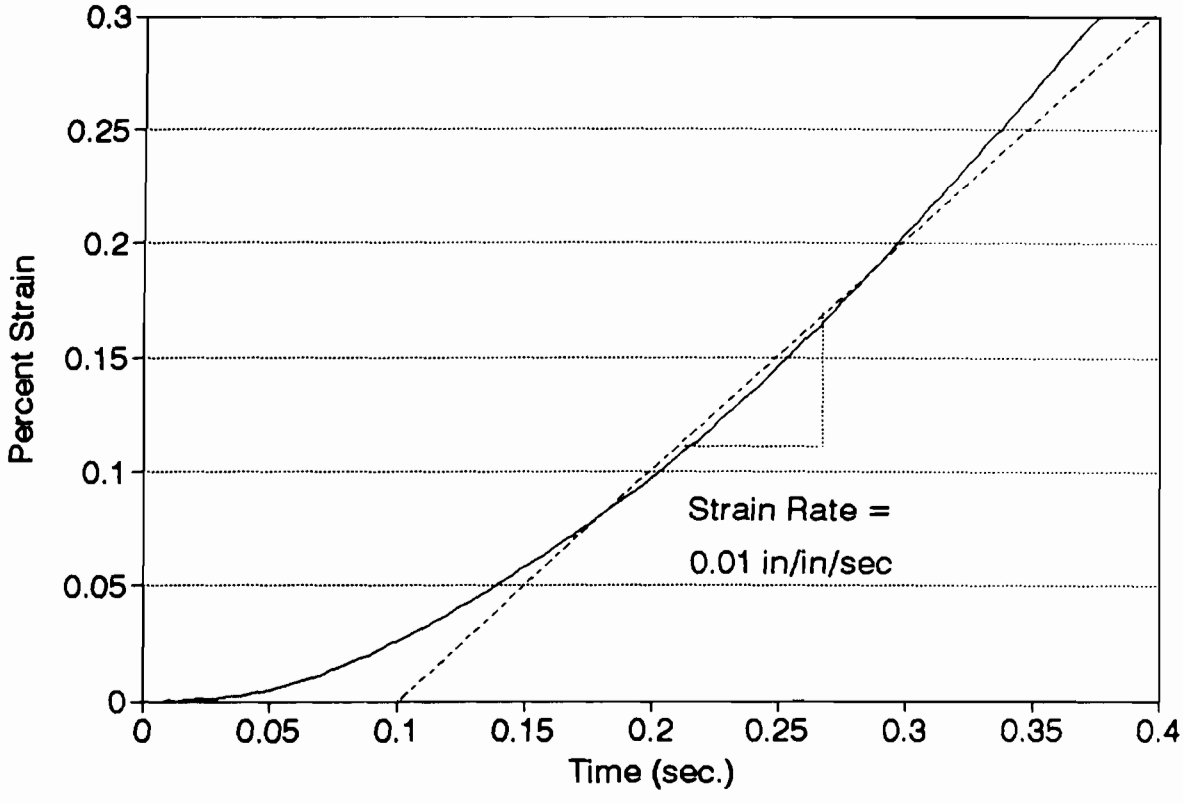

Figure 3.28 Typical Plot of Strain-Time Relationship for Beam Specimen under a Strain Rate of 0.01 in./in./sec (Spec. 3B3BW)

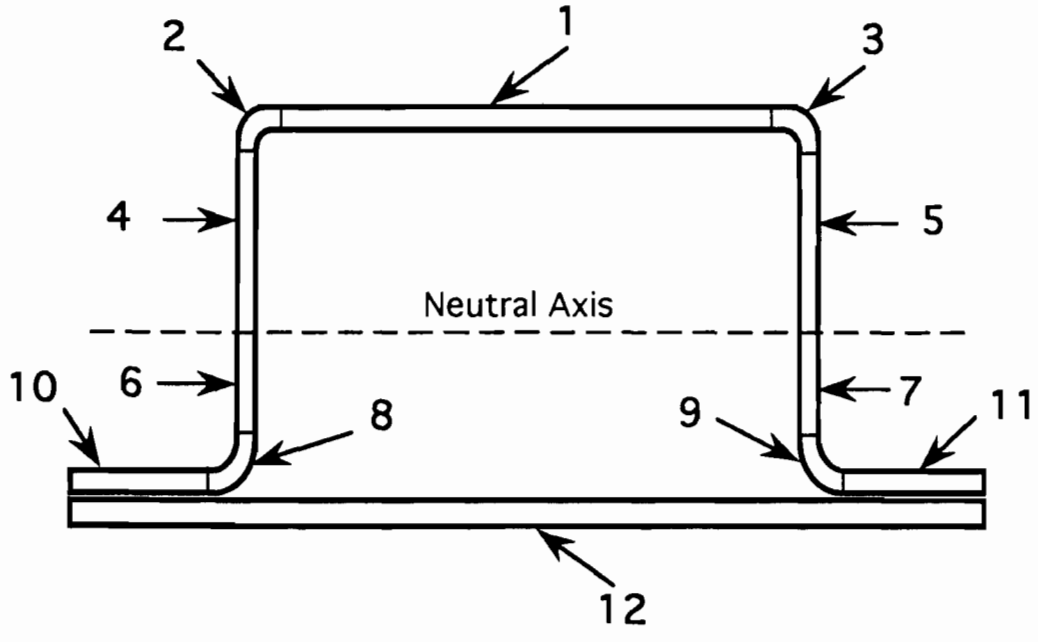

Figure 4.1 Location of Elements for Determination of the Neutral Axis of a Beam Specimen

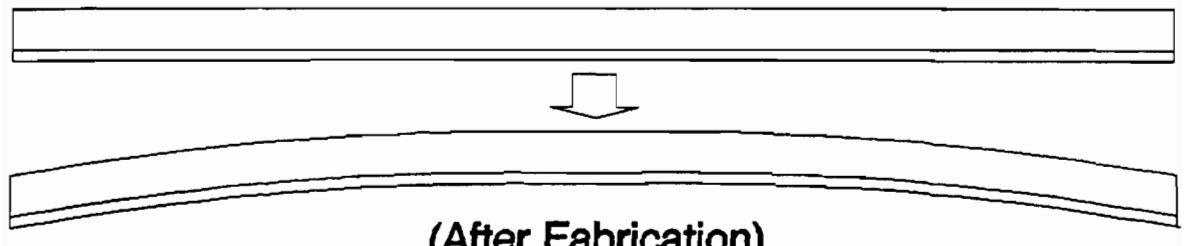

(After Fabrication)

Groups W and S

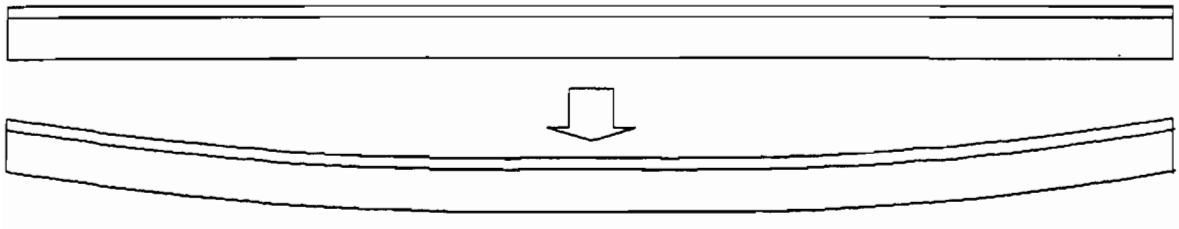

(After Fabrication)

Groups Z and K

Figure 4.2 Schematic Diagram for Specimens after Fabrication

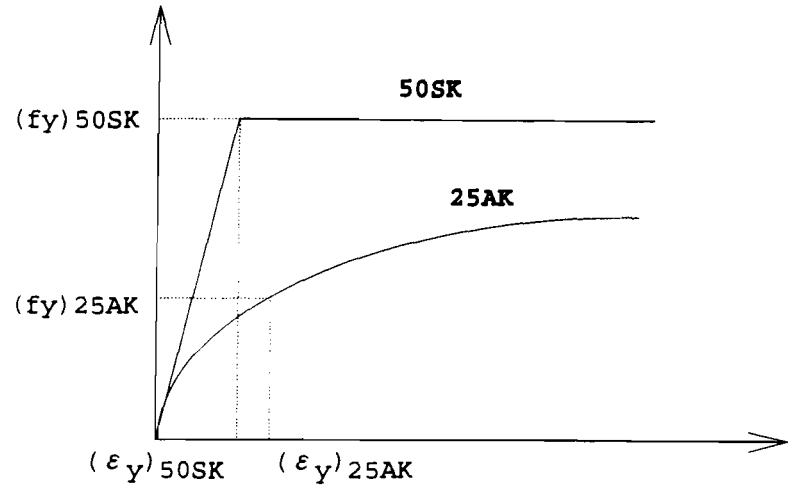

Figure 4.3 Real Stress-Strain Relationships for 25AK and 50SK Sheet Steels

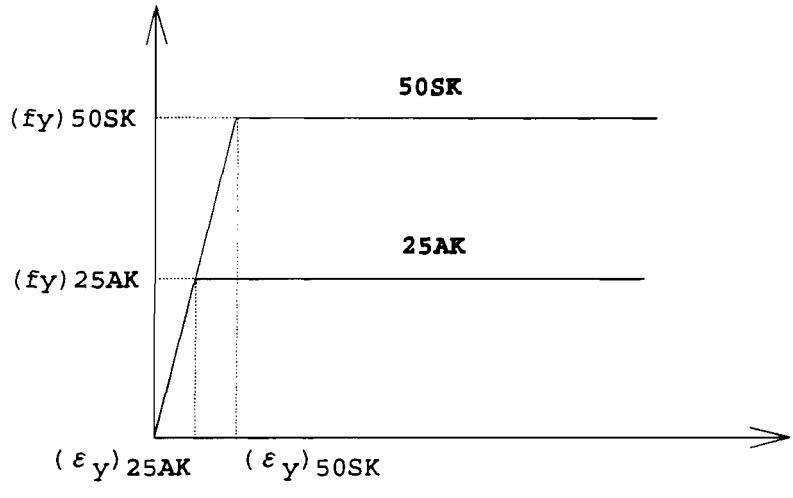

Figure 4.4 Idealized Stress-Strain Relationships for 25AK and 50SK Sheet Steels

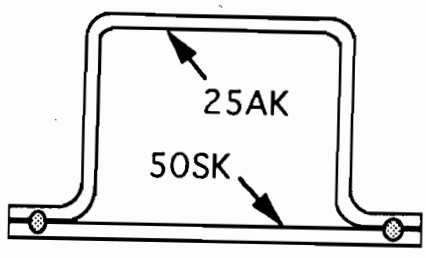

Group W

(a) Cross Section

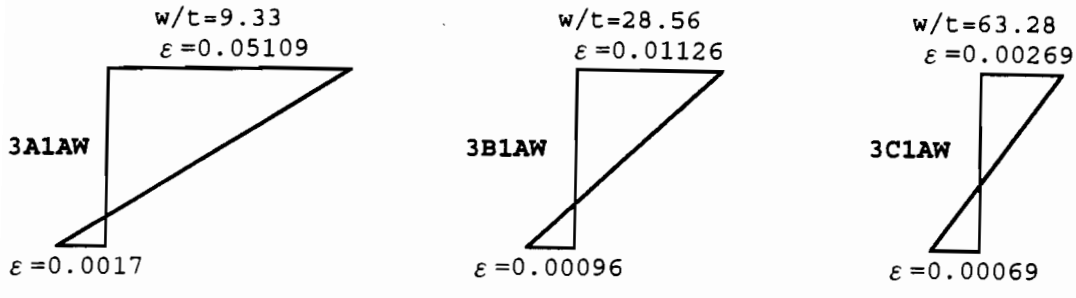

(b) Strain Diagram

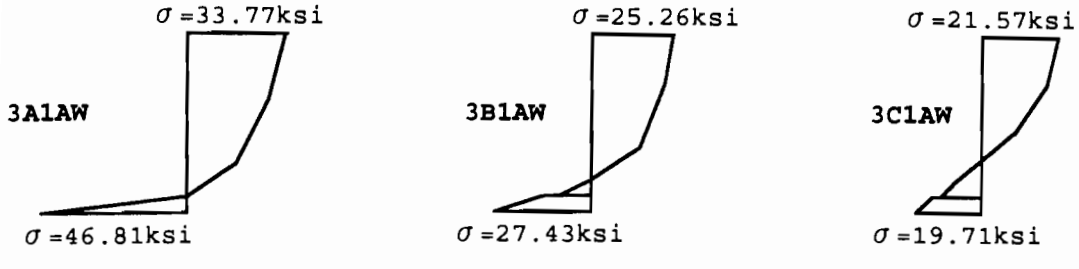

(c) Stress Diagram

Figure 4.5 Stress and Strain Diagram for Group W Specimens Subjected to Ultimate Moments

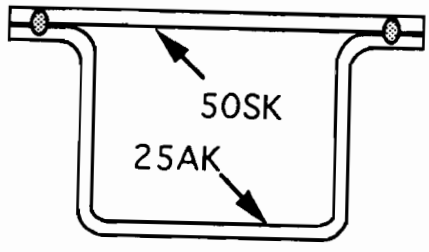

Group Z

(a) Cross Section

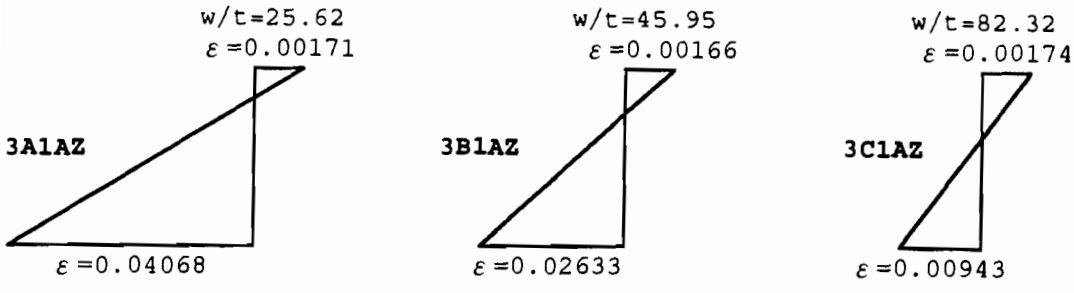

(b) Strain Diagram

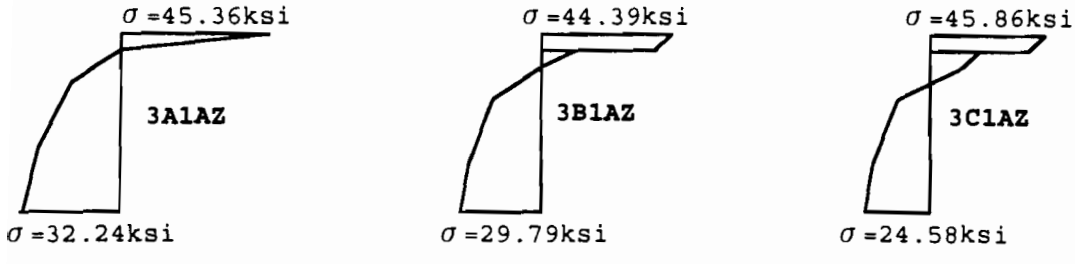

(c) Stress Diagram

Figure 4.6 Stress and Strain Diagram for Group Z Specimens Subjected to Ultimate Moments

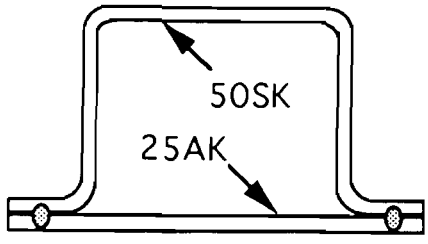

Group S

(a) Cross Section

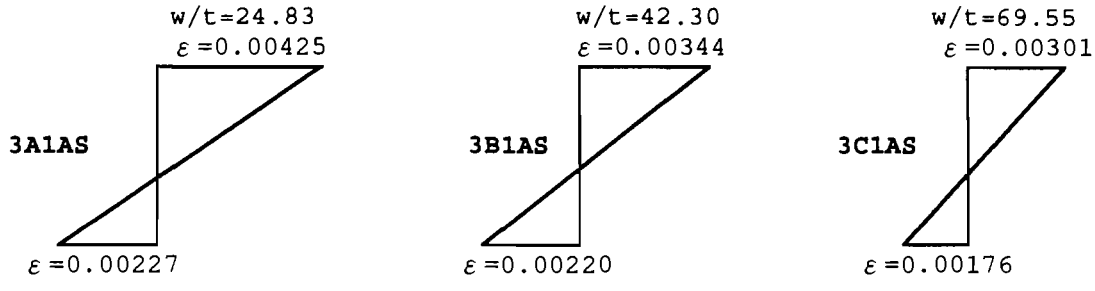

(b) Strain Diagram

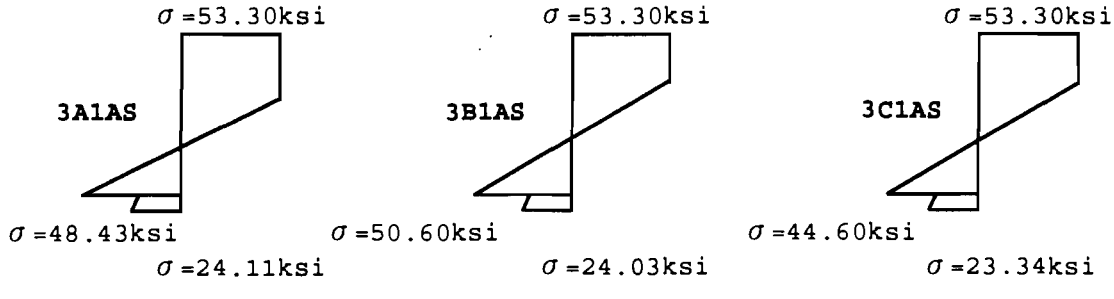

(c) Stress Diagram

Figure 4.7 Stress and Strain Diagram for Group S Specimens Subjected to Ultimate Moments

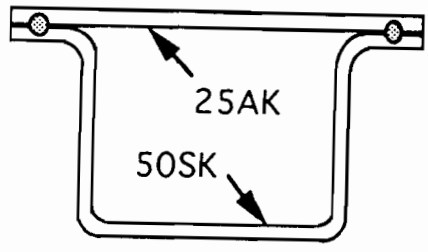

Group K

(a) Cross Section

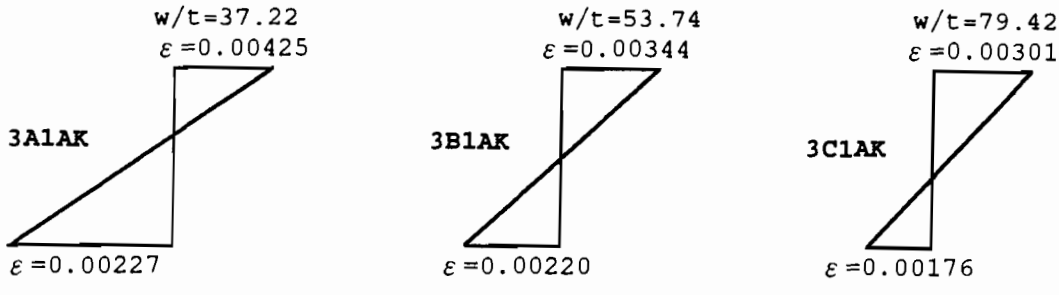

(b) Strain Diagram

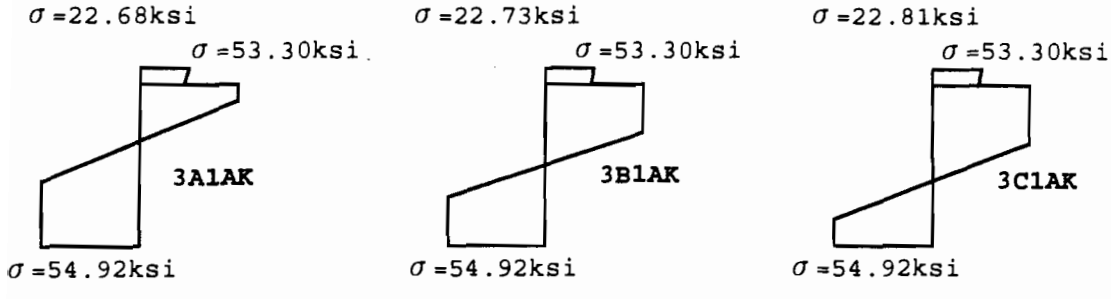

(c) Stress Diagram

Figure 4.8 Stress and Strain Diagram for Group K Specimens Subjected to Ultimate Moments

NOTATION

The following symbols are used in this report:

b	Effective width of a compression element
D	Flexural rigidity of plate
E	Modulus of elasticity of steel, 29,500 ksi
f	Edge stress in the compression element
f_{cr}	Critical local buckling stress
$(f_{cr})_E$	Elastic critical local buckling stress
$(f_{cr})_I$	Inelastic critical local buckling stress
F_{pr}	Proportional limit
F_y	Yield stress
F_u	Ultimate tensile strength
k	Buckling coefficient
L	Span length of beam specimen
P_{cr}	Critical local buckling load
$(P_{cr})_{comp}$	Computed critical local buckling load
$(P_{cr})_{test}$	Tested critical local buckling load
P_u	Ultimate load
$(M_u)_{comp}$	Computed ultimate moment
$(M_u)_{test}$	Tested ultimate moment
$(M_y)_{comp}$	Computed yield moment
$(M_y)_{test}$	Tested yield moment
R	Inside bend radius
S_x	Elastic section modulus of the full cross section relative to the compression element
S_e	Elastic section modulus of effective section
t	Thickness of element

w	Flat width of a compression element
	Transverse distance between spot welds for plate element
λ	Slenderness factor
ω	Lateral deflection of the plate
μ	Poisson's ratio
ρ	Reduction factor
α	Aspect ratio
ε_{pr}	Strain under proportional limit
ε_{y}	Strain under yield point